Coastal Resiliency and Morphodynamic Responses to Storm Surge and Seiche in Eastern Lake Erie

Final Report | Report Number 22-02 | August 2021

NEW YORK STATE | NYSERDA

NYSERDA's Promise to New Yorkers:

NYSERDA provides resources, expertise, and objective information so New Yorkers can make confident, informed energy decisions.

Our Vision:

New York is a global climate leader building a healthier future with thriving communities; homes and businesses powered by clean energy; and economic opportunities accessible to all New Yorkers.

Our Mission:

Advance clean energy innovation and investments to combat climate change, improving the health, resiliency, and prosperity of New Yorkers and delivering benefits equitably to all.

Coastal Resiliency and Morphodynamic Responses to Storm Surge and Seiche in Eastern Lake Erie

Final Report

Prepared for

New York State Energy Research and Development Authority

Albany, NY

Amanda Stevens
Project Manager

Prepared by:

Stony Brook University

Ali Farhadzadeh, Ph.D., P.E.
Assistant Professor

and

University at Buffalo

Joseph F. Atkinson, Ph.D., P.E.
Professor

NYSERDA Report 22-02 NYSERDA Contract 105162 August 2021

Notice

This report was prepared by Ali Farhadzadeh, PhD and Joseph Atkinson, PhD in the course of performing work contracted for and sponsored by the New York State Energy Research and Development Authority (hereafter "NYSERDA"). The opinions expressed in this report do not necessarily reflect those of NYSERDA or the State of New York, and reference to any specific product, service, process, or method does not constitute an implied or expressed recommendation or endorsement of it. Further, NYSERDA, the State of New York, and the contractor make no warranties or representations, expressed or implied, as to the fitness for particular purpose or merchantability of any product, apparatus, or service, or the usefulness, completeness, or accuracy of any processes, methods, or other information contained, described, disclosed, or referred to in this report. NYSERDA, the State of New York, and the contractor make no representation that the use of any product, apparatus, process, method, or other information will not infringe privately owned rights and will assume no liability for any loss, injury, or damage resulting from, or occurring in connection with, the use of information contained, described, disclosed, or referred to in this report.

NYSERDA makes every effort to provide accurate information about copyright owners and related matters in the reports we publish. Contractors are responsible for determining and satisfying copyright or other use restrictions regarding the content of reports that they write, in compliance with NYSERDA's policies and federal law. If you are the copyright owner and believe a NYSERDA report has not properly attributed your work to you or has used it without permission, please email print@nyserda.ny.gov

Information contained in this document, such as web page addresses, are current at the time of publication.

Abstract

Extreme coastal events and abrupt changes in atmospheric pressure in an enclosed or semi-enclosed basin can trigger low-frequency water surface oscillations known as seiches. This exploratory study numerically quantifies the effects of seiches on morphological changes along the eastern Lake Erie shoreline and examines their impact on flooding in a coastal urban setting, using the Buffalo River (Buffalo, New York) as an example. The quantification is made by simulating the hydrodynamics of the lake using the coupled circulation, ADCIRC, (ADvanced CIRCulation), and spectral wave, SWAN (Simulating WAves Nearshore) model, providing the flow boundary conditions to the two-dimensional nearshore morphodynamic model, XBeach. The process-based XBeach model is used to simulate the nearshore morphological variations under two water-level conditions: the lake's actual water level, and the synthetically generated seiche-free water level. The XBeach model is cross-calibrated using the one-dimensional cross-shore morphodynamic model, CSHORE, which was extensively validated using lab and field data. It is found that the seiching motions have a contribution of ~1.5% to the erosion of beaches along a 2 kilometer (km) stretch of the shoreline in eastern Lake Erie. The Environmental Fluid Dynamics Code (EFDC) was used to model flow conditions in the Buffalo River, using upstream flows obtained from United States Geological Survey (USGS) gauges and downstream water-level simulations from the ADCIRC model. Frequency analysis results for flows and downstream water level were also used with the Army Corps of Engineers (ACOE) Hydrologic Engineering Center-River Analysis System (HEC-RAS) model to simulate water levels along the river and to evaluate the impact of seiches on flooding. Because of side bank protections installed along the lower parts of the river, seiches were found to have limited impact on flooding locations, but the amount of flooding increased upstream with increased downstream water level. It is suggested that unprotected rivers would suffer increased risks of flooding as a result of seiches, and the procedures developed here can be used generally to evaluate those risks.

Keywords

Seiching, low-frequency oscillation, the Great Lakes, suspended sediment, bed load, flooding

Acknowledgments

This study was funded by The New York State Energy Research and Development Authority (NYSERDA) under agreement No. 105162. The authors would like to thank the funding agency for this support.

Table of Contents

List of Figures

List of Tables

Executive Summary

Responding to a need to plan for impacts of future climate change as encoded in the New York State Law, Coastal Risk and Resiliency Act (Bill no. A06558, effective 2017), this project was designed to evaluate resilience for Lake Erie coastal and riverine environments as well as to support planning, development, and management activities that would be conducted to develop such resilience. Furthermore, the project included an analysis of the potential for flooding as a result of the combined effects of precipitation-generated flows and lake level variations controlled by seiching, where seiches are low-frequency water surface oscillations that are triggered by extreme winds or abrupt changes in atmospheric pressure in an enclosed or semi-enclosed basin. Both precipitation and seiching are driven by meteorological factors. The primary goals of the project were the following:

- Examine coastal and littoral processes in coastal Lake Erie for short-term events and long-term climate, and to consider the potential impacts of climate change (Woodlawn Beach, along the New York State shoreline south of Buffalo, was chosen for detailed analysis).
- Evaluate waves, storm surge, and post-storm seiche-induced water-level variations and current patterns and their contributions to riverine and coastal sediment transport and morphological changes.
- Understand the extent and distribution of flooding due to in-lake extreme events in both coastal and riverine areas (the Buffalo River in Buffalo, NY was used to demonstrate an approach to analyzing the statistical risk of flooding due to the combined effects of extreme flow and lake-water level).
- Disseminate project findings among State and government officials, stakeholders, the scientific community, and the public.

These goals were pursued using a primarily modeling-based approach, as well as frequency analyses of flows and water levels for the Buffalo River. The frequency analyses considered flows and water levels independently as well as in conjunction, to develop a risk of flooding as a combined effect of both processes. Quantification of the effects of seiches on morphological changes along the eastern Lake Erie shoreline was done by simulating the hydrodynamics of the lake using the coupled circulation, ADCIRC (ADvanced CIRCulation), and spectral wave, SWAN (Simulating WAves Nearshore), model, providing the flow-boundary conditions to the two-dimensional nearshore morphodynamic model. The two-dimensional, process-based morphodynamic (XBeach) model was used to simulate nearshore morphological variations under two water-level conditions: the lake's actual water level and the

synthetically generated seiche-free water level. The model was cross-calibrated using a one-dimensional cross-shore morphodynamic model (CSHORE), already validated using lab and field data. It was found that seiching motions contribute approximately 1.5% of the erosion of beaches along the 2 kilometer (km) stretch of shoreline in eastern Lake Erie that was considered for detailed analysis.

The Environmental Fluid Dynamics Code (EFDC) was used to model flow conditions in the Buffalo River, using upstream flows obtained from United States Geological Survey (USGS) gauges and downstream water-level simulations from the ADCIRC model and also direct analysis of lake water-level data. Frequency analysis results for flows and downstream water levels were also used with the Army Corps of Engineers (ACOE) Hydrologic Engineering Center River Analysis System (HEC-RAS) model to simulate water levels along the river and to evaluate the impact of seiches on flooding. A copula analysis was used to evaluate the combined effects of upstream flows and downstream water levels on flooding conditions in the river. Because of side-bank protections installed along the lower parts of the river, seiches were found to have limited impact on flooding locations, but the amount of flooding increased upstream with increased downstream water level.

Results show that seiches can have an impact on flooding and the compounding effects of seiche and high flow can increase the inundation area. The study also shows that the present Federal Emergency Management Agency (FEMA) 100-year flood scenario for the study site is equivalent to a compound 100-year high flow and 10-year water-level scenario, and the 100-year high flow and corresponding most probable water level (slightly larger than the long-term average lake level) is approximately seven times more likely to occur than the FEMA scenario. This analysis framework can provide insight into the compounding effects of seiche and high flow on inundation, and on the probability of occurrence of such events for overall flood engineering in a freshwater coastal river. It is suggested that unprotected rivers would suffer increased risks of flooding as a result of seiches, and the procedures developed here can be used generally to evaluate those risks.

1 Introduction

1.1 Background

This project was designed and carried out with funding provided through the NYSERDA Climate Change Adaptation Research and Strategies Program Opportunity Notice (PON) 3242. The motivation for this program is based on New York State's recognition of the need for resiliency and adaptation under future climate conditions, as enacted under the Coastal Risk and Resiliency Act, Bill no. A06558, effective 2017. Specifically, Category B of the PON lists the need for climate change adaptation strategies "to build resiliency in all sectors of NYS, such as agriculture, buildings, coastal zones, ecosystems, public health, telecommunications, transportation, and water resources." This project addresses the evaluation of coastal resilience along the New York State shoreline of Lake Erie. Specifically, we consider the impacts of lake seiches on changes in coastal morphodynamics and on flooding in a coastal river. Lake Erie is well-known for its seiches, and it is anticipated that both the frequency and magnitude of seiches will increase in the future.

Lake Erie is the fourth largest lake among the five Laurentian Great Lakes in North America and eleventh in surface area worldwide. It accommodates approximately twelve million people in seventeen metropolitan areas with more than 50,000 residents around the watershed, which is ~30% of the total population in the Great Lakes basin. The lake, with an average depth of 19 meters (m), comprises three basins: a very shallow western basin, a large central basin, and a relatively deep eastern basin. Its length and width are about 390 kilometers (km) and 90 km, respectively. The western basin, with an average depth of 7.4 m, is covered with fine sediments and is the most turbid region of the lake. The central basin has a relatively uniform average depth of 18.3 m and a maximum depth of 25 m. The eastern basin has an average depth of 24 m and a maximum depth of 64 m (United States Environmental Protection Agency, 2019). Additional details on the Lake Erie physical and environmental specifications are referenced in the Great Lakes Atlas (USEPA Great Lakes Atlas), among other resources.

Lake Erie is known for its seiche—a standing wave in an enclosed or semi-enclosed body of water originated by strong winds (e.g., storms, hurricanes), earthquakes, tsunamis, or rapid large-scale atmospheric pressure changes. Following such an event, the water surface begins oscillating at a range of frequencies, from hours to days, until it reaches equilibrium (Kamphuis 2010a; Kim 2009; National Oceanic and Atmospheric Administration 2019b). Typically, Lake Erie's seiches occur when a strong wind blows along the lake's longer axis, from southwest to northeast. Following such events, large

wind setups forming at one end (on the west) of the lake initiate long waves propagating toward the opposite end (on the east) of the lake. In 1844, for example, a 14-foot-high seawall was destroyed and 78 people were drowned by a 22-foot rise of the water level due to a seiche event in Buffalo (National Ocean Service, 2019). A powerful storm in 2008 resulted in flooding near Buffalo (National Oceanic and Atmospheric Administration, 2019b) and generated significant seiching oscillations (Farhadzadeh *et al.*, 2018). Recently, a large seiche occurred in November 2019 when 60 miles per hour (mph) winds were recorded and, according to the Capital Weather Gang (Washington Post, November 1, 2019), "High winds [whipped] a powerful seiche into Buffalo, causing coastal flooding." The extent of seiche-induced flooding is evaluated below, in particular with a comparison to the 100-year floodplain defined by the Federal Emergency Management Agency (FEMA).

Seiches occurring in the lakes have been the focus of numerous studies over the past decades (Cueva *et al.* 2019; Trebitz 2006). The following summarizes the studies that investigated Lake Erie's seiches. Platzman and Rao (1964a) spectrally analyzed Lake Erie's hourly water levels and identified distinct peaks at periods of 14.1hr, 9.2hr, 6.0hr, and 4.1hr. Platzman and Rao (1964b) analytically showed that those periods were attributed to the first four seiche modes and the low-frequency oscillations were found to be more energetic in winter than summer. Furthermore, the diurnal constituent of the lake level was found to be an amphidromic Kelvin-type wave (Hamblin, 1987; Irish and Platzman, 1961; Kite, 1992; Mortimer, 1987; Platzman and Rao, 1964a, b).

Palmer and Izatt (1972) investigated the effects of surface ice on the Lake Erie seiche by analyzing current velocity data collected from northern Lake Erie during and soon after ice cover formation, and several months later. The velocity spectra for the period of ice formation were similar to those of the ice-free condition. The spectral density of the current velocity peaked at the frequencies corresponding to the free-oscillation modes. On the other hand, the maximum current velocity of the second timeframe was less than half of that for the first period, the ice-free condition. The velocity spectral density was not peaked at this period, pointing to the absence of seiching oscillations. Dingman and Bedford (1984) investigated the response of partially ice-covered Lake Erie to the cyclone of January 26, 1978, by analyzing the power spectral density of the lake-level fluctuations. They stated that the surface ice played a significant role in suppressing the seiches such that the tidal oscillations—which are very small for the lake—became dominant. Gerbush *et al.* (2008) and Wang *et al.* (2010) showed that the presence of the surface ice led to a reduced momentum flux exchange between the atmosphere and the lake, decreasing oscillations of the lake level. This finding supported the conclusions by Palmer and Izatt, (1972) and Dingman and Bedford (1984).

Varying water levels contribute to morphological changes in beaches. The majority of Lake Erie's New York State shorelines are at a high risk of erosion (New York State Division of Homeland Security, 2014). The quantification of shore erosion requires understanding the effects of factors that influence the erosion processes. For enclosed water bodies, this includes, among others, the interpretation of seiches and their potential contribution to the beach erosion. Most of the past studies focused on the hydrodynamics of seiches, as reviewed above. On the other hand, studies on beach morphology are mainly concentrated on the morphological changes by short waves (*e.g.,* Bruun 1954; Dean 1991; Dean and Houston 2016; Kamphuis 1996, 2010b; Kriebel and Dean 1985, 1993; Tomasicchio *et al.* 2011) and long waves such as infragravity waves, edge waves, *etc.* (*e.g.,* Aagaard and Greenwood 2008; de Bakker *et al.* 2016; Bertin *et al.* 2018; Russell 1993; Wright and Short 1984).

As the shallowest among the five Great Lakes, Lake Erie responds relatively quickly to changes in temperature. As a result, the extent of the winter ice cover on Lake Erie is greatly reduced with warmer winters (United States Environmental Protection Agency, 2019)—this has been a trend in recent years (National Oceanic and Atmospheric Administration, Great Lakes Environmental Research Laboratory, 2019). Figure 1[a] shows the historical ice cover (percent of total surface area) for Lake Erie during 1973–2017. There is evidence that shows reduced surface ice can lead to an intensification in the low-frequency oscillations following an extreme event (Farhadzadeh, 2017; Farhadzadeh and Gangai, 2017). Farhadzadeh *et al.* (2018) highlighted the contribution of seiches to beach profile changes in Lake Erie. Their study, however, was limited to a six-month timespan. Further, they used a one-dimensional numerical model, disregarding the longshore variations of such changes.

The present study extends the work by Farhadzadeh *et al.* (2018) by quantifying the contribution of the seiche to the beach evolutions in eastern Lake Erie using a suite of 2D numerical models and for an extended period of time (*e.g.*, one year). A broader range of variables and processes are studied here. The simulations were carried out for the entire year of 2012 during which Lake Erie's ice cover was historically low and mostly concentrated in the western basin (Figure 1[b]). Hence, the impact of the surface ice on the seiche in eastern Lake Erie was believed to be negligible. Furthermore, the quality of the meteorological and hydrological data during the selected year is more complete than that of other warm winters.

1.1.1 Statistical Analysis of Combined Effects of Flow and Lake Level on Flooding in a Freshwater Coastal River

For analysis of coastal resilience, an important impact of seiches is their effect on calculations of water level. Water-level predictions are important for storm readiness, and variations along rivers and streams discharging into the lake are affected in ways that depend on river flows and physical conditions along the river course. In this study we applied a copula to evaluate the impacts of lake-level variations on calculations of different return period flooding.

Compound effects on flooding in a freshwater coastal river depend on multiple statistically dependent variables and, therefore, a conventional univariate statistical analysis cannot give accurate information regarding the multivariate nature of these events (Bevacqua et al., 2017). Even if there is only a weak statistical correlation between variables, a joint probability distribution approach is needed. Previous studies have evaluated compound flood risks in a coastal environment using joint probability analysis with Monte Carlo simulation, Bayesian networks, or other statistical methods, such as threshold excess, point process, and conditional methods (Hawkes et al., 2002; Leonard et al., 2014; Zheng et al., 2014). Several of these approaches are reviewed by Saharia et al. (2021), who also argue for the use of copula functions, which have become increasingly popular as a means of describing the dependence between random variables (Wang et al., 2018; Xu et al., 2019).

A copula is a multivariate cumulative distribution function used to describe the statistical relationship between random variables and to evaluate their joint probability (Sklar, 1973). The main benefit of using copula functions is that it allows an independent investigation of the marginal properties and dependence structure of each of the random variables (Grimaldi and Serinaldi, 2006). Copula functions are increasingly used to evaluate compound flooding due to the flexible selection of different marginal distributions to construct the joint distribution function (Xu et al., 2019; Zhang et al., 2013). Several examples of this type of application are summarized by Saharia et al. (2021).

Although the joint probability of heavy rainfall and high tides in marine systems has been analyzed, to the best of our knowledge, compound flooding in freshwater coastal systems due to seiching and river streamflow has not been studied. Both the downstream and upstream boundary conditions are important in determining water flows and elevations along the river reach under consideration. However, previous

studies mostly focused on the joint probability of storm surge and rainfall but lacked quantification of their combined effects on flooding (Xu et al., 2019). Here, this research gap is filled by investigating the joint impact of high streamflow and wind seiche processes leading to compound flooding in a freshwater coastal system, using a combined statistical and hydrodynamic modeling approach.

The goal of this part of the study is to characterize the combined effects of seiches and high-streamflow discharge on flooding in a freshwater coastal river. Adequate data are available for both streamflow and water level to carry out this analysis. The copula joint distribution is introduced to determine the conditional probability of streamflow discharge and seiche water level at the upstream and downstream boundaries of the river, respectively. The HEC-RAS model was used to simulate river water levels and flooded areas, and the hydraulic performance graph (HPG) was used to visualize the backwater profile in the river channel under different boundary conditions. The framework used here, based on copula, hydrologic model, and HPG, can be used for other freshwater coastal rivers to understand the compound effects of seiche and high discharge on flooding.

1.1.2 Area of study

The study area is the eastern portion of Lake Erie (Figure 2), focusing on the New York State shoreline, and the Buffalo River. To illustrate the effect of seiching, Figure 3 shows lake-level variations at the stations shown in Figure 2 for the aforementioned storm of 2008. These fluctuations in water level can obviously be significant. The Buffalo River discharges to Lake Erie just south of downtown Buffalo and is designated as one of 43 Areas of Concern (AOCs) in the Great Lakes Water Quality Agreement of 1987 (New York Department of Environmental Conservation: Great Lakes Areas of Concern; USEPA Great Lakes Areas of Concern). As with other AOCs, it has suffered from environmental degradation and exhibits beneficial use impairments, many of which are associated directly or indirectly with sediment quality, which in turn is related to water movements. The AOC is defined as extending from Lake Erie to the farthest point upstream to which the backwater condition reaches during Lake Erie's highest monthly average lake level, a distance of approximately 10 km, and this is the region considered in the present study.

Figure 1. Lake Erie Ice Cover

[a] Annual maximum ice cover for Lake Erie; [b] Lake Erie surface ice coverage in 2012.

Source: National Oceanic and Atmospheric Administration, Great Lakes Environmental Research Laboratory, (NOAA/GLERL).

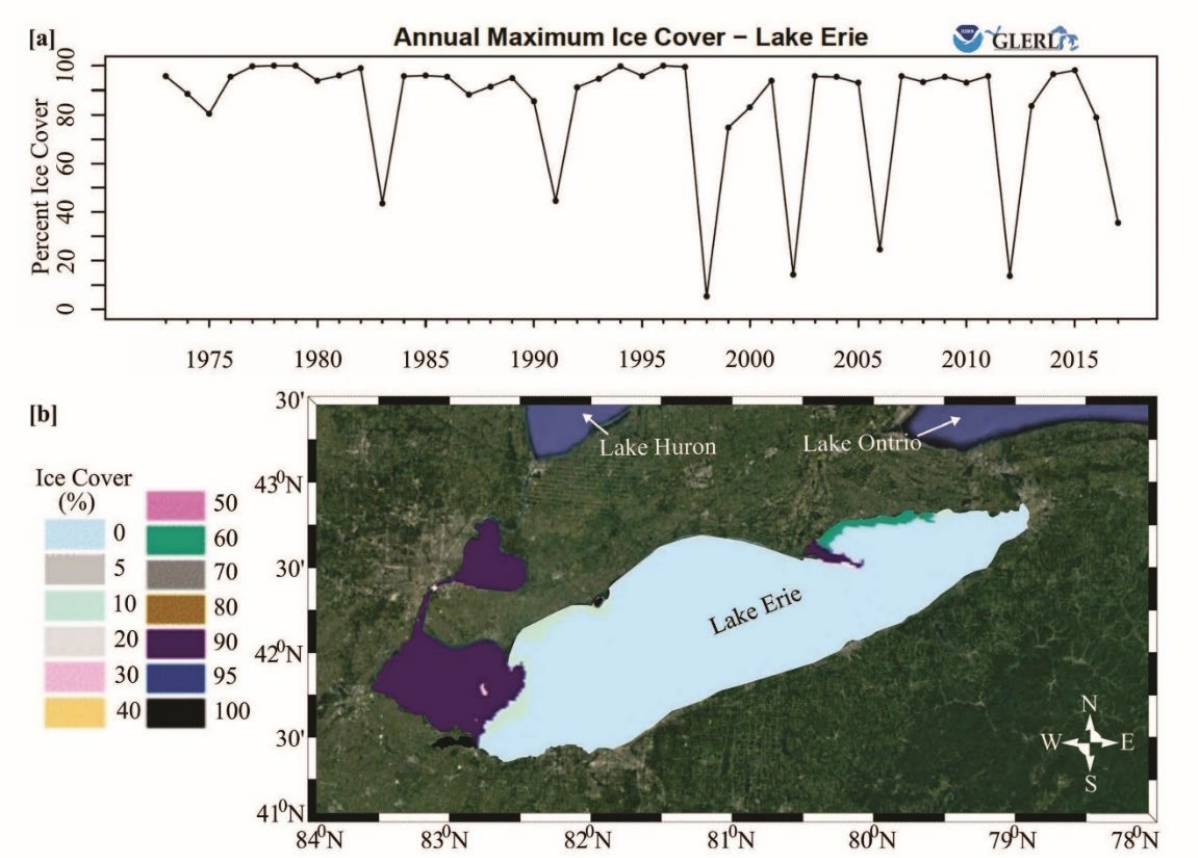

Figure 2. Lake Erie Water-Level Gauges

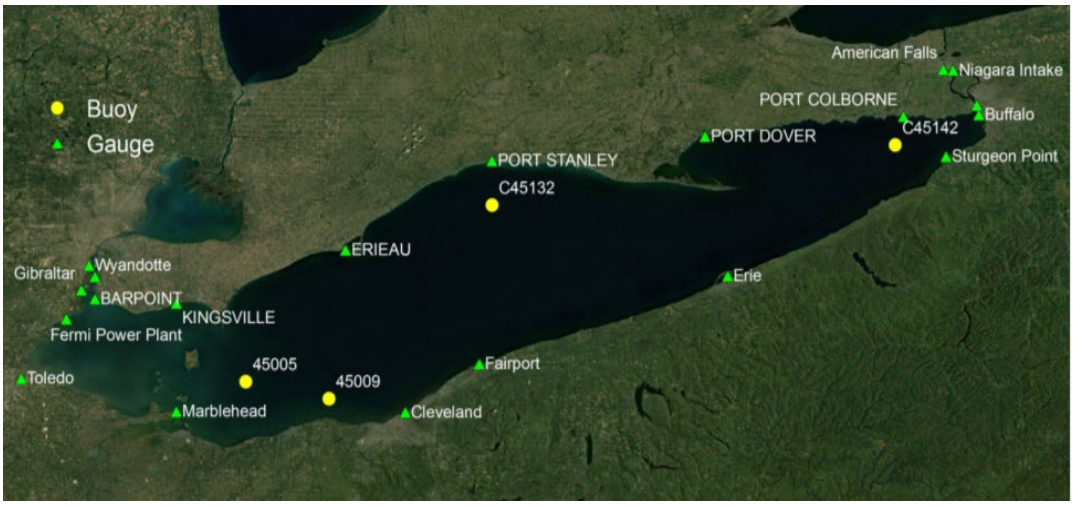

Figure 3. Water-Level Variations During Storm of 2008

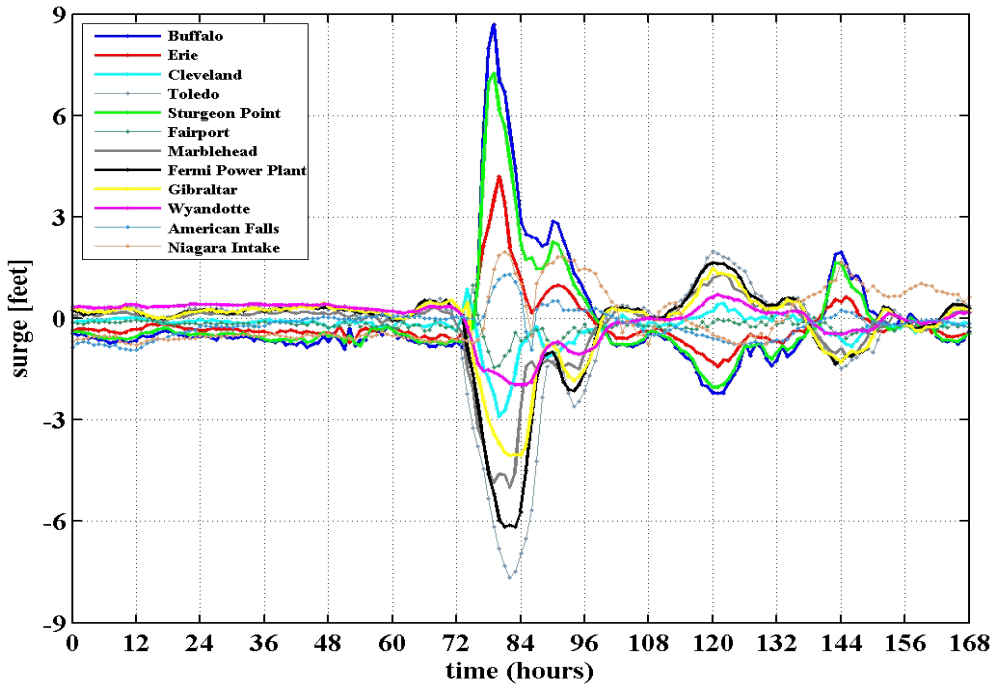

In addition, Figure 4 highlights the location of Woodlawn Beach on the eastern end of the lake, where the seiche is pronounced. The beach is located in the vicinity of National Oceanic and Atmospheric Administration (NOAA) Gauge 9063028. This site was selected because its sandy beach is located at the anti-node where the seiching motions are the greatest (Farhadzadeh 2017). The selected shoreline is approximately 2 km long and is relatively straight. The beach is composed of fine sand with a median grain size of approximately D_{50} = 0.11 mm (Dusini 2005; Farhadzadeh *et al.*, 2018; Sogut and Farhadzadeh, 2018; Thomas *et al.*, 1976). The initial and final beach profiles and the spatial variation of the beach erosion for the actual and no-seiche water-level boundary conditions are presented in the top and bottom panels of Figure 5, respectively (these are modeling results that were developed in preliminary runs to identify areas for more detailed analysis; further modeling details are provided below). As the model results suggest, the actual water-level time series result in slightly more erosion than the seiche-free condition. Given the beach length of about 2,000 m, the difference between the erosions induced by the actual and seiche-free lake conditions would be approximately 600 m^3 over a duration of 178 days.

Figure 4. Lake Erie and Woodlawn Beach Study Area

Figure 5. Beach Profile Evolution Using (left) Actual Lake Level and (right) Seiche-Free Water Level

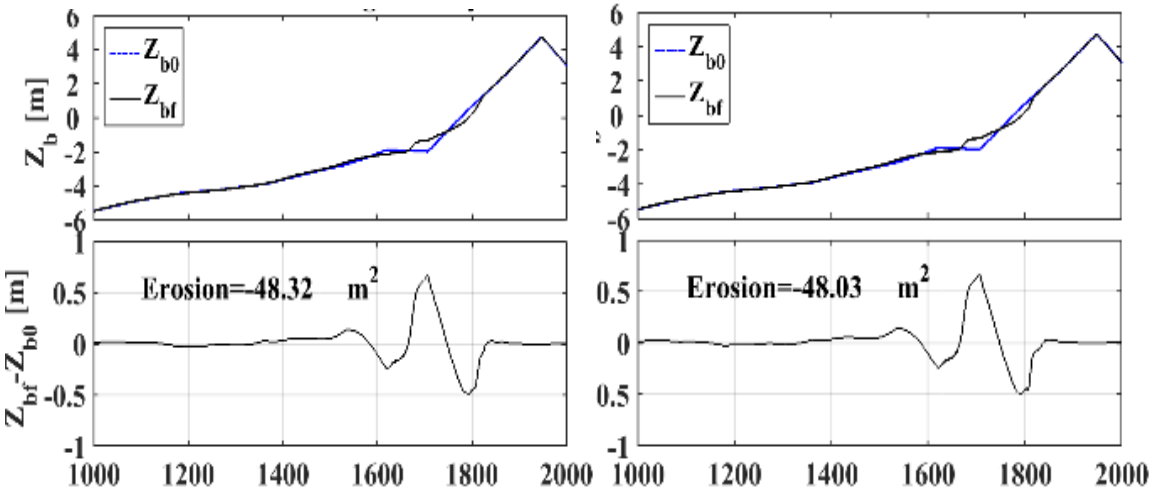

1.2 Hypotheses and Objectives

The proposed research is based on the hypothesis that surges and seiches induced by extreme storm events contribute to sediment resuspension and transport in riverine and coastal areas of eastern Lake Erie. We assume that these impacts will become more severe with changing climate, and a major objective was to develop a modeling framework with which these impacts can be measured. Seiche

impact on coastal erosion has not been considered in Great Lakes coastal planning, engineering, and design, mainly because existing methodologies have been developed only for ocean coasts. In fact, preliminary results of our previous studies (Farhadzadeh et al. 2018) indicate that there are some meaningful morphological variations in the eastern Lake Erie coastal areas due to long-term storm induced seiches.

Wave impact on nearshore morphology depends, to a great extent, on water depth. Seiching can change local water depth and surf zone width. This is one way that seiches could play a role in nearshore morphological evolution. Furthermore, seiche-induced currents and waves can interact and modify the nearshore hydrodynamics and morphology. In particular, there is a strong potential for seiching to impact flooding in a coastal region, as demonstrated by past events. To study such effects, we will develop an integrative numerical modeling framework to look into both coastal erosion and Lake Erie-Buffalo River interactions during extreme coastal events.

The objectives of this research project are the following:

1. Investigate general trend of storms in the region and characterize extreme wave and storm surge events.
2. Implement an integrative lake-river modeling system for hydrodynamics, sediment transport, and morphology for eastern Lake Erie and the Buffalo River.
3. Simulate extreme events to predict the contribution of short-term events in sediment resuspension and transport in eastern Lake Erie coastal areas.
4. Predict the extent of coastal flooding due to potential future extreme events for the Buffalo River area.
5. Predict morphological evolution due to short-term storm surge, wave and seiche events in a number of locations identified as areas with coastal erosion hazard risk.
6. Evaluate cumulative (long-term) effects of seiches on coastal morphology.
7. Enhance knowledge on Lake Erie hydrodynamics, seiching and associated sediment transport, using workshop, journal, and conference publications.

2 Methodology

The lake-wide water level and wave fields, for 2012, were simulated using the coupled ADCIRC (Luettich *et al.*, 1992) and SWAN (Booij *et al.*, 1999) model. This coupled modeling framework uses an unstructured mesh to generate the lake's hydrodynamics. The coupling of ADCIRC and SWAN allows the circulation model to use radiation stress gradients calculated by the wave model as an additional forcing for storm surge predictions. Subsequently, the wave model runs on updated water-level predictions to calculate the wave field (Dietrich *et al*., 2011). The use of the coupled model in a shallow water body such as Lake Erie, with a historical storm surge of up to 3 m (and set-downs of nearly -3 m) is critical for an accurate prediction of wave and water level (Farhadzadeh, 2017; Farhadzadeh and Gangai, 2017).

The spatial variations of the nearshore morphology in response to seiche motions were evaluated for the beach at Woodlawn Beach State Park in eastern Lake Erie (Figure 6). The nearshore morphodynamics were simulated using both one-dimensional (CSHORE, Johnson *et al.*, 2012; Kobayashi and Farhadzadeh, 2008) and two-dimensional (XBeach, Roelvink *et al.*, 2009, 2010) process-based morphodynamic models. The offshore boundary conditions for the morphodynamic models were supplied from the lake-wide hydrodynamic model, ADCIRC+SWAN. The XBeach model in its 1D mode was cross calibrated against CSHORE which has been extensively calibrated using laboratory and field data. The model was used for previous FEMA Great Lakes flood studies (Johnson, 2012; Johnson *et al.*, 2012).

2.1 Lake-Wide Hydrodynamics

To obtain offshore boundary conditions for the morphodynamics models, lake-wide water levels and waves were generated by the coupled ADCIRC+SWAN on Lake Erie during 2012. The year of 2012 was selected because it experienced a low-ice coverage and the quality of data available was better than the previous years. In the following subsections, descriptions are provided for the circulation (ADCIRC) and spectral wave (SWAN) models, as well as the model setup.

Figure 6. Woodlawn Beach State Park

[a] Study area: Woodlawn Beach State Park; [b] The topography and near-shore bathymetry of Woodlawn Beach State Park used in the 2D XBeach simulations.

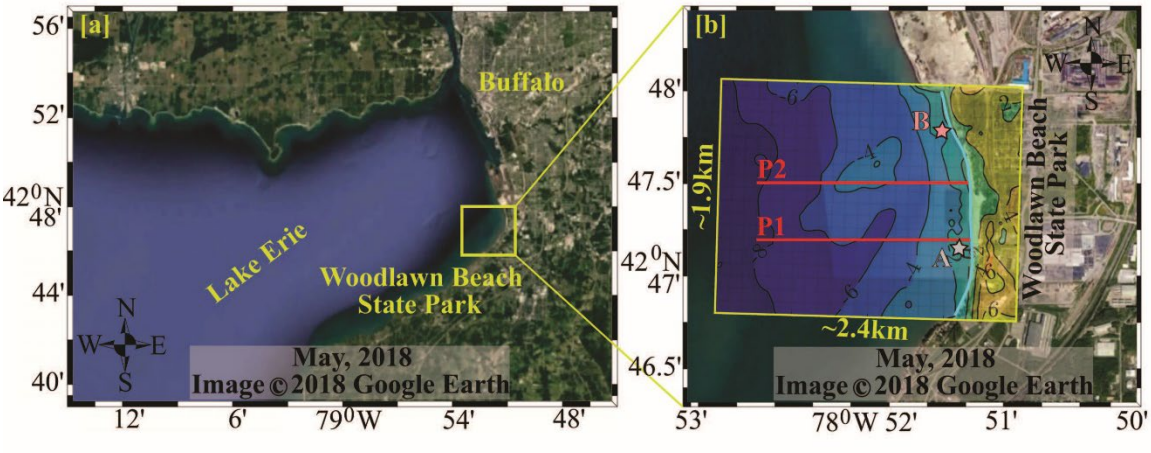

2.1.1 ADCIRC model

ADCIRC is a finite element, time-dependent, long wave model that can simulate water level and current over an unstructured gridded domain. It can be applied to varying scales of motion and a broad range of hydrodynamic problems from deep-ocean and lakes to flows in inlets, floodplains, and waterways. The use of an unstructured grid enables the use of finer grids where bathymetry is complex or in areas of interest. This leads to minimizing both local and global errors. In ADCIRC, elevations are obtained by solving the depth-integrated continuity equation in the Generalized Wave-Continuity Equation (GWCE) form. Velocities are computed from the solutions of the momentum equations which include all nonlinear terms (Luettich *et al.*, 1992; Luettich and Westerink, 2004; Westerink *et al.*, 2008). The model can run with either Cartesian or spherical coordinates. The model forcing mechanisms includes tide, wind, and pressure as well as radiation stress. In the coupled ADCIRC+SWAN model, the radiation stress forcing is provided to the ADCIRC model by the spectral wave model, SWAN. This is particularly important for the surf zone where wave setup, resulting from wave breaking, can be large.

2.1.2 SWAN Model

The SWAN model is a third-generation wave model, simulating random waves in coastal regions and inland waters (Booij et al., 1999). It is spectral in frequencies and directions and includes important physical processes such as wave generation, shoaling, refraction, transmission, reflection, diffraction, breaking, three- and four-wave nonlinear interactions, white-capping, and effects of bottom friction. The SWAN modeling can be done on a regular, curvilinear, or unstructured grid in a cartesian or

spherical coordinate system. The unstructured grid allows for a higher resolution where it is needed. The model output includes one- and two-dimensional wave spectra, wave height, period, direction, directional spreading, wave forces, near-bed orbital velocities, and radiation stress. The spectral wave field is predicted by solving the wave-action equation. The spectral density is computed at the vertices of an unstructured triangular mesh and physical processes are represented at scales of wavelengths.

2.1.3 Lake-Wide Hydrodynamic Model Setup

Figure 7 shows the bathymetry of Lake Erie, as well as the water-level stations, and wave buoys. The depth is relative to 174.0 m (NAVD88), which corresponds to the long-term average lake level. The main driving forces of water-level variations in the Great Lakes are wind and pressure fields as tides are very small (Farhadzadeh and Gangai 2017). Hence, the use of the most accurate wind and pressure fields is critical for an accurate prediction of the water levels and waves in Lake Erie. In this study, the wind data are obtained from the NOAA/GLERL Great Lakes Coastal Forecasting System (GLCFS), which has a grid resolution of 2 km × 2 km and covers the entire lake area. The pressure fields are obtained from Climate Forecast System Reanalysis (CFSR) developed by the National Center for Atmospheric Research (NCAR) with 0.5 global geographical resolution at 1-hour intervals provided on a Gaussian grid (Saha *et al.* 2010, 2011). To account for the land use and modify the wind field accordingly, the surface canopy coefficient is also implemented in the lake-wide hydrodynamic model depending on National Land Cover Database (Wickham *et al.* 2014). In addition to the wind and pressure fields, the water surface elevations at the Detroit and Niagara Rivers, *i.e.*, Fort Wayne and American Falls stations (Figure 2) are provided to the model as boundary conditions.

2.1.3.1 Wind and Pressure Data

Hourly wind data were collected from the NOAA GLCFS Great Lakes Coastal Forecasting System (NOAA/GLERL GLCFS). Hourly pressure data were obtained from The National Centers for Environmental Prediction (NCEP) Climate Forecast System Reanalysis (CFSR). The NOAA/ GLERL GLCFS wind data and CFSR pressure data were refined to computational grid nodes of the coupled ADCIRC+SWAN model using the natural neighboring method.

Figure 7. Lake Erie Bathymetry and Locations of Water-Level Gauges and Wave Buoys

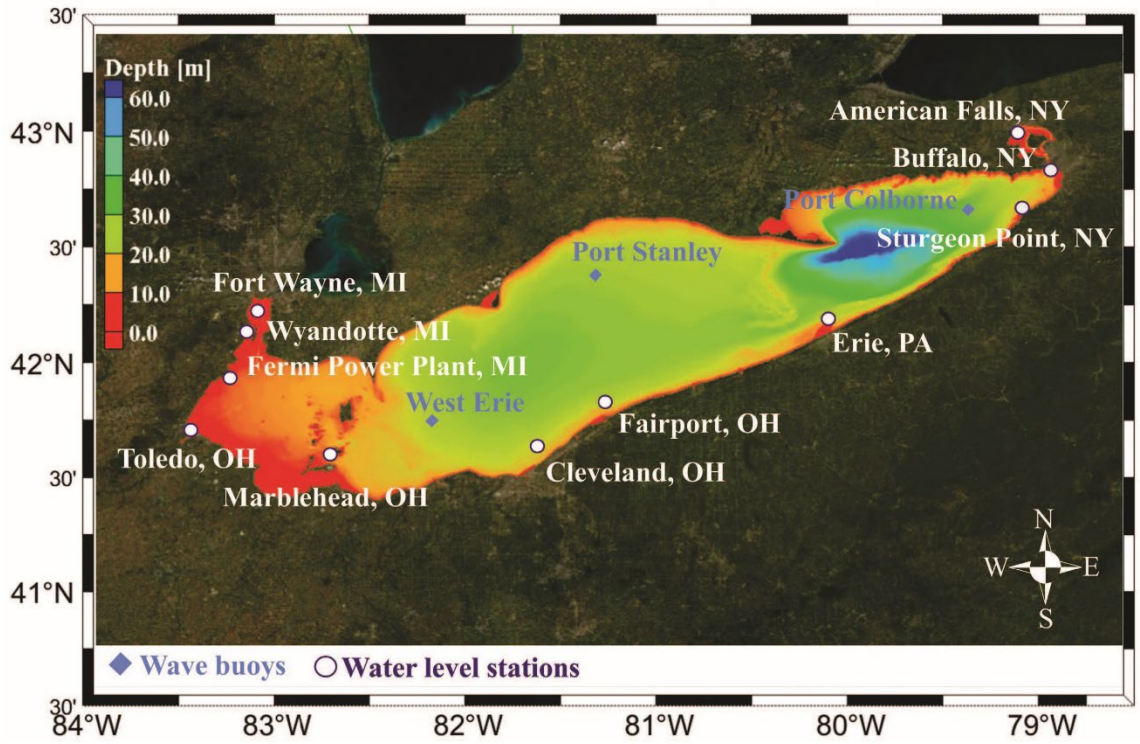

Wind and Pressure Calibration/Validation

Figures 8 and 9 show the comparisons of the model input and measured wind speed and direction, respectively, for the storm event of October 15, 2002 as an example. Figure 10 shows the atmospheric pressure data comparisons for the same period. The CFSR data were calibrated to be consistent with the measured data. The calibrated data are also shown in Figures 8–10, which demonstrate a good fit with the data.

Figure 8. Wind Speed Comparisons for the October 15, 2012, Storm

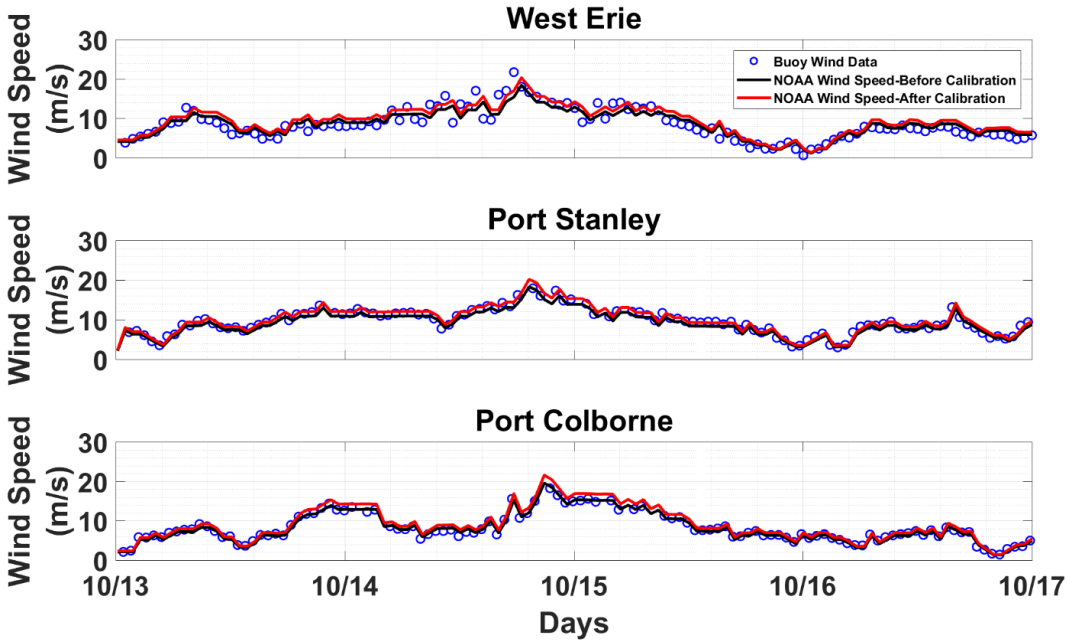

Figure 9. Wind Direction Comparisons for the October 15, 2012, Storm

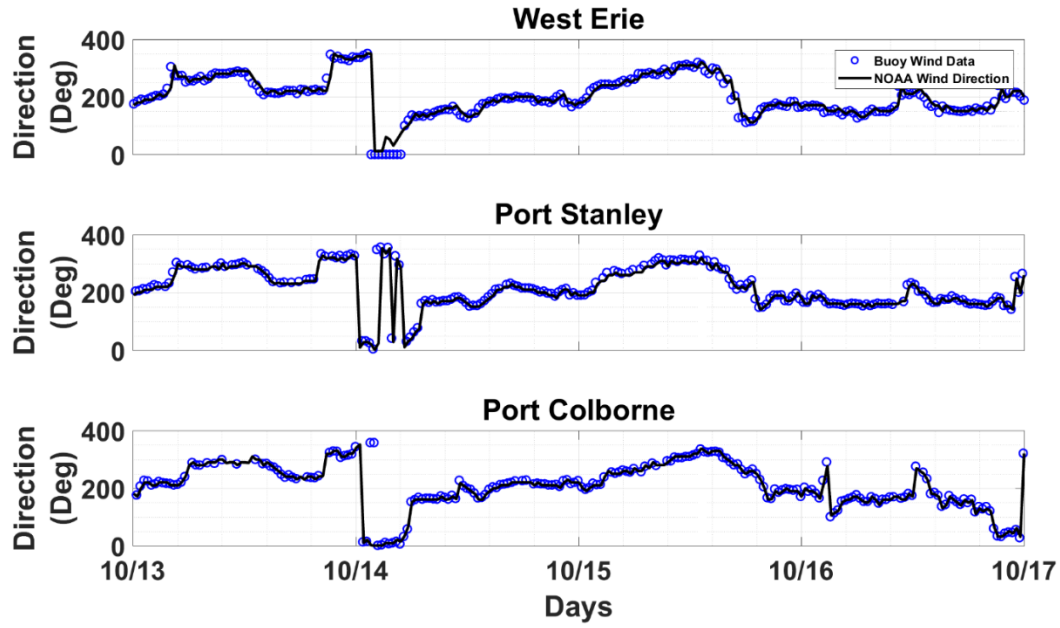

Figure 10. Atmospheric Pressure Comparisons for the October 15, 2012, Storm

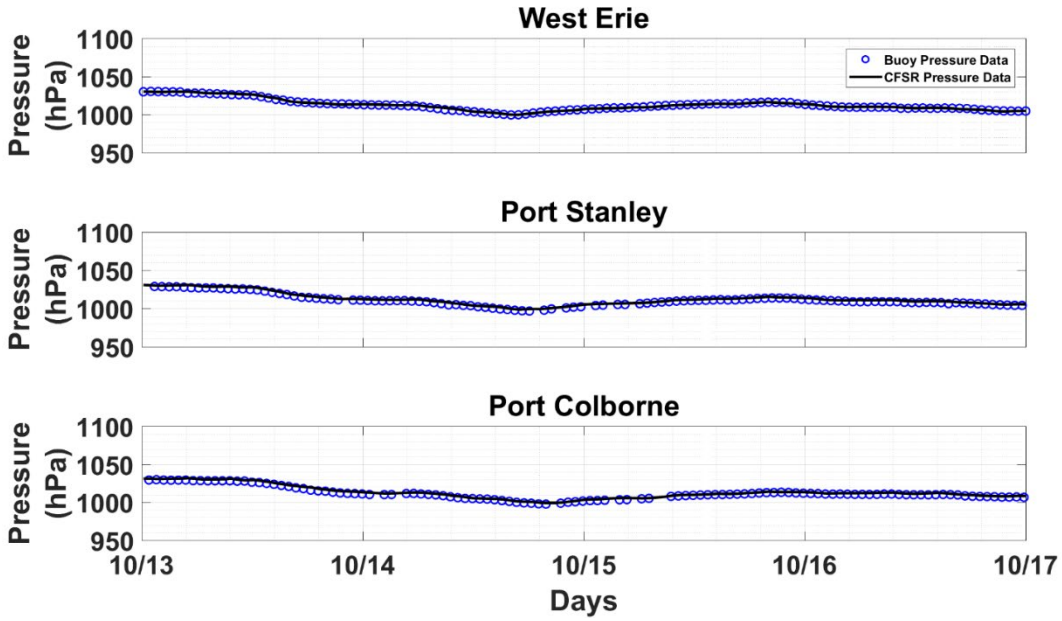

Validation of Surge and Wave Height

Figures 11-14 show comparisons of the ADCIRC+SWAN model results for a period of six months in 2001, as an example.

Figure 11. Comparison of Simulated and Measured Storm Surge

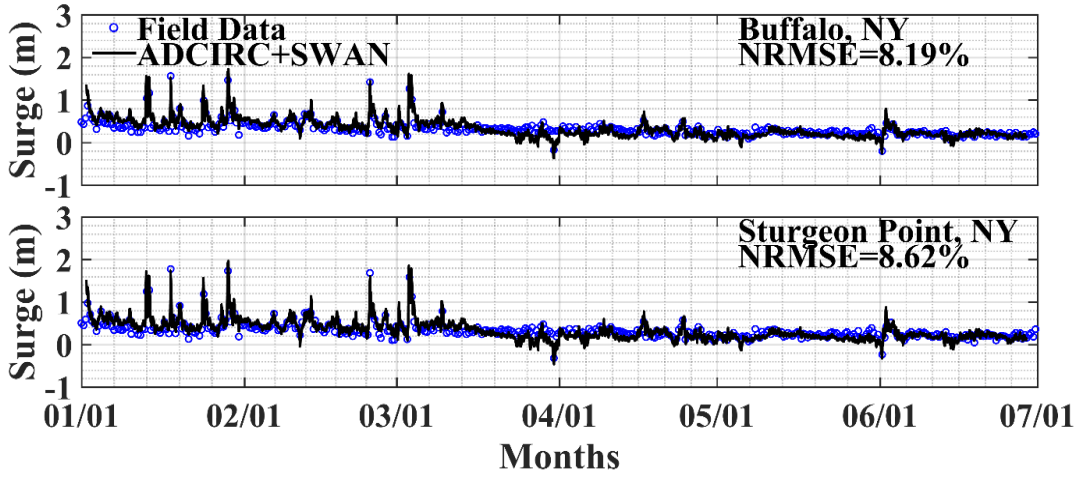

Figure 12. Comparison of Simulated and Measured Significant Wave Height

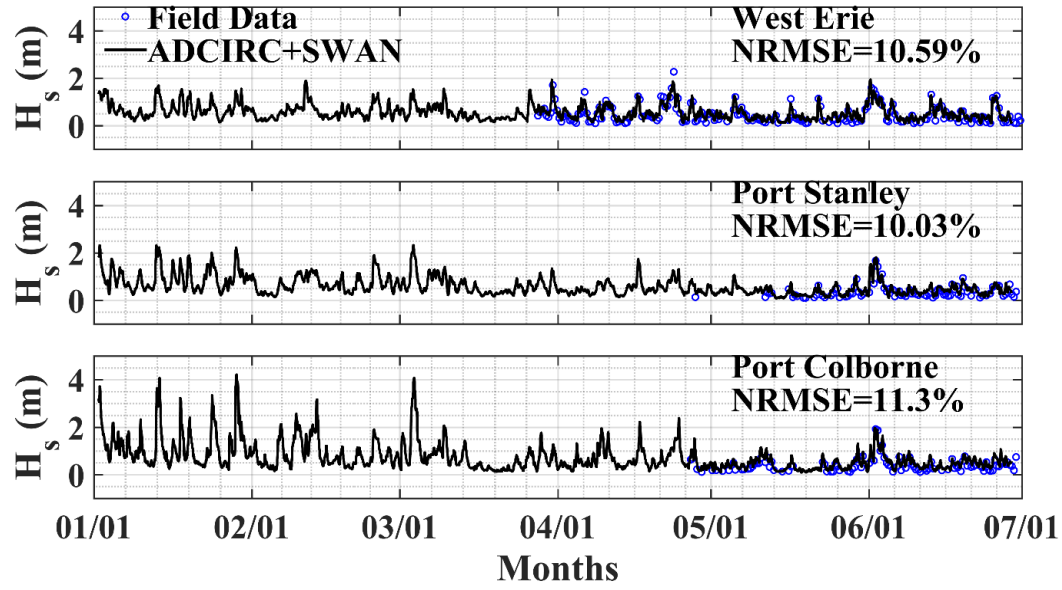

Figure 13. Comparison of Simulated and Measured Significant Peak Wave Period

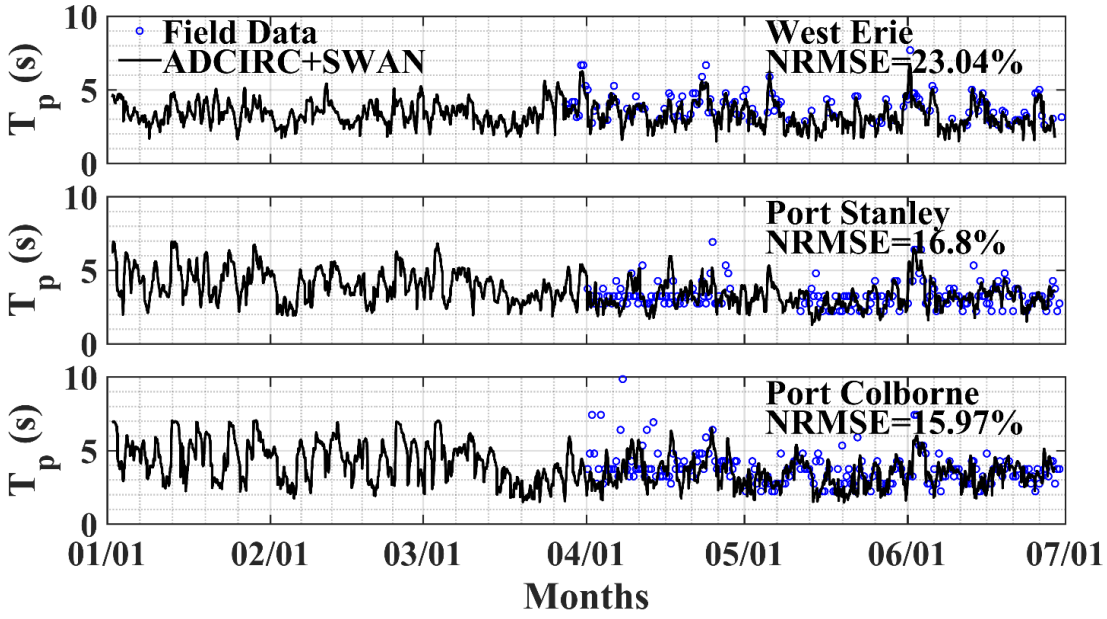

Figure 14. Comparison of Simulated and Measured Wave Direction

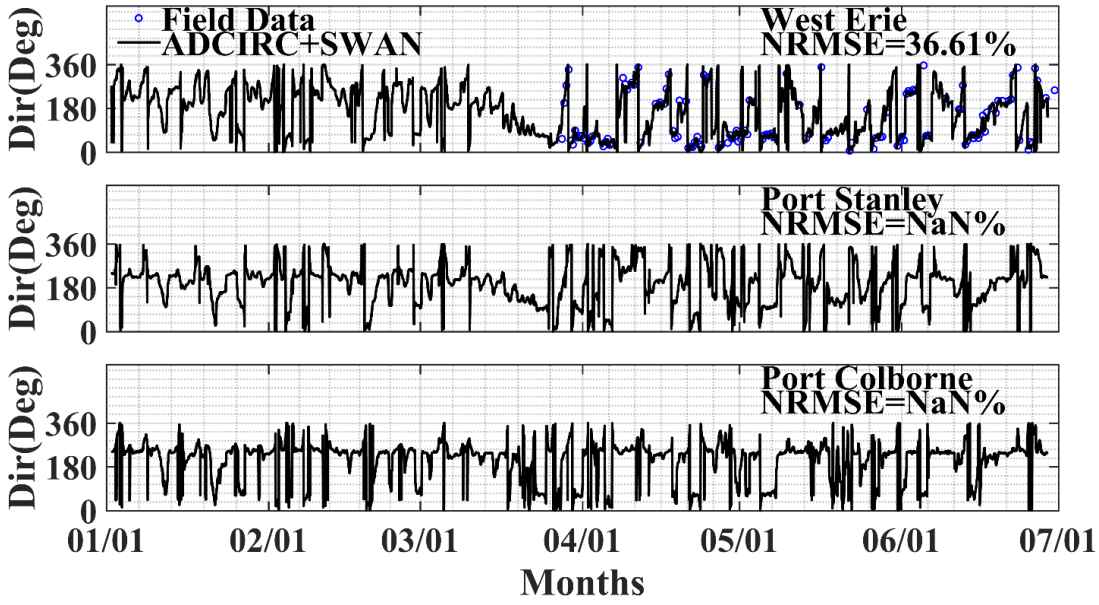

2.2 Nearshore Morphodynamics

The water levels and waves generated by the coupled ADCIRC+SWAN models are used as input offshore boundary conditions for the morphodynamics models, quantifying the morphological changes of the nearshore bathymetry on eastern Lake Erie during 2012. In the following subsections, descriptions are provided for the models, study area, grid sensitivity, and the model setup.

2.2.1 XBeach model

XBeach is a process-based numerical model for simulating the morphodynamic processes of sandy coasts (Roelvink *et al.,* 2009, 2010). The model simulates hydrodynamic processes of short wave transformation, including refraction, shoaling and breaking, long wave (infragravity wave) generation, propagation and dissipation, wave-induced setup and unsteady currents, as well as overwash and inundation (Sallenger, 2000). The morphodynamic processes include, among others, bedload and suspended sediment transport, dune erosion, and breaching. The model has been validated extensively using analytical, laboratory, and field data.

The wave action equation is solved for the wave height variations on the scale of wave groups. It employs a dissipation model with wave groups and a roller model accounting for momentum at the water surface once waves break. The forcing applied on the water column through the radiation stress gradients can

generate low-frequency harmonics such as infragravity waves as well as unsteady currents. These processes are solved in XBeach using the nonlinear shallow water equations. Thus, wave-induced currents such as longshore current, rip currents and undertow can be simulated by the model.

The sediment transport formulation is based on the depth-averaged advection-diffusion equation (Galappatti and Vreugdenhil, 1985) to calculate sediment concentration in the water column, using a source-sink term, depending on the equilibrium suspended sediment and bed load concentrations. The sediment is assumed to be mobilized or deposited depending on the comparison of the actual sediment concentration with the equilibrium sediment concentration. If the actual sediment concentration is less than the equilibrium sediment concentration, the sediment will be transported. Otherwise, it is considered to be deposited. The bottom elevation is updated based on the gradient in sediment transport formulation.

2.2.2 CSHORE model

The CSHORE model, which is currently used for FEMA flood mapping studies, among other coastal-related applications, is a process-based nearshore morphodynamic model. The current version of CSHORE includes a combined wave and current model based on time-averaged continuity, momentum, wave action, and roller energy equations; a sediment transport model for bed and suspended load coupled with the continuity equation of bottom sediment; a permeable layer model for porous flow; and a probabilistic swash model on impermeable (fine sand) and permeable (gravel and stone) bottoms (Johnson *et al.*, 2012; Kobayashi and Farhadzadeh, 2008).

CSHORE assumes unidirectional irregular waves and alongshore uniformity along each cross-shore line. The hydrodynamic model in the CSHORE predicts the mean and standard deviation of the free surface elevation above the still water level and depth-averaged, cross-shore and longshore velocities. The equivalency of the time and probabilistic averaging is assumed to reduce computation time considerably. In the wet zone, the probability distributions of the free surface and velocity are assumed to be Gaussian. In the wet and dry zone, the wave angle was assumed to be small and remain the same as the wave angle at the still water shoreline. The probability distribution of water depth in the swash zone is assumed to be exponential. The time-averaged continuity and momentum equations are used together with the wet probability for the presence of water (Kobayashi *et al*. 2010).

The sediment components of CSHORE are as follows: a cohesionless sediment transport model for suspended load and bedload, a continuity equation of sand bottom for beach profile evolution prediction, and a soft cliff erosion model for downward erosion of consolidated sediment composed of both cohesive and cohesionless materials (Kobayashi and Weitzner 2015; Kobayashi and Zhu 2020).

2.2.3 Morphodynamic Model Setup

The model validation is carried out by the "cross-calibration" procedure through which input parameters of XBeach were calibrated until it produced nearly identical results as CSHORE, which has already been validated for Great Lakes shore erosion and flooding applications as discussed earlier. This procedure was followed due to the lack of beach survey data for the study area. The simulations were done using the actual water level and wave conditions for the two selected transects shown in Figure 6[b] (P1 and P2). The cross-calibrated model parameters are summarized in Table 1.

The sensitivity of the cross-calibrated 1D XBeach and CSHORE models to the grid resolution was evaluated for selecting the optimal grid size. Three different grid sizes: dx = 5 m, 10 m, and 20 m, were considered. The results show that the two models are relatively insensitive to the grid resolution. Table 2 summarizes the comparisons of the eroded area above mean sea level for pairs of grid sizes.

Although XBeach is more sensitive to the grid resolution than CSHORE, refining the grid size by four times, from 20 m to 5 m, results in only an 8.6% difference in the computed eroded area. Hence, to reduce the computation cost, dx = 10 m was selected for the 2D morphodynamics modeling.

Table 1. Parameters of the Cross-Calibrated XBeach and CSHORE Morphodynamic Models

XBeach			CSHORE		
Parameter	Value	Unit	Parameter	Value	Unit
dx	10.00	m	dxc	10.00	m
gamma	0.78	-	gamma	0.65	-
wetslp	0.10	-	effb	0.15	-
dryslp	1.00	-	D50	0.11	mm
hswitch+	0.10	m	tanphi	0.63	-
D50	0.11	mm			
facua	0.01	-			
reposeangle	32.00	deg			

Table 2. Grid Sensitivity Analysis of XBeach and CSHORE Morphodynamics Models

Comparison	Difference [%]	
	XBeach	CSHORE
5 m - 10 m	5.0	0.3
5 m - 20 m	8.6	3.3
10 m - 20 m	3.6	3.6

2.3 River Modeling

The focus of the river modeling in this project was to evaluate the combined impacts of upstream flows and downstream water levels on flooding risk in the Buffalo River. A typical concept used in evaluating flood risk, as used by FEMA, is that of the 100-year floodplain, which is calculated using a hydrological model with a fixed downstream water depth. Those models solve the backwater curve and often use the critical flow depth for the downstream boundary condition. In the present study the downstream water surface elevation is that of the lake and impacts of seiching on the water surface are included in the calculations. The main goal of this part of the study was to evaluate changes in floodplain calculations as a result of including the variable downstream water surface. This analysis is necessarily stochastic in nature, and a copula-based approach is used, as previously introduced.

2.3.1 Hydrodynamic and Hydrological Modeling

Preliminary modeling was performed using the Environmental Fluid Dynamics Code (EFDC), which is a three-dimensional, time-dependent model that solves the continuity, momentum, and energy governing equations to predict water flow and temperature distributions, and turbulence and mixing characteristics. EFDC is an EPA-supported, public domain, open-source surface water modeling system. Cartesian or curvilinear, orthogonal coordinates can be used for horizontal discretization. Vertical discretization is accomplished using generalized vertical coordinates, an approach that combines sigma coordinates with "*z*" coordinates and allows better representation of systems in which there are significant variations in depth. The upstream flow conditions are provided by three United States Geological Survey (USGS) tributary gauges. Downstream boundary conditions are set in the lake nearshore region not far from the discharge point of the river and are specified as time-varying water level obtained either directly from data or from the lake modeling results. EFDC also includes modules for sediment and contaminant fate and transport modeling, although these modules were not used in the present study. EFDC was successfully applied as part of the Buffalo River Feasibility Study (Environ 2011), which provided a significant head start for the present study to understanding hydrodynamic conditions in the river.

It was found that the simpler, one-dimensional hydrologic model HEC-RAS was more useful in evaluating floodplains, as it provided longitudinally varying (along the river path) water surface values that could be directly compared with topographic features (ground elevations) along the river. This model was also used to calculate the hydraulic performance graphs (HPGs). An already existing HEC-RAS model of the Buffalo River was identified. It was developed by LimnoTech (Environ Intl. Corp., 2011) and used to simulate river hydraulics and flooding. The model was originally used to conduct hydraulic investigations including flood evaluations and remedial options, in support of the Great Lakes National Program Office (GLNPO) Legacy Act process (US EPA, 2020). For further information on calibration of this model, see Environ Intl. Corp. (2011).

2.3.1.1 Model Calibration and Validation

The river EFDC model was already validated as part of the Feasibility Study (Environ, 2011). Model comparisons were made with previous studies (e.g., Gailani et al., 2006). Limited velocity data also were available, both published and unpublished (J. Singer, Buffalo State College, pers. comm.), and these were used for model comparisons as well. The results were deemed to be reasonable in comparison with limited data for water velocity and elevation. Note that the upstream flows were obtained from USGS gauges on three tributaries that join to form the Buffalo River AOC (Figure 15). Primarily, the HEC-RAS model was calibrated with results from the EFDC model. Using two different modeling approaches is a powerful validation of the results. For the desired HPGs, the primary results desired were the water-level profiles, and as already noted, these were more conveniently calculated (shorter set up and run times) with the HEC-RAS model.

Figure 15. Buffalo River Location with Locations of Water Level (#1) and Upstream Flow Gauges (#2-4) on Three Tributaries

Reproduced from Saharia et al. (2021)

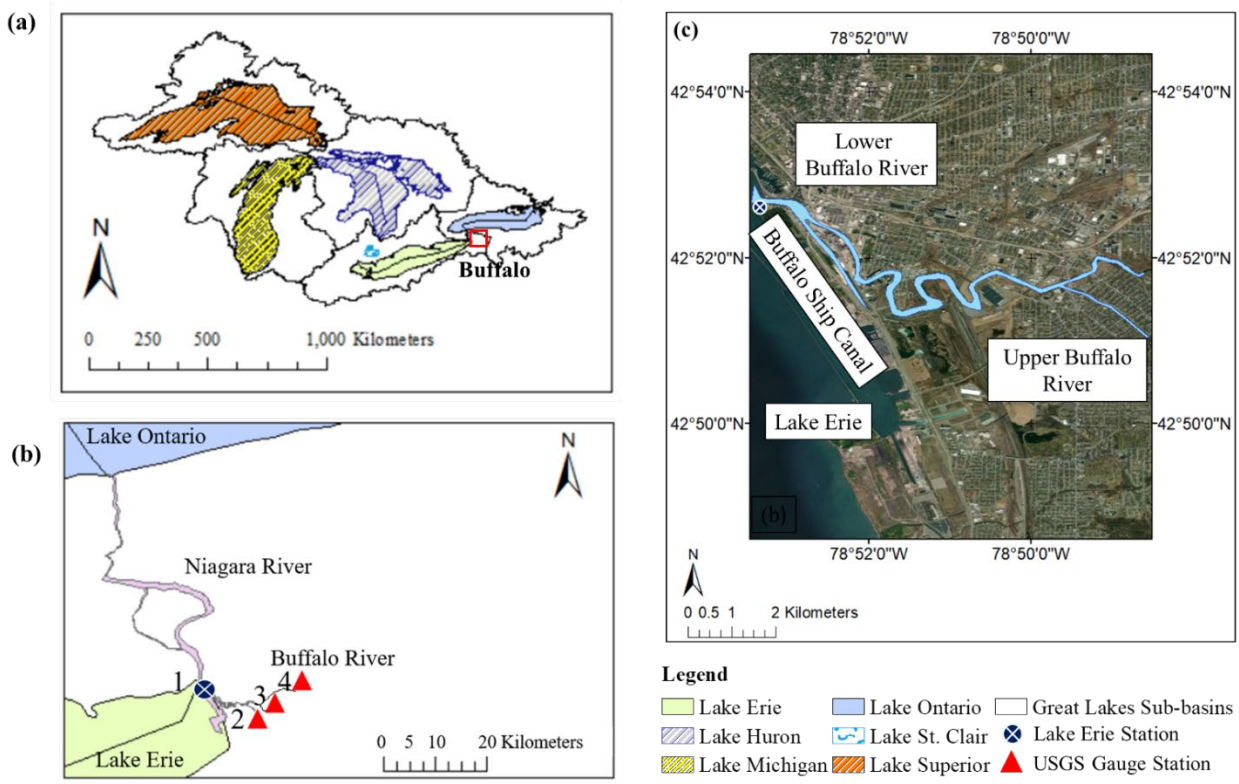

2.4 Statistical Calculations

The highest accuracy for the constructed copula functions can be obtained by selecting marginal and joint distributions that provide the best fits to the data. Candidate marginal distributions considered were the Normal (NORM), two-parameter lognormal (LN), Generalized Extreme Value (GEV), Frechet or Extreme Value 2 (EV2), Gamma or Pearson type 3 (P3), and the log-Pearson type 3 (LP3), which are commonly used to describe statistical variations of hydrological parameters (Laio et al., 2009). The candidate bivariate copula functions commonly used for compound flooding include Clayton copula, Gumbel copula, Frank copula, Joe copula, Gaussian copula, and Student's t copula (Genest and Rivest, 1993; Huard et al., 2006; Lian et al., 2013; Xu et al., 2019). The model selection criteria are based on the Akaike information criterion (AIC), corrected Akaike information criterion (AICc), Bayesian information

criterion (BIC), log-likelihood (logLik) and the Anderson-Darling criterion (ADC). To select the marginal distribution, AIC, AICc, and ADC are used, and for joint distribution logLik, AIC, and BIC are used, based on recommendations from previous studies, which are shown to be suitable for prediction and cross-validation, and allows consistent estimation of the underlying data generating process (Laio et al., 2009; Wang et al., 2010; Wang et al., 2018).

The procedures for application of the copula-based analysis are described in Saharia et al. (2021) and summarized here. The methodological framework is shown in Figure 16 (this is Figure 1 in Saharia et al.). Two logical pathways are shown. The "seiche-driven" events are based on the data acquired from frequencies of the lake's seiching modes by Farhadzadeh (2017). From the seiche data, the annual maximum seiche events were selected. The "streamflow-driven" events are based on annual maximum discharge data from USGS stations. Along the left-hand side of Figure 15, calculations start with creating marginal distributions for seiche water levels and river discharges, and then the joint probability of different discharge values, for given water levels, is carried out after considering the non-parametric correlation coefficient to investigate dependency. This scenario is referred to herein as "seiche-driven." The right-hand side follows an alternative approach, in which marginal distributions for annual maximum discharge are first evaluated, and the probability of different downstream water levels is then considered. The joint distribution is carried out similarly for water level and annual maximum discharge values after considering the non-parametric correlation coefficient. This scenario is referred to as "streamflow-driven."

The non-parametric dependence measurement (i.e., Kendall's tau) is used to investigate the functional association among the variables under consideration. In "seiche-driven" and "streamflow-driven" scenarios the calculated Kendall's tau values were 0.13 and 0.22, respectively, representing significance at a confidence level of 95%. These results indicated there is a significant, but weak correlation between the two variables for both scenarios and therefore a bivariate joint probability distribution based on copula functions was conducted. In either approach, copula analysis was carried out by constructing marginal and joint probability distribution functions and fitting the data to select the best models (see below). The first step to create the marginal distributions for the water level and river discharge are described below. The copula functions were created from the marginal distributions, based on selecting the best fit distributions for the data sets used in this study.

The preferred approach for either the "seiche-driven" or "streamflow-driven" scenarios can be selected based on the flooding severity depending on the upstream and downstream boundary conditions of the river. In general, it is important to consider both the streamflow and seiche-driven scenarios, as either can lead to significant flooding. Therefore, the copula analysis along with the probability framework was carried out for both scenarios. The copula joint distribution coupled with the probability-based framework is useful to quantify the conditional probability of compounding boundary conditions. The HEC-RAS model was then used to predict inundation areas that resulted from different combinations of upstream and downstream boundary conditions (i.e., presenting flood risk). The HEC-RAS model results were also used to create the hydraulic performance graph (HPG), which can be used to conveniently look up water levels under each set of boundary conditions.

Data used for the statistical calculations are summarized in Table 3.

Figure 16. Workflow Schematic for Copula Analysis (Taken from Saharia et al. 2021)

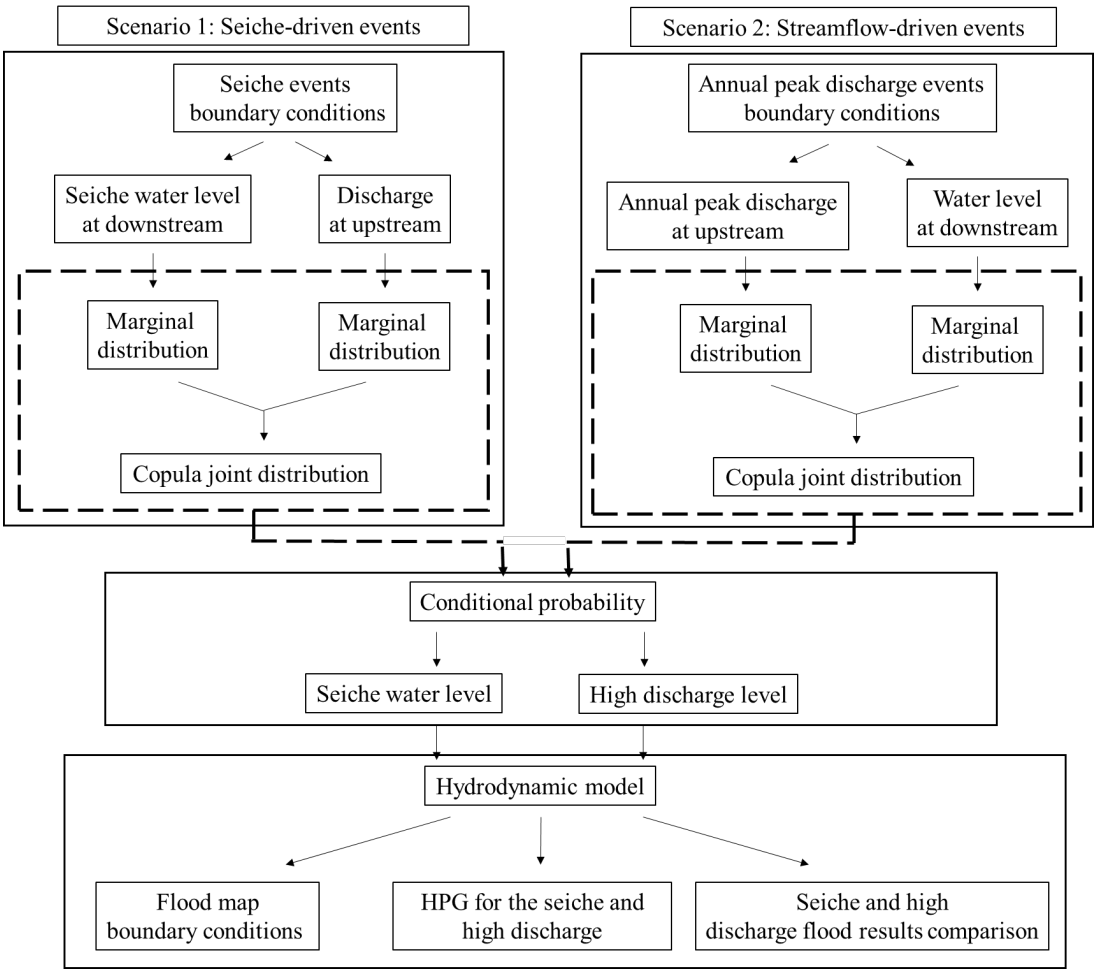

Table 3. Overview of the Water Level and Discharge Data for the Buffalo River

Scenario	Data type	Station no.	Data sources	Duration
Seiche-driven	Water level	9063020	NOAA	1975-2017
	Discharge	04215500	USGS	1975-2017
		04214500		
		04215000		
Streamflow-driven	Water level	04215900	USGS	1960 -2019
	Discharge	04215500	USGS	1960 -2019
		04214500		
		04215000		

3 Results

3.1 Lake and Coastal Morphodynamic Calculations

To evaluate the performance of the lake-wide hydrodynamic model, the simulated water levels were compared with the measurements at the water-level stations, operated by NOAA and Canada's Department of Fisheries and Oceans (Figure 2). The normalized root mean square error (NRMSE) is used to quantify the accuracy of the ADCIRC+SWAN model results. The NRMSE of the surge levels calculated based on the long-term average lake level (Figure 17) ranges between 3.4% and 7.6%. The largest differences are observed in the southern part of the lake, Fairport, OH and Cleveland, OH. Although the error values are relatively high at these stations, the range of water-level variations is small and perhaps within the error range.

In addition to the surge comparisons, the coupled model is evaluated for the prediction of the wave field. Figure 18 shows comparisons of the simulated and measured significant wave height (H_s), peak wave period (T_p) and mean wave direction (Dir^0) for the three wave buoys (Figure 2) operated by the National Data Buoy Center (NDBC). Although the model predicts the significant wave height within an approximately 3–5% error margin, the error increases to ~5–14% for the peak wave period. The simulated and measured mean wave directions are in agreement for the West Erie wave buoy which is the only buoy with these data. Overall, it is concluded that the coupled ADCIRC+SWAN model performed well in predicting the water level and wave fields for 2012.

Figure 17. Comparison of Simulated and Measured Surge Levels at Nine NOAA Stations around Lake Erie

Dashed line represents perfect agreement.

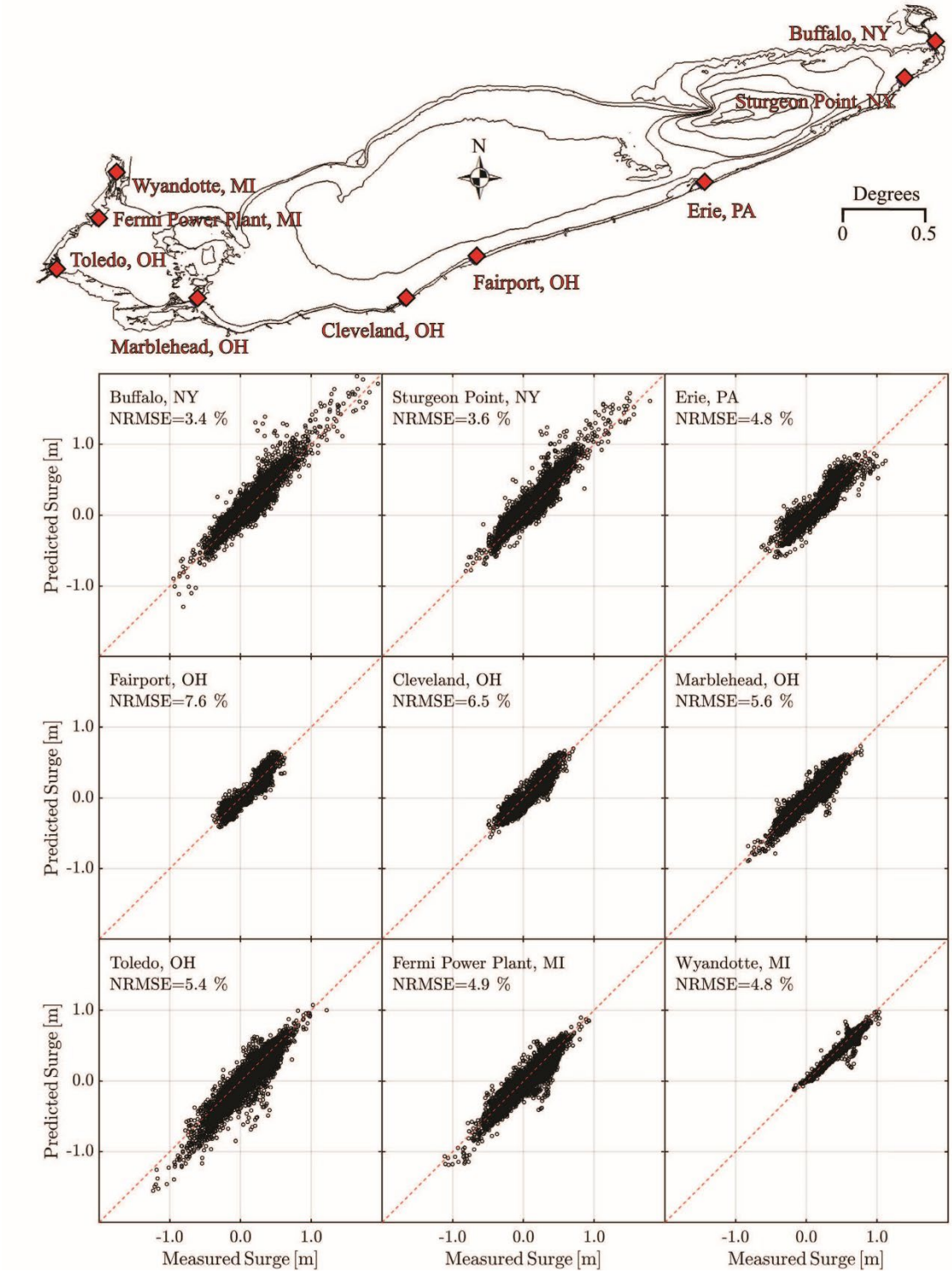

Figure 18. Comparisons of Predicted and Measured

Dashed line represents perfect agreement.[a] Significant Wave Height; [b] Peak Wave Period; [c] Mean Wave Direction for West Erie Wave Buoy.

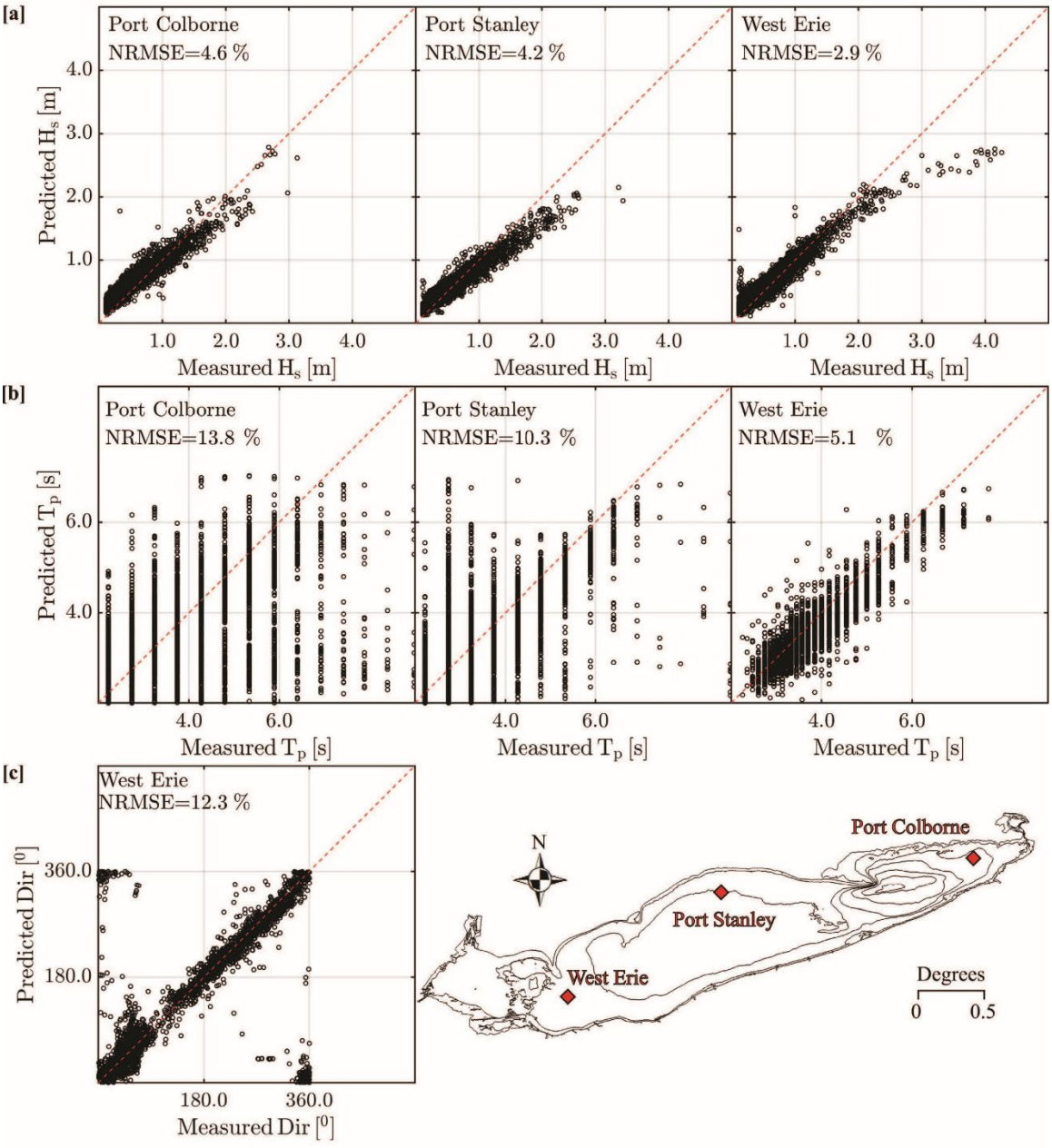

Figure 19 shows results from the calibrated morphodynamics models for the two selected transects shown in Figure 6[b] (P1 and P2). The hourly time series of the wave and water level, obtained from the ADCIRC+SWAN model, are applied as the offshore flow boundary condition for the transects P1 and P2. The comparisons of the initial (z_0) and final (z_f) bed profiles show that erosion occurred mostly above the mean sea level (MSL) and the eroded material is deposited offshore of the shoreline where the depth is 1 m - 2 m.

Figure 19. Cross-Calibrated Cross-Shore Profiles for Transects: [a] P1, and [b] P2 Shown in Figure 6

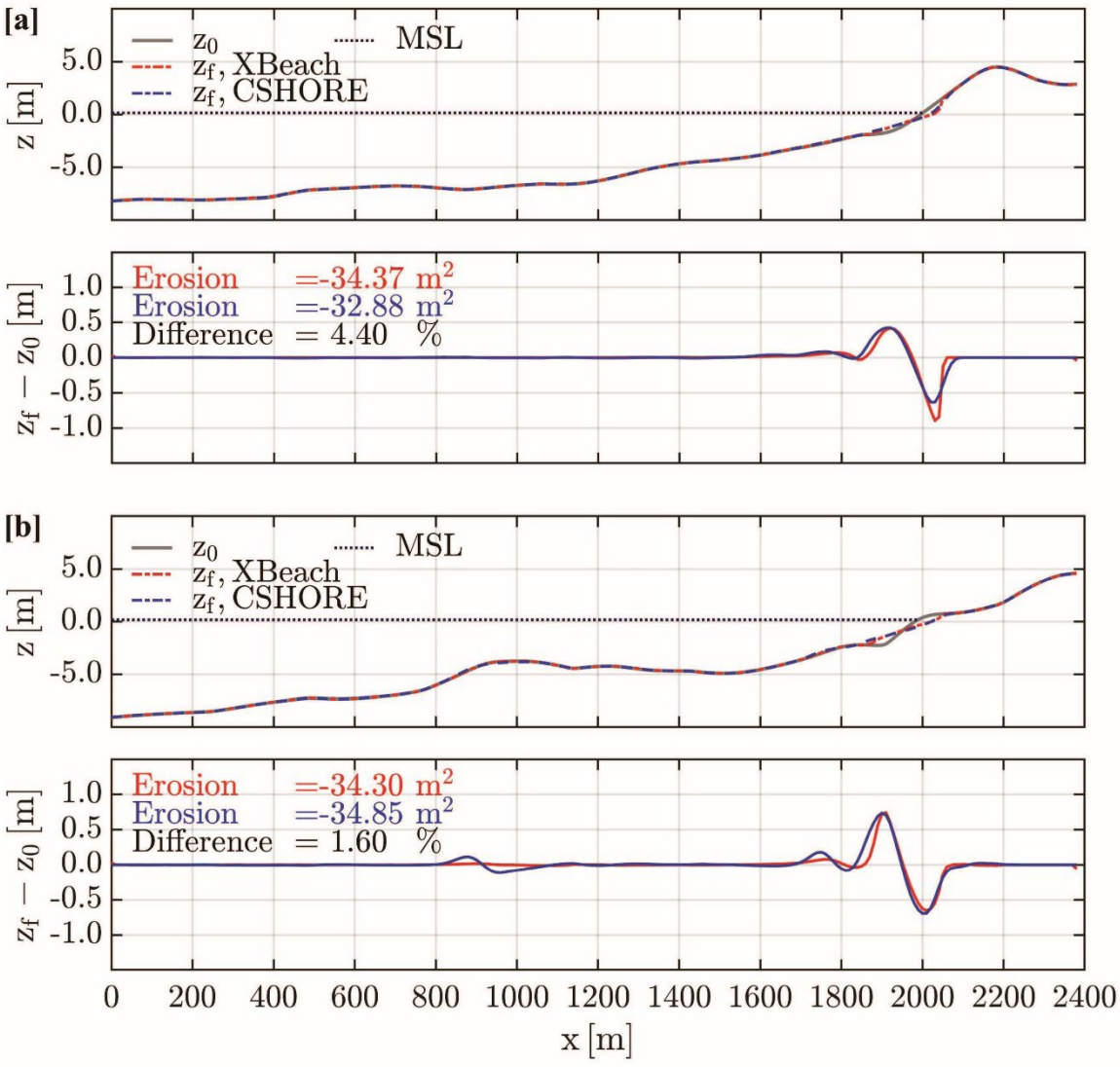

The water-level output from the lake-wide hydrodynamic model at the offshore boundary of the nearshore morphodynamics model is filtered to synthetically create a seiche-free condition. To remove the seiching oscillations, first, the low-frequency oscillations in Lake Erie were identified through a spectral analysis of the hourly water levels. The power spectral density (PSD), $S_{xx}(\tau)$, of a real stationary signal, $x(t)$, is the Fourier transform of its autocorrelation, $R_{xx}(\tau)$.

Equation 1

$$S_{xx}(f) = \int_{-\infty}^{\infty} R_{xx}(\tau) e^{-2\pi i f \tau} d\tau$$

$$R_{xx}(f) = \int_{-\infty}^{\infty} S_{xx}(\tau) e^{-2\pi i f \tau} df$$

The predominant storm-induced seiching motions are considered to have a period larger than 2.5 hr but shorter than two weeks, consistent with previous studies (Farhadzadeh, 2017; Farhadzadeh *et al.*, 2018). Hence, to generate the synthetic seiche-free water levels, the oscillations beyond this range were filtered by applying a band-pass filter. Figure 20 shows the PSD of the measured and computed lake levels for Buffalo, NY and Sturgeon Point, NY stations for 2012. Several distinct peaks can be identified at frequencies of 1.7, 2.6, 4.1 and 5.8 cycles per day (CPD) which are related to the first four seiche modes corresponding to periods of 14.2, 9.2, 5.9, and 4.1 hr (Farhadzadeh, 2017; Platzman and Rao, 1964a; Sogut and Farhadzadeh, 2018). The comparison of the measured and modeled water levels spectra for the two stations (Figure 20) indicates that the lake-wide hydrodynamic model can satisfactorily reproduce the spectra of low-frequency motions where the spikes correspond to the seiche motions.

Figure 20. Power Spectral Density of Measured and Predicted Water Levels for Eastern Lake Erie for Year of 2012. fs1, fs2, fs3 and fs4 Correspond to the First Four Seiche Modes

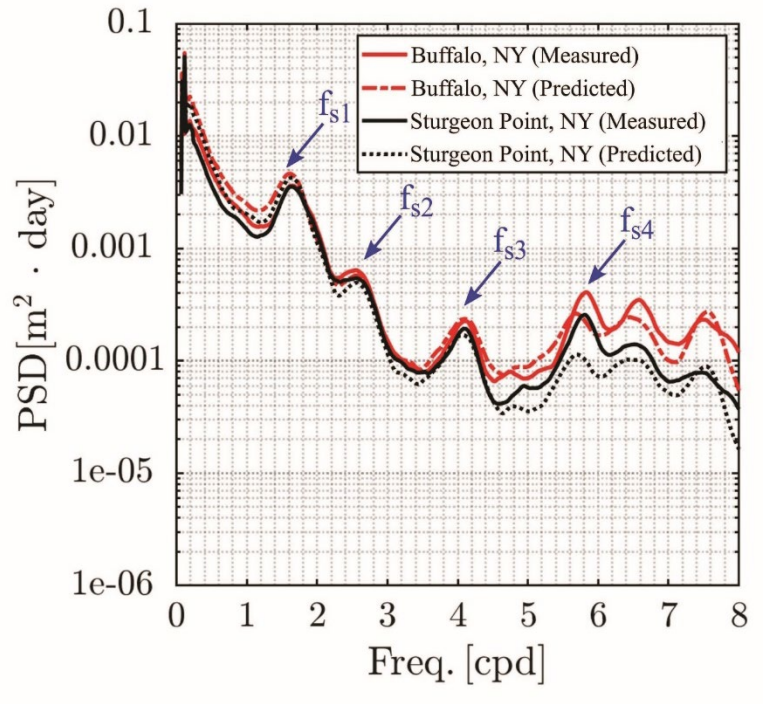

To quantify the contribution of the seiche to the annual beach evolutions in eastern Lake Erie, the 2D XBeach simulations were carried out under the actual (A) and the synthetically created seiche-free (SF) water-level conditions. The wave data, generated by the lake-wide hydrodynamics model, were directly used at the offshore boundary with the two water-level conditions without any modifications, assuming that the effects of the low-frequency lake-level variations on the waves at the offshore boundary are negligible.

Figures 21[a] and 21[b] show the time history of the water level measured at the nearest water-level station to the study area (i.e., Sturgeon Point, NY) during 2012, as well as the simulated water level at the offshore boundary of the XBeach model. The lake-level time series indicates that major storms took place in the winter and fall, during the timespans of January–March, and October–December, while the spring and summer months, *i.e.*, May–September, were relatively calm. The figure also shows that the water level gradually decreased throughout the year by about 0.5 m.

Figure 21. Time Histories

[a] Actual water levels (WL_A) at Sturgeon Point, NY (measurement: black circles and predicted: red solid line); [b] Actual (black solid line) and seiche-free (WL_{SF}: red dashed line) water levels at the offshore boundary of XBeach model in 2012 [c] Comparison of post-storm actual (WL_A) and seiche-free (WL_{SF}) water levels at the offshore boundary of XBeach model in 2012.

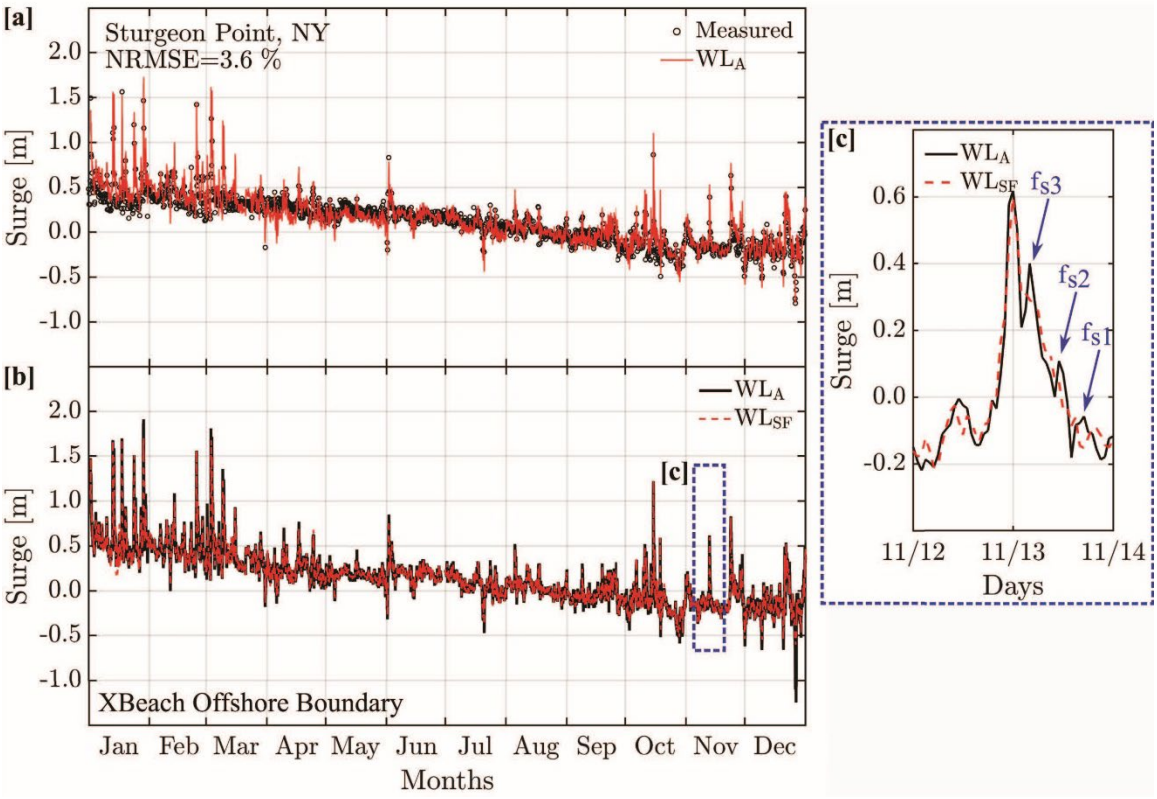

The synthetic seiche-free water-level time series was derived by applying a band-pass filter, in the frequency domain, to the water-level data and eliminating the oscillations corresponding to the first four modes of the seiche. Then, the signal was transformed back to the time domain. The comparison of the actual and seiche-free water levels at the offshore boundary of the model following a major storm in mid-November in 2012 is represented in Figure 21[c]. Note that the filtered oscillations following the peak of the storm correspond to the post-storm seiching motions.

Figure 22 shows plan views of the 2D XBeach model results for the monthly-averaged root mean square wave height (H_{rms}), wave direction (Dir), current velocity ($U=\sqrt{u^2+v^2}$), bed load (q_b) and suspended load (q_s), as well as the bottom variation for each month ($z_{ch} = z_{final} - z_{initial}$) under the actual lake level conditions. The parameters $z_{initial}$ and z_{final} are the bottom elevations at the beginning and end of each

month, respectively. As indicated in the figure, the plots are related to the storm season in 2012. It is expected that seiching motions contribute to the nearshore morphological changes during the storm season. Figure 23 presents the model results for the same quantities under the synthetic seiche-free condition.

Figure 22. Spatial Variations Predicted by XBeach

Actual water-level condition of monthly-averaged root mean square wave height (H_{rms}), wave direction in nautical coordinates (Dir), current velocity (U), bed load (q_b), suspended load (q_s), as well as bed level change (z_{ch}).

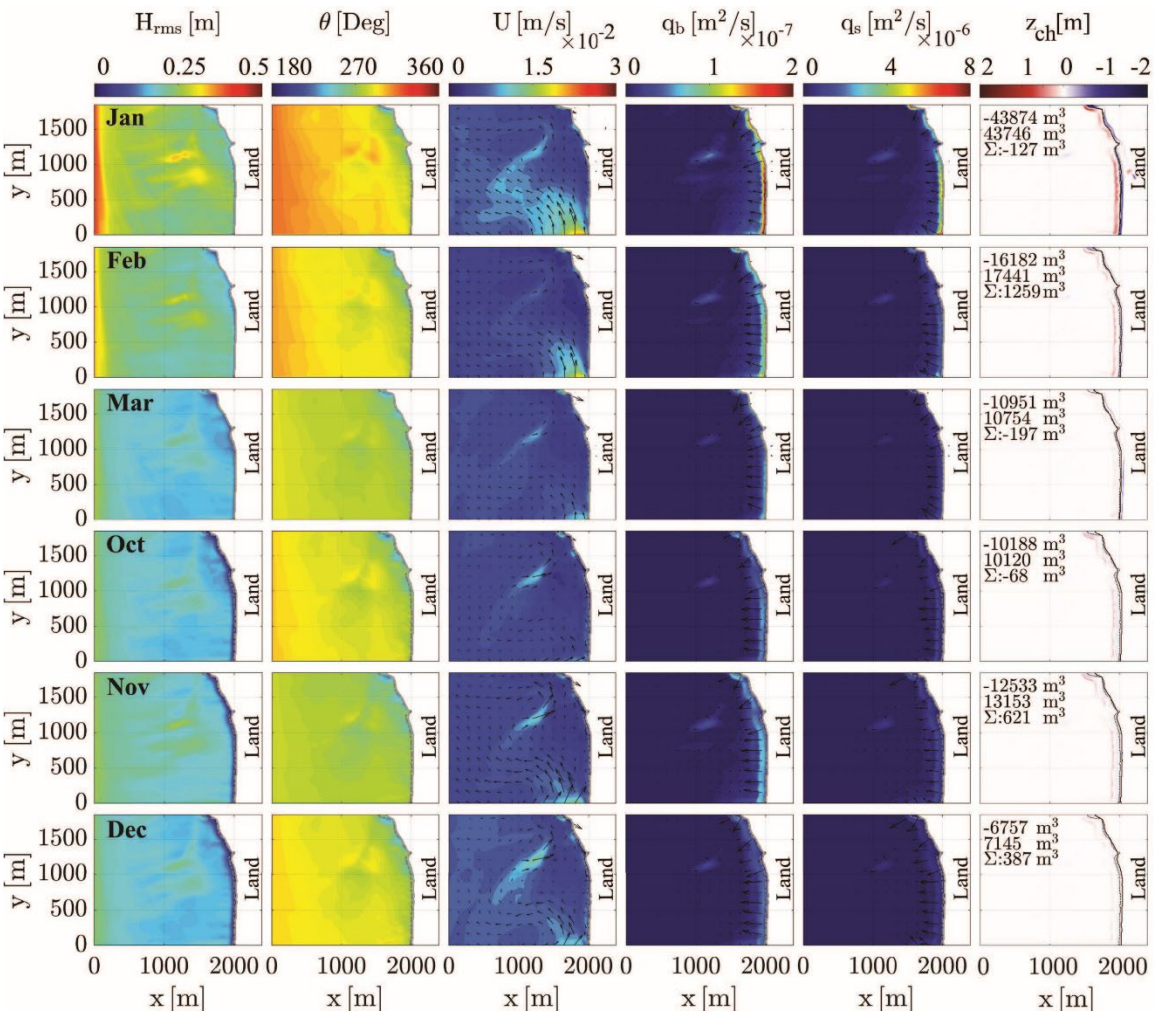

Figure 23. Spatial variations predicted by XBeach

Seiche-free water-level condition of monthly-averaged root mean square wave height (H_{rms}), wave direction in nautical coordinates (Dir), current velocity (U), bed load (q_b), suspended load (q_s), as well as bed level change (z_{ch}).

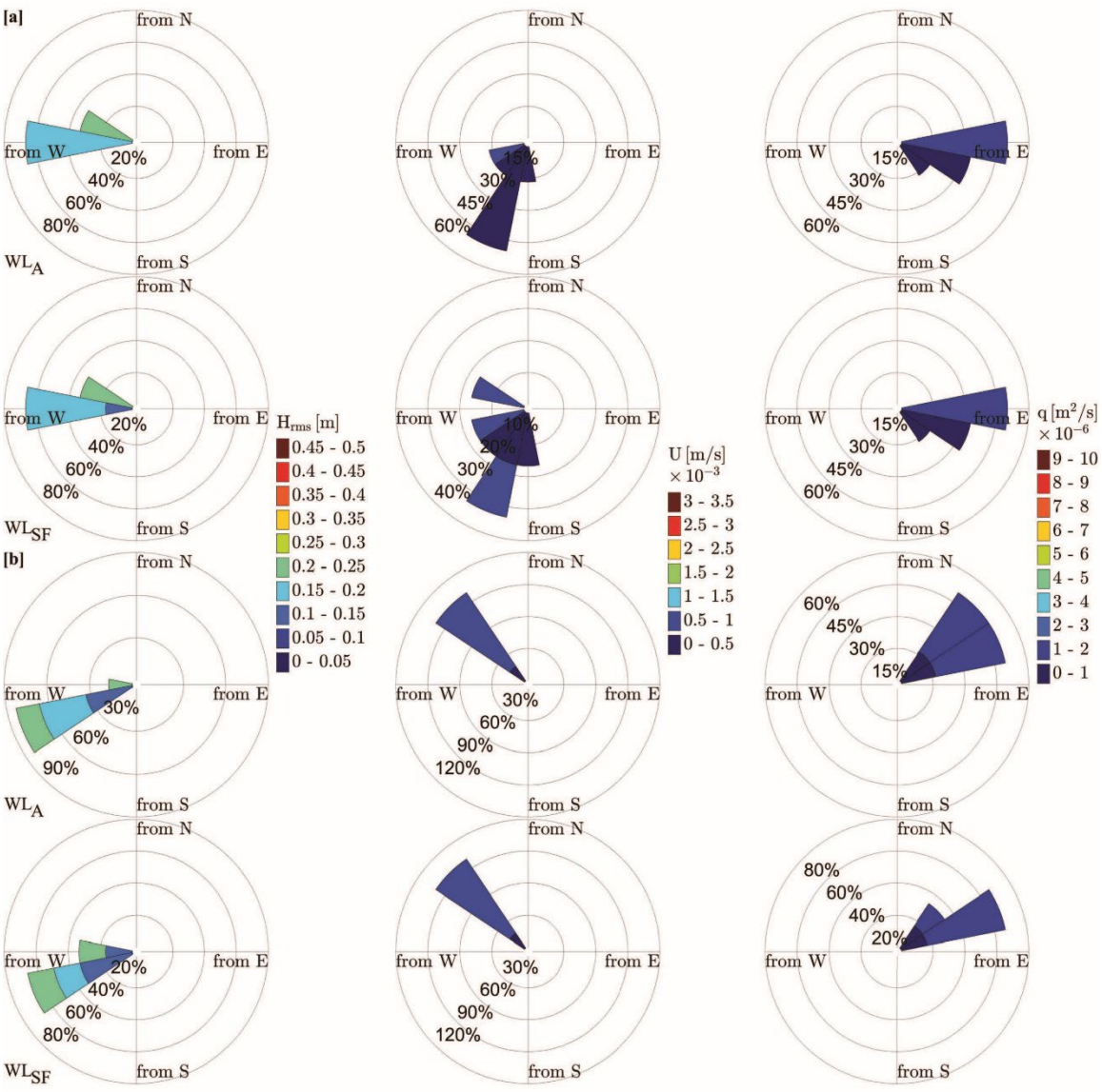

3.2 River (Probabilistic) Calculations

Marginal distribution fitting tests for seiche-driven and streamflow-driven event scenarios were calculated. The best marginal distribution models were selected on the basis of lowest value of AIC, AICc, BIC, and ADC. In the seiche-driven scenario, the Pearson type 3 distribution was found to provide the best fit to the data for the seiche water-level marginal distribution, while

the lognormal distribution provided the best fit for the river discharge distribution. In the streamflow-driven scenario, the lognormal distribution was selected for both the river discharge and downstream water level.

The best joint distribution models were selected using criteria listed by Joe and Kurowicka (2011). In the seiche-driven scenario the Frank copula is found to provide the best fit for annual maximum seiche water level and corresponding river discharge. In the streamflow-driven scenario, the Clayton copula was found to provide the best fit for annual maximum river discharges and corresponding downstream water levels.

A comparison of empirical and theoretical frequencies is shown in Figure 24 for both scenarios. It can be seen that there is a reasonable fit, with root mean square error (RMSE) values of 0.0647 and 0.0604 for the seiche-driven and streamflow-driven cases, respectively. The joint cumulative distributions are shown in Figure 25, using the Frank copula for the seiche-driven scenario (Figure 25[a]) and the Clayton copula for the streamflow-driven scenario (Figure 25[b]). From Figure 25[a], it can be seen that most of the seiche water-level data are in the range of 1.5 m to 2.5 m.

Figure 24. Empirical Frequency versus Theoretical Frequency

[a] Seiche-driven events based on Frank copula; and [b] streamflow-driven events based on Clayton copula.

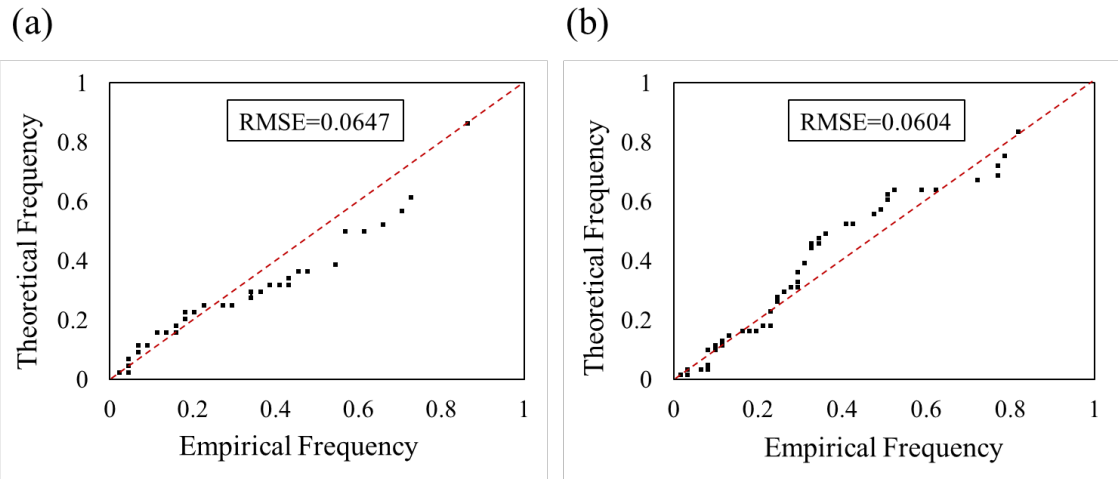

Figure 25. Cumulative Distribution

[a] Seiche water level and river discharge for seiche-driven events; and [b] river discharge and downstream water level for streamflow-driven events.

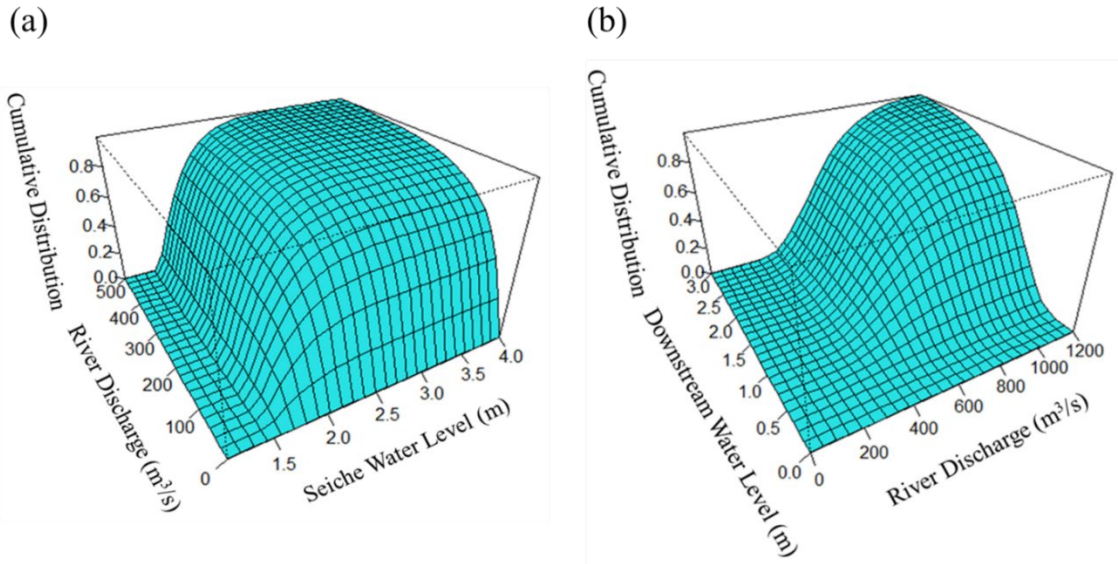

Figure 26 shows the probability of seiche water level and river discharge interval occurring jointly. The seiche water-level intervals are from 1.5 m to 4 m, where the lower limit is chosen based on results in Figure 25[a], showing most of the seiche water levels to be above this value, and the higher limit is based on the largest seiche observed at this site, which is the previously mentioned event in 1844, when a "4.3 m high seawall" was breached (NOAA, 2018). The interval width for flow is chosen as 20 m^3/s and the largest interval is up to 285–305 m^3/s when the conditional probability drops below 1% for all scenarios. Based on a frequency analysis of the annual maximum discharges for the Buffalo River, 305 m^3/s represents a 1.5-year return period flood.

Figure 26. Conditional Probability of River Discharge Intervals under Different Seiche Water Levels

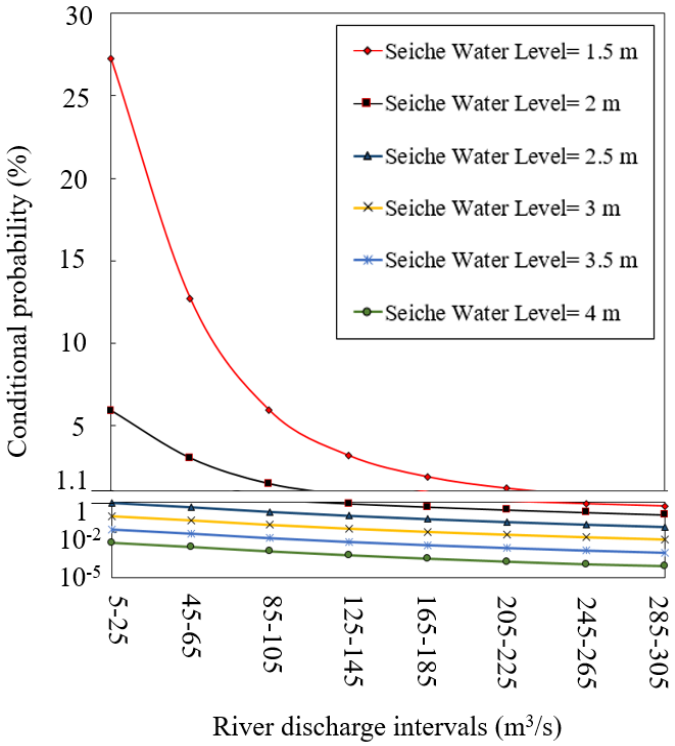

The seiche water level of 1.5 m shows the highest probability of occurrence (27.2%) for the discharge interval of 5 to 25 m3/s. As the river discharge increases, the conditional probability decreases. It is worth noting that the median daily discharge of the river is approximately 15 m^3/s, falling into the highest-probability interval. The conditional probability of discharge occurring in the 285–305 m^3/s interval under the 1.5 m seiche water level decreases to 0.57%. As seiche water level increases, the

values of conditional probability decrease because the probability of a higher water level is smaller. It is observed that when the seiche water level is at 3 or 4 m, the conditional probability is 0.12% or 0.002%, respectively, for the 5 to 25 m^3/s interval, and decreases further with higher discharge.

Figure 27 shows the results for different discharges between 200 m^3/s and 1000 m^3/s. For the Buffalo River, 200 m^3/s and 1000 m^3/s represent the lowest annual peak flow and the 100-year flood flow, respectively. A unimodal shape for conditional probability is observed for all discharges and the selected downstream water-level intervals. The peak for all different discharge scenarios is observed at the 0.75 to 1 m water level-interval, with the long-term average lake level being 0.75 m (note that all lake levels are reported with respect to IGLD85 datum). The peak probability value decreases from 22.6% to 0.84% as discharge increases from 200 m^3/s to 1000 m^3/s.

The highest water-level interval considered in Figure 27 is 2.75 to 3 m, since the 100-year seiche water level is 2.76 m. The conditional probabilities of the 2.75 to 3 m water-level interval are 0.66%, 0.62%, 0.12%, and 0.03% under 200, 400, 800, and 1000 m^3/s discharges, respectively. Similar to the seiche-driven scenarios, since each curve shows the probability of two events occurring jointly, the curve for a larger discharge, e.g., 1000 m^3/s, generally is lower than that for a smaller discharge.

Figure 27. Conditional Probability of Downstream Water-Level Intervals under Different River Discharges

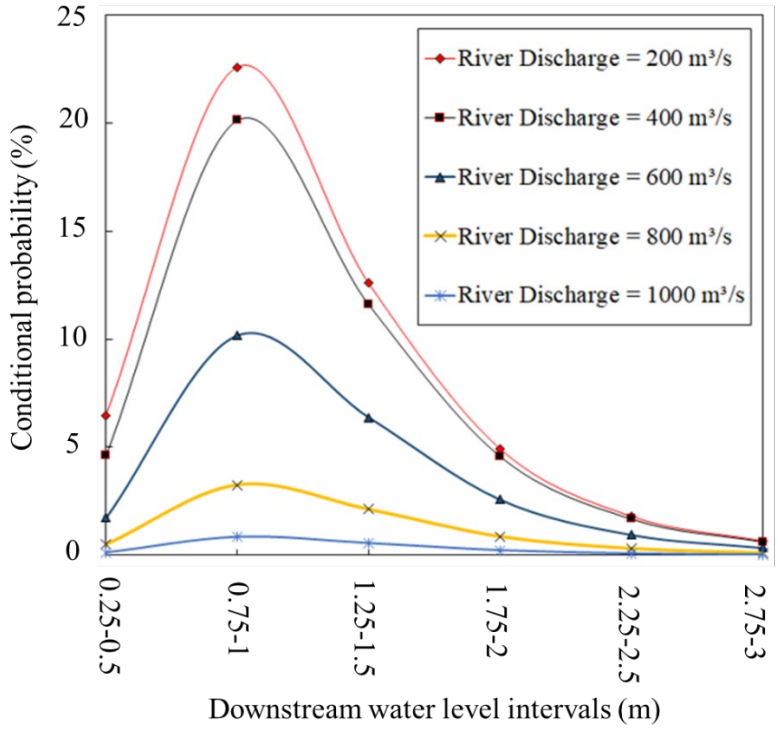

The FEMA flood map for the Buffalo River is based on the 100-year discharge and a downstream water level of 2.22 m. This water level represents an extreme lake level, approximately 1.5 m higher than the long-term average of 0.75 m. It may be supposed that using an extreme water level should provide a conservative (or worst-case) scenario for flooding prediction. Here we investigated the impact of conditional probabilities on the predicted flood areas for a 100-year event. The copula-based methodology incorporates the joint distribution for both the upstream discharge and downstream water-level boundary conditions, rather than a flood map based on the marginal distribution of the discharge data only.

Figure 28 shows the inundation areas under four scenarios: (a) long-term average lake level (0.75 m) and median discharge (15 m^3/s); (b) 10-year flood flow (736 m^3/s) and 100-year water level (based on seiche analysis (2.76 m); (c) 100-year flood flow (1056 m^3/s) and 10-year seiche (2.22 m); and (d) 100-year flood flow (1056 m^3/s) and 100-year seiche (2.76 m) (Table 6). It should be noted that the FEMA 100-year flood map is generated using conditions almost equivalent to scenario (c). Flooding results are discussed further in the following section.

Figure 28. Flood Flow

The red dots show the upstream and downstream locations used in this study.
[a] Median flow discharge and long-term average lake level; [b] 10-year flood flow and 100-year seiche; [c] 100-year flood flow and 10-year seiche (FEMA 100-year flood map scenario); and [d] 100-year flood flow and 100-year seiche.

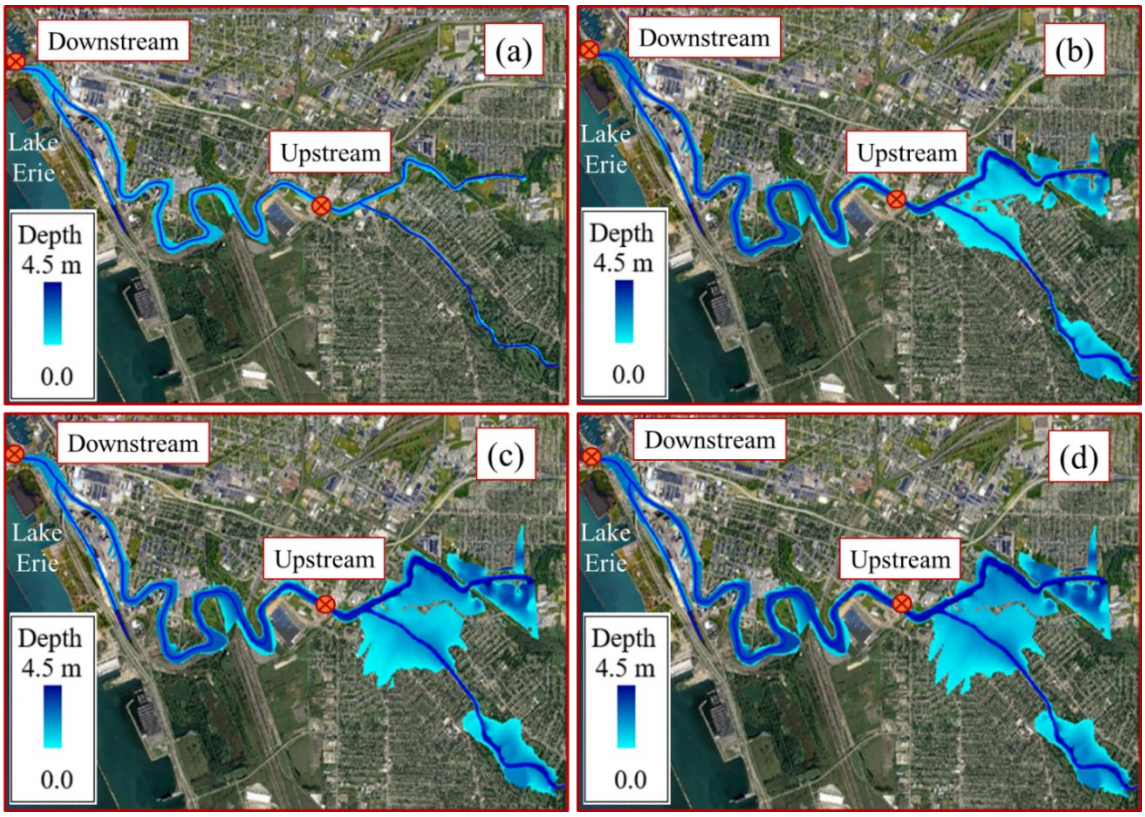

3.3 Dissemination of Results

Products published or presented at conferences resulting from this project include Sogut and Farhadzadeh (2018) and Saharia et al. (2021). In addition, we worked with New York Sea Grant Extension to develop a "fact sheet" on seiching in the Great Lakes that includes an image of the impact of seiches on flooding in the Buffalo River (this is similar to Figure 28). A copy of this fact sheet is included as appendix B.

We also worked with New York State Department of Environmental Conservation (NYSDEC) and gave a presentation to the Eastern Lake Erie Action Agenda group on November 15, 2019, entitled "Seiche Events and Climate Change: Effects in Eastern Lake Erie and Buffalo River." This presentation was made in person to about 25 stakeholders from Western New York representing a variety of interests.

Several people also participated remotely. Also working with NYSDEC, we gave a presentation as part of a regular webinar series on September 30, 2020, entitled “Coastal Resiliency and Morphodynamic Responses to Storm Surge and Seiche in Eastern Lake Erie.” This presentation was made virtually, and we were told there was an audience of almost 70 people from around New York State and other Great Lakes states. Copies of either of these presentations can be made available upon request.

4 Discussions

4.1 Coastal Morphology

At the southern boundary of the domain, the nearshore current velocity is strong likely because of the shoreline alignment. There, the relative orientation of the predominant incident waves with respect to the curved shoreline leads to the formation of a strong longshore current. As Figures 22 and 23 show, the longshore current was strongest in January, when a higher number of storms took place, followed by February and December. The velocity field demonstrates a relatively similar pattern for the six storm months—the current near the southern boundary is directed northwards and then offshore before turning northwards and onshore around the northern boundary.

A shoal in the northern part of the study area (Figure 6[b]), formed possibly due to the sediment deposit discharged from the Blasdell Creek and Rush Creek at Woodlawn Beach State Park, appears to influence the current velocity pattern. At this shallow zone, the current velocity is higher than that of the nearshore area. Furthermore, at this shoal, the current velocity for the seiche-free condition is greater than that of the actual water-level condition. Additionally, the shoal creates a sheltering effect by reducing the wave height on its leeside which is extended further north. The central and southern parts of the study area are more exposed to the direct impacts of larger waves and thus are morphologically more dynamic, resulting in a higher rate of sediment transport, thanks to a more regular bathymetry and a straight shoreline.

The monthly average shore evolutions presented in Figures 22 and 23 show an erosion zone closer to the shoreline and an accretion area at a distance offshore, indicating a net offshore-directed sediment transport during the storm season. The beach profile between the shoreline and the 2 m deep contour line is morphologically the most active zone. Because the beach material is mainly fine sand, the transport mode is primarily suspended load which is nearly 10 times the bed load. The comparisons of the maxima of the wave height (H_{rms}) along the initial shoreline position indicate that seiche motions increase the maximum wave height ~3 mm for the actual water-level condition, ~0.179 m. This small increase in the maximum nearshore wave height results in a slightly larger maximum current velocity, U ~0.0001m/s, for the actual water-level condition, 0.013m/s. On the other hand, the minimum current velocity for the seiche-free water-level condition is determined to be ~0.0001m/s larger than the one for actual water-level condition. This difference is assumed to be related to the depth-limited wave breaking. The maxima of the bed load (q_b), ~ 2.3×10^{-7} m^2/s, and suspended load (q_s), ~ 4.6×10^{-6} m^2/s, along the initial shoreline position for the actual water-level condition are found to be ~ 0.1×10^{-7} m^2/s and 0.4×10^{-6} m^2s larger compared to those of seiche-free condition, respectively.

The winter wave height, current velocity, and total sediment transport ($q=q_s + q_b$) roses for the actual and seiche-free water conditions at points A and B, located at approximately 100m offshore (Figure 6), are presented in Figure 29. Although the patterns of the nearshore wave heights and current velocity are not significantly different for the actual and seiche-free conditions for point B, the current velocity for point A, near the southern boundary, is much stronger under the seiche-free condition. Such a difference is likely due to the depth-limited wave-breaking which is reflected in the wave rose of point A. Comparing the total sediment transport for the actual and seiche-free water-level conditions, the contribution of the seiche motions on the sediment transport appears along the northeast direction at point B. However, for point A the total transport patterns for the two water-level conditions appear to be similar. This is likely related to the shoreline orientation as well as the presence of the shoal offshore of point B. The alongshore variations of the accretion and erosion, as well as the total transport rate, are presented in Figure 30 for three distinct regions: The straight section of the shoreline (region 1), the leeside of the shoal (region 2), and the northwest oriented shoreline (region 3). For region 1, the total erosion and accretion for the actual water-level condition are approximately 2% more than those of the seiche-free condition. The presence of the shoal in region 2, which provides a shelter for the shoreline from the wave, influences the nearshore flow patterns, hence, reducing the beach evolution. The eroded and deposited sediment volumes for region 2 are around 1.5% more under the actual water level compared to those of the seiche-free condition. For region 3, where the shoreline is oriented toward the northwest, the actual water-level results in about 1% more erosion and deposition than those of the seiche-free condition. Figures 30 [c] and 30 [d] show the alongshore variations of the deposited and eroded sediment volumes for the actual and seiche-free water-level conditions. Since the seiche-induced current flows in a counterclockwise direction in the lake (Hamblin 1987; Irish and Platzman 1961; Kite 1992; Mortimer 1987; Platzman and Rao 1964a; b), the difference between total deposited and eroded materials could be attributed to the longshore sediment transport gradient along the shoreline in the computation domain.

The variations of the monthly eroded and deposited sand volumes for the entire shoreline under the actual water-level condition are plotted in Figure 31[a]. The deviations of the accreted and eroded sediment volumes for the seiche-free condition from those of the actual water level are presented in Figure 31[b]. As mentioned before, during May–September fewer storms occur which results in a significant reduction in the bathymetric changes. Therefore, the difference between the actual and seiche-free bottom changes are insignificant during this calm period. This difference becomes greater during the winter months.

Over the one-year period, the total accretion and erosion under the actual water-level condition are estimated to be approximately 114,630 m^3 and 112,745 m^3, respectively. Under the seiche-free condition, the accreted and eroded sand volumes are ~112,889 m^3 and 110,878 m^3, respectively–approximately 1.5% and 1.7% less than the ones for the actual water-level condition, respectively. Overall, the eroded or deposited sand volume, during the one-year period, is found to be ~1.5% greater under the actual lake condition compared to that of the seiche-free lake–this difference can be attributed to the contribution of the seiches.

Figure 29. Winter wave height (H_{rms}), Current Velocity (U), and Total Sediment Transport Rate ($q=q_s + q_b$)

Roses under actual and seiche-free water-level conditions obtained from XBeach simulations, for 2012, at [a] Point A and [b] Point B shown in Figure 2.

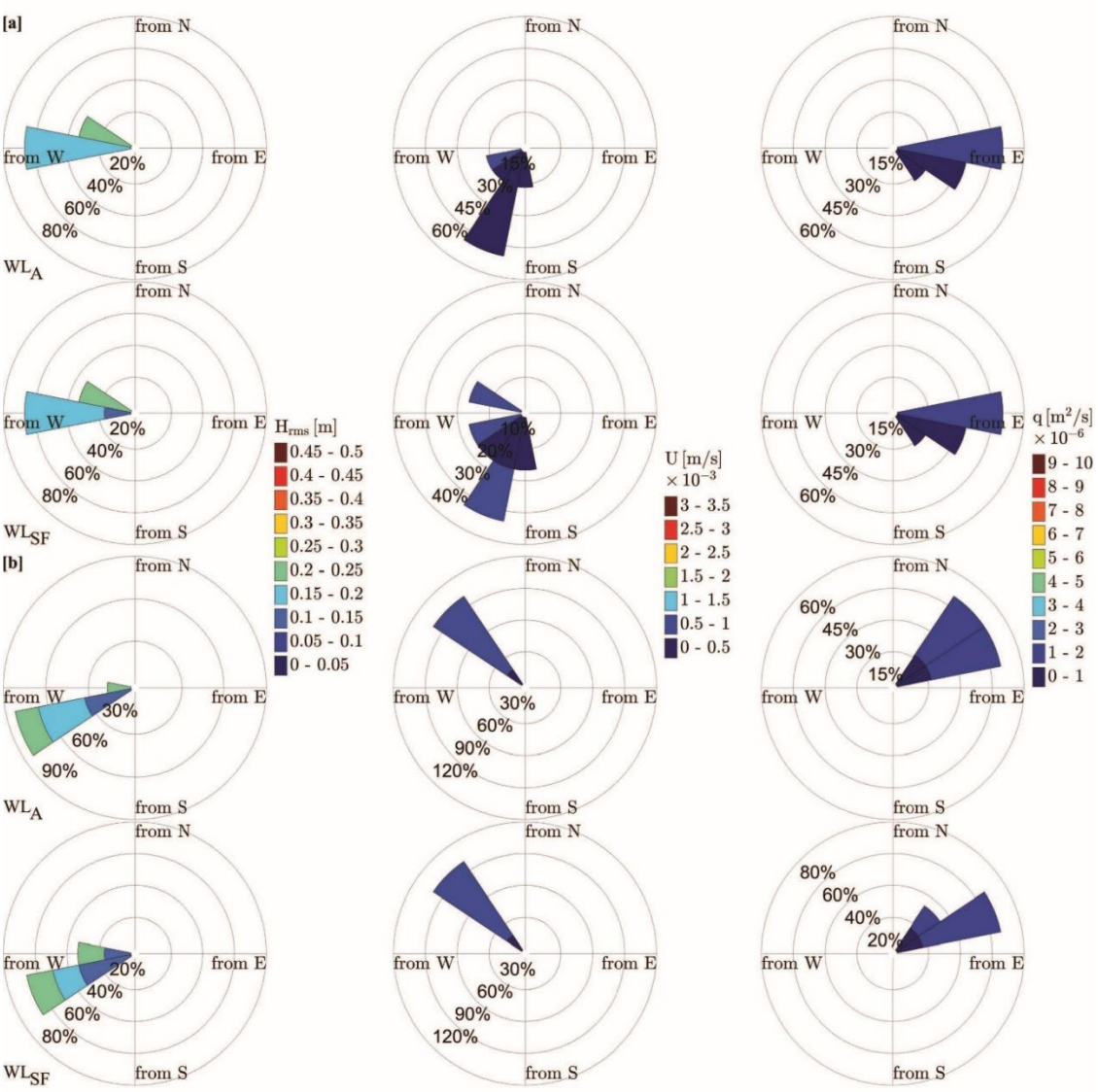

Figure 30. Alongshore Variations of Bottom Elevation Changes During 2012

Under: [a] Actual water-level condition [b] Seiche-free water-level condition. Alongshore variation of: [c] Accretion and erosion under seiche-free water-level condition (VSF) compared to actual water-level condition (VA) [d] Total accretion, erosion, and net transport under seiche-free water-level condition (ΣVSF) compared to actual water-level condition (ΣVA). Red, blue, and black represent accretion, erosion, and total transport, respectively.

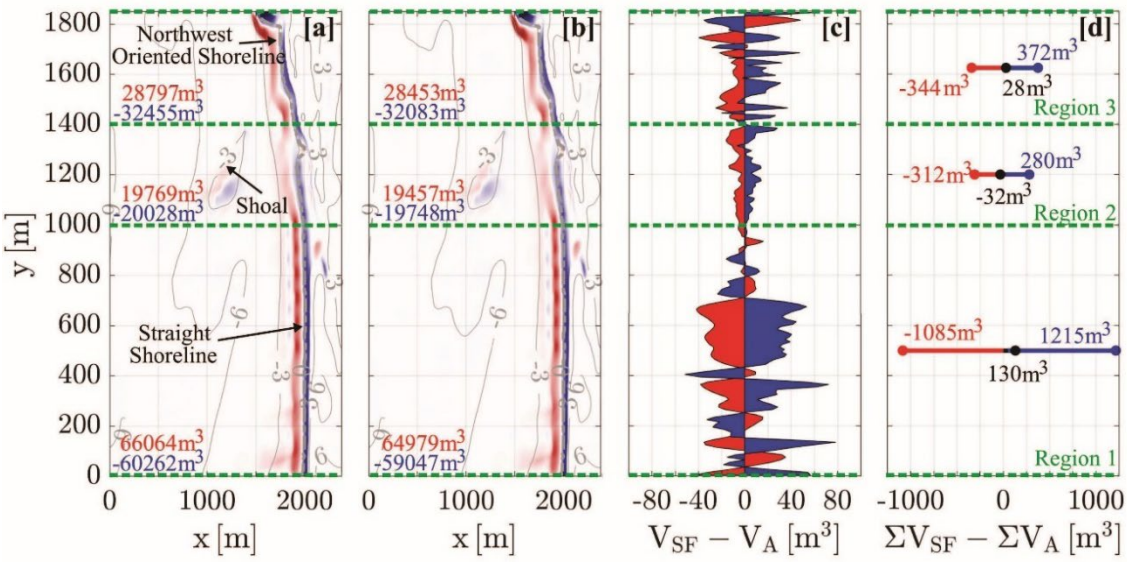

Figure 31. Variations Continued

[a] Variations of computed monthly accretion (ΣVa) and erosion (ΣVe) for actual water-level condition [b] Variations of monthly accretion and erosion under seiche-free water-level condition (ΣVSF) compared to actual water-level condition (ΣVA).
Black solid line represents accretion and black dashed line represents erosion.

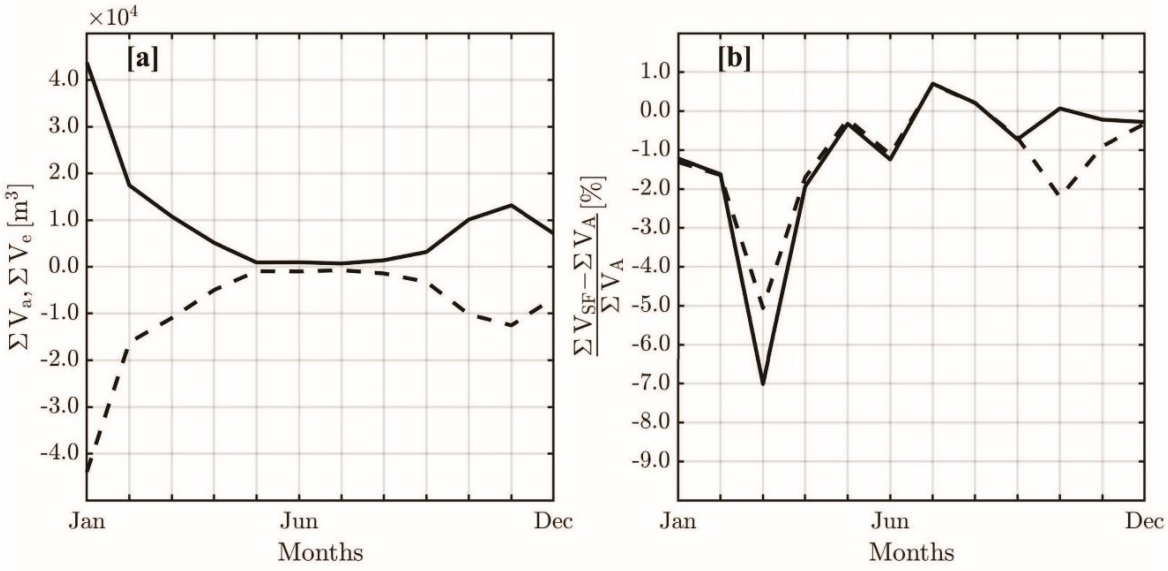

4.2 Copula Analysis and Flooding Risk

The ratio of the conditional probability between the 5–25 m^3/s and 285–305 m^3/s intervals under different seiche scenarios is shown in Table 4. The ratio decreases as the seiche water-level increases, indicating that the probability of high river discharge (i.e., 285-305 m^3/s) compared to that of normal river discharge (i.e., 5-25 m^3/s) actually increases as the seiche water-level increases. The ratio drops greatly from 47.5 to 39.5 when the water level increases from 1.5 m to 2 m. When the water level is higher than 2 m, further changes become small. This finding suggests that although normal discharge is always the most probable, higher discharge becomes relatively more probable when seiches occur, likely because the heavy wind on Lake Erie that caused a seiche could also be related to storms in the Buffalo River watershed.

Table 4. Ratio of Conditional Probability between the Most Probable Interval and Largest Considered Interval under Different Seiche Scenarios

L	Seiche water level, *s* (m)					
	***s*>1.5**	***s*>2**	***s*>2.5**	***s*>3**	***s*>3.5**	***s*>4**
P(5<*r*<25)/P(285<*r*<305)	47.5	39.5	37.6	37.3	37.2	36.7

Note: r = river discharge, m^3s.

From the conditional probability analysis described previously, the most probable downstream water-level interval under the 100-year flow should be 0.75-1 m, which is more probable than a higher water-level interval such as the 10-year-seiche-equivalent. With the interval width of 0.25 m for copula computation, the 2.1–2.35 m interval and the 2.63–2.88 m interval are used for a 10-year seiche and a 100-year seiche, respectively. The probability of the 100-year flow occurring with water level in the 0.75 m–1 m range, relative to the probability of the same flow with water level in the 2.1 m–2.35 m range is approximately equal to 7, meaning the 100-year flood flow and the most probable water level (slightly larger than the long-term average lake level) is approximately 7 times more likely to occur than the FEMA 100-year flood scenario. Similarly, the probability of river discharge being greater than 1056 m^3s and water level being between 0.75 and 1 m, relative to a discharge greater than 736 m^3s with water level between 2.63 and 2.88 m is about 3, but the probability of a flow greater than 1056 m^3s with water level between 0.75 and 1 m, relative to the same discharge but with water level between 2.63 and 2.88 m is about 20. This comparison indicates that the 100-year flood flow and the most probable water level is likely to occur 3 and 20 times more frequently than cases (b) and (d), respectively, as shown in Figure 28.

This result indicates that conditions with downstream water level different from the one considered in the FEMA analysis, while still using the 100-year flood value, are likely to occur more frequently. Figure 32 shows a comparison of inundation areas resulting from several combinations of discharge and downstream water level. The inundation area for the FEMA scenario is 2.85 km^2. For the 100-year seiche and 100-year flood scenario, and 100-year seiche and 10-year flood the inundation areas are 3.1 km^2 and 1.95 km^2, respectively. The FEMA scenario is thus seen to produce a lower water level compared to the 100-year seiche, 100-year flood scenario. From the copula analysis, the most probable flood scenario for the 100-year flood flow is with water level in the 0.75–1 m range. Therefore, from Figure 32 the most probable 100-year flood flow with the 0.75–1 m water-level flood will cause an inundation of 2.4–2.5 km^2, slightly less than for the FEMA scenario. In terms of flooding, therefore, it may be concluded that the FEMA result is relatively conservative.

Figure 32. Inundation Area as a Function of Downstream Water-Level and Upstream Discharge

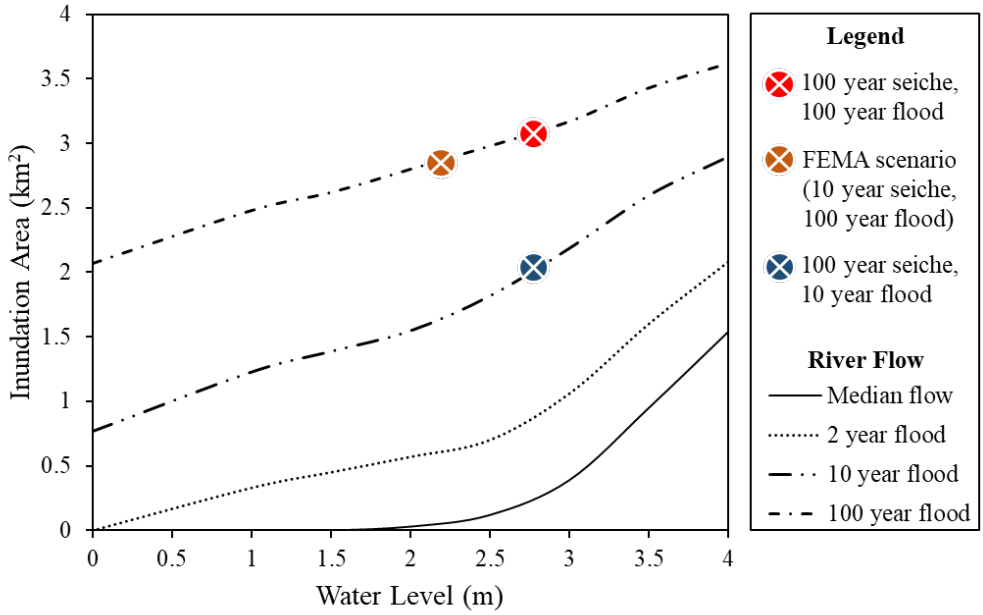

4.2.1 Hydraulic Performance Graph

The HPG is made up of a family of hydraulic performance curves (HPCs) for discharges ranging from 15 m^3/s to 1000 m^3/s, as shown in Figure 33. The HPG provides a convenient way to look up water level at the upstream boundary (as in Figure 33) or at any given location (which can be created separately) under all combinations of compound flood scenarios. The IGLD85 datum is used in Figure 33, which represents a low water level. The HPCs are bounded by the 45-degree straight line on the right, labelled

as the Z-line. The Z-line represents a horizontal water surface for which there is no flow. The N-line represents the locus of normal flow profiles, and it divides the HPCs into two regions. The region between the N-line and Z-line contains the pairs of upstream and downstream water levels corresponding to all possible M1-type profiles, whereas the region between the vertical axis and the N-line contains the pairs of water levels corresponding to all M2-type profiles (Yen et al., 2000). Figure 33 shows that there will always be an M1-type profile in the river for discharges less than 400 m^3/s, while for discharges larger than 800 m^3/s the profile will always be M2-type. For a 600 m^3/s discharge, the profile switches from M2 to M1 when the downstream water level is at 1.5 m, with a corresponding upstream water level of 2.2 m.

Figure 33. HPG for the Buffalo River Seiche and High-Discharge Assessment

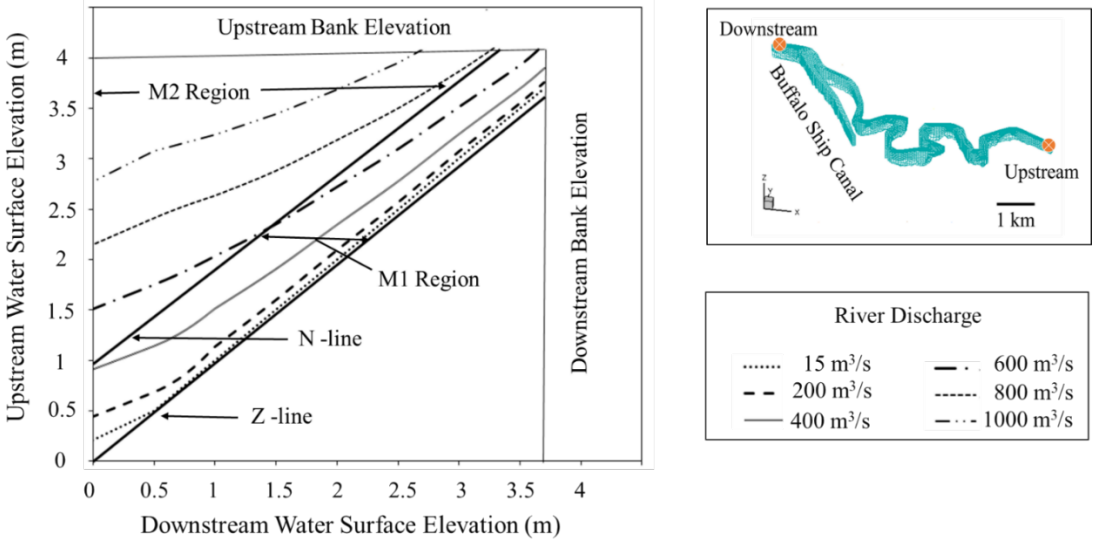

This flow profile analysis enables engineers to learn beforehand the possible flow profiles associated with the downstream seiche and upstream flow boundary conditions. It is also useful to learn about these flow profiles before constructing any weirs, dams, or control structures in the river. M1 profiles are considered common water surface profiles where mild slope streams enter a pool, while M2 profiles occur at a sudden drop of the channel or the channel outlet into a lake if the slope becomes steeper (Chaudhry, 2007). Though the flow profile usually depends mostly on the channel slope, it is seen here that the water level and upstream flow boundary conditions can alter the river flow profile.

The upstream and downstream bank elevations also are marked in Figure 33 (note that much of the Buffalo River has hard siding installed, with artificially high-stream bank elevations). It is observed from the HPCs that as discharge increases from 600 m^3/s to 1000 m^3/s, it is more likely that water surface elevation will overtop the upstream bank first. This effect also is evident in Figure 28, where it is seen that most of the flooding occurs upstream of the study area. Therefore, in the case of the Buffalo River, the "streamflow-driven" scenario should be considered for flood analysis, and flooding is much more of a concern in upstream areas rather than downstream. The "seiche-driven scenario" may still be used to look into seiche event conditional probability for the range of available data but would not be as useful for the flood analysis in this case. In general, the choice of "streamflow-driven" or "seiche-driven" will probably not be known when considering applying the type of analysis described here to a new site. However, for the Buffalo River, with its artificially protected streambanks, it is clear that discharge is the main factor in controlling flooding. This result is not, however, expected to be true for all applications.

5 Conclusions

This exploratory study numerically demonstrates the contribution of the seiche to the morphological changes in eastern Lake Erie. The lake-wide hydrodynamics model, coupled with the circulation and spectral wave model (ADCIRC+SWAN) provided the flow boundary conditions for the 2D process-based morphodynamic model, XBeach for the entire year of 2012. The computational domain for XBeach includes an area of nearly 2 km alongshore and 2 km cross-shore, encompassing Woodlawn Beach State Park, south of Buffalo, NY, where the beach is composed of fine sand. The model results indicate that suspended sediment transport is the dominant transport mode in the study area and the seiches exacerbate the erosion processes along the beach.

The alongshore variations of accretion and erosion, as well as the total transport rate are divided into three distinct regions: In region 1, in the south where the shoreline is straight, the total erosion and accretion for the actual water-level condition are approximately 2% more than those of the seiche-free condition; for region 2, the central section of the study area, an offshore shoal provides a shelter for the shoreline from the wave. This shoal appears to influence the nearshore flow patterns, hence, reducing the beach evolution. The eroded and deposited sediment volumes for region 2 are around 1.5% greater under the actual water-level condition compared to those of the seiche-free condition. Region 3, the northern segment of the shoreline, is oriented toward the northwest. In this region, the actual water-level results in about 1% more erosion and deposition than those of the seiche-free condition. Furthermore, it is found that over the one-year period, 2012, the seiche motions contribute to approximately 1.5% of the total accretion/erosion, along the selected stretch of shoreline. These findings are the results of the numerical simulations which require validations using field data including beach profiles and sediment sampling. In addition, techniques such as composite modeling (Kamphuis 1996, 2010b; Tomasicchio *et al.* 2011) can potentially be used to further analyze the effects of seiching on beach morphology.

The compound flooding due to seiche (i.e., high downstream water level) and high discharge can have an enormous impact on a community near a coastal freshwater river. The compound impacts of both upstream discharge and downstream water level—potentially affected by lake seiching—on flooding were examined using copula probability and a hydrologic model. The hydrologic model was found to

be more useful than a full hydrodynamic model for this purpose. The probability-based framework proposed in this study can be applied to quantify the conditional probability of compounding boundary conditions for any freshwater coastal river, although it is not expected that the same conclusions would necessarily be reached as in the Buffalo River. Perhaps the most important conclusion to be reached for the Buffalo River is that the FEMA floodplain represents a relatively conservative estimate, and that seiching does not significantly affect the inundation area when discharge is high.

6 References

Aagaard, T., and Greenwood, B., 2008. Infragravity wave contribution to surf zone sediment transport - The role of advection. *Marine Geology*.

de Bakker, A. T. M., Brinkkemper, J. A., van der Steen, F., Tissier, M. F. S., and Ruessink, B. G., 2016. Cross-shore sand transport by infragravity waves as a function of beach steepness. *Journal of Geophysical Research: Earth Surface*.

Bertin, X., de Bakker, A., van Dongeren, A., Coco, G., André, G., Ardhuin, F., Bonneton, P., Bouchette, F., Castelle, B., Crawford, W. C., Davidson, M., Deen, M., Dodet, G., Guérin, T., Inch, K., Leckler, F., McCall, R., Muller, H., Olabarrieta, M., Roelvink, D., Ruessink, G., Sous, D., Stutzmann, É., and Tissier, M., 2018. Infragravity waves: From driving mechanisms to impacts. *Earth-Science Reviews*.

Bevacqua, E., Maraun, D., Hobæk Haff, I., Widmann, M., Vrac, M., 2017. Multivariate statistical modelling of compound events via pair-copula constructions: analysis of floods in Ravenna (Italy). *Hydrology and Earth System Sciences*, 21(6): 2701-2723.

Booij, N., Ris, R. C., and Holthuijsen, L. H., 1999. A third-generation wave model for coastal regions: 1. Model description and validation. *Journal of Geophysical Research: Oceans*, Wiley Online Library, 104(C4), 7649–7666.

Bruun, P., 1954. *Coast erosion and the development of beach profiles*. US Beach Erosion Board.

Chaudhry, M.H., 2007. Open-channel flow. Springer Science & Business Media.

Cueva, D. A., Monzón, C. O., Filonov, A., Tereshchenko, I., Covarrubias, P. L., and González, J. R. G. 2019. Natural frequencies of seiches in Lake chapala. *Scientific reports*, Nature Publishing Group, 9(1), 1–11.

Dean, R. G., 1991. Equilibrium beach profiles: characteristics and applications. *Journal of coastal research*, JSTOR, 53–84.

Dean, R. G., and Houston, J. R., 2016. Determining shoreline response to sea level rise. *Coastal Engineering*, Elsevier, 114, 1–8.

Dietrich, J. C., Zijlema, M., Westerink, J. J., Holthuijsen, L. H., Dawson, C., Luettich Jr, R. A., Jensen, R. E., Smith, J. M., Stelling, G. S., and Stone, G. W., 2011. Modeling hurricane waves and storm surge using integrally coupled, scalable computations. *Coastal Engineering*, Elsevier, 58(1), 45–65.

Dingman, J. S., and Bedford, K. W., 1984. The Lake Erie response to the January 26, 1978, cyclone. *Journal of Geophysical Research: Oceans*, Wiley Online Library, 89(C4), 6427–6445.

Dusini, D. S., 2005. The effect of Lake Erie water level variation on sediment resuspension. The Ohio State University, Ph.D. Dissertation.

Environ International Corporation, Mactec Engineering and Consultants, Inc., and LimnoTech (2011), Feasibility Study for the Buffalo River, New York. Report prepared for Buffalo River Great Lakes Legacy Act Project Coordination Team, October 5, 2011.

Environmental Protection Agency Great Lakes Atlas, accessed at http://epa.gov/greatlakes/atlas/index.html

Farhadzadeh, A., 2017. A study of Lake Erie seiche and low frequency water level fluctuations in the presence of surface ice. *Ocean Engineering*, Elsevier, 135, 117–136.

Farhadzadeh, A., and Gangai, J., 2017. Numerical modeling of coastal storms for ice-free and Ice-covered Lake Erie. *Journal of Coastal Research*, The Coastal Education and Research Foundation, 33(6), 1383–1396.

Farhadzadeh, A., Ghazian, A. M., and Bokuniewicz, H., 2018. Contribution of Seiche to Beach Profile Evolution in Eastern Lake Erie. *Shore and Beach*.

Gailani, J., Lick, W., Ziegler, C.K. and Endicott, D. (1996), "Development and Calibration of a Fine-Grained Sediment Transport Model for the Buffalo River," *J. Great Lakes Research*, 22(3), 765–778.

Galappatti, G., and Vreugdenhil, C. B., 1985. A depth-integrated model for suspended sediment transport. *Journal of Hydraulic Research*, Taylor & Francis, 23(4), 359–377.

Genest, C., Rivest, L.-P., 1993. Statistical inference procedures for bivariate Archimedean copulas. *Journal of the American Statistical Association*, 88(423): 1034-1043.

Gerbush, M. R., Kristovich, D. A. R., and Laird, N. F., 2008. Mesoscale boundary layer and heat flux variations over pack ice--covered Lake Erie. *Journal of Applied Meteorology and Climatology*, 47(2), 668–682.

Grimaldi, S., Serinaldi, F., 2006. Asymmetric copula in multivariate flood frequency analysis. *Advances in Water Resources*, 29(8): 1155-1167.

Hamblin, P. F., 1987. Meteorological forcing and water level fluctuations on Lake Erie. *Journal of Great Lakes Research*, Elsevier, 13(4), 436–453.

Hawkes, P.J., Gouldby, B.P., Tawn, J.A., Owen, M.W., 2002. The joint probability of waves and water levels in coastal engineering design. *J. Hydraulic Research*, 40(3): 241-251.

Huard, D., Evin, G., Favre, A.-C., 2006. Bayesian copula selection. *Computational Statistics & Data Analysis*, 51(2): 809-822.

Irish, S. M., and Platzman, G. W., 1961. *An investigation of the meteorological conditions associated with extreme wind tides on Lake Erie*. University of Chicago, Department of Meteorology.

Joe, H., Kurowicka, D., 2011. Dependence modeling: vine copula handbook. World Scientific.

Johnson, B. D., Kobayashi, N., and Gravens, M. B., 2012. *Cross-shore numerical model CSHORE for waves, currents, sediment transport and beach profile evolution*. (No. ERDC/CHL-TR-12-22). Engineer Research and Development Center Vicksburg MS Coastal and Hydraulics Lab.

Johnson, B. D. 2012. *Lake Michigan: Prediction of Sand Beach and Dune Erosion for Flood Hazard Assessment* (No. ERDC/CHL TR-12-16). Engineer Research and Development Center Vicksburg MS Coastal and Hydraulics Lab.

Kamphuis, J. W., 1996. Coastal hydraulic models. Physical Modelling Workshop. 25th International Conference on Coastal Engineering.

Kamphuis, J. W., 2010a. *Introduction to coastal engineering and management: 2nd edition*. Advanced Series on Ocean Engineering.

Kamphuis, J. W., 2010b. Coastal modeling--indispensable design tool, but how? *In Proc. Coastlab 2010 Conf.* 10, 29-30. IAHR, Madrid.

Kim, Y. C., 2009. *Handbook of coastal and ocean engineering*, World Scientific, Singapore.

Kite, G. W., 1992. Spectral analysis of selected Lake Erie levels. *Journal of Great Lakes Research*, Elsevier, 18(1), 207–217.

Kobayashi, N., and Farhadzadeh, A., 2008. *Cross-shore numerical model CSHORE for waves, currents, sediment transport and beach profile evolution. Research Rep.* No. CACR-08-01, Center for Applied Coastal Research, Univ. of Delaware, Newark, Del.

Kobayashi, N., Farhadzadeh, A., Melby, J., Johnson, B., and Gravens, M. 2010. Wave overtopping of levees and overwash of dunes. *Journal of Coastal Research*, BioOne, 2010(265), 888–900.

Kobayashi, N., and Weitzner, H., 2015. Erosion of a seaward dike slope by wave action. *Journal of Waterway, Port, Coastal, and Ocean Engineering*, American Society of Civil Engineers, 141(2), 4014034.

Kobayashi, N., and Zhu, T., 2020. Erosion by wave action of consolidated cohesive bottom containing cohesionless sediment. *Journal of Waterway, Port, Coastal, and Ocean Engineering*, American Society of Civil Engineers, 146(2), 4019041.

Kriebel, D. L., and Dean, R. G. 1985. Numerical simulation of time-dependent beach and dune erosion. *Coastal Engineering*, Elsevier, 9(3), 221–245.

Kriebel, D. L., and Dean, R. G. 1993. Convolution method for time-dependent beach-profile response. *Journal of Waterway, Port, Coastal, and Ocean Engineering*, American Society of Civil Engineers, 119(2), 204–226.

Laio, F., Di Baldassarre, G., Montanari, A., 2009. Model selection techniques for the frequency analysis of hydrological extremes. *Water Resources Research*, 45(7).

Leonard, M. et al., 2014. A compound event framework for understanding extreme impacts. *Wiley Interdisciplinary Reviews: Climate Change*, 5(1): 113-128.

Lian, J., Xu, K., Ma, C., 2013. Joint impact of rainfall and tidal level on flood risk in a coastal city with a complex river network: a case study of Fuzhou City, China. *Hydrology and Earth System Sciences*, 17(2): 679-689.

Luettich Jr, R. A., Westerink, J. J., and Scheffner, N. W., 1992. *ADCIRC: An Advanced Three-Dimensional Circulation Model for Shelves, Coasts, and Estuaries. Report 1*. Theory and Methodology of ADCIRC-2DDI and ADCIRC-3DL.

Luettich, R. A., and Westerink, J. J., 2004. *Formulation and numerical implementation of the 2D/3D ADCIRC finite element model version 44*. XX,74.

Mortimer, C. H., 1987. Fifty years of physical investigations and related limnological studies on Lake Erie, 1928-1977. *Journal of Great Lakes Research*, Elsevier, 13(4), 407–435.

National Oceanic and Atmospheric Administration (NOAA), 2018. National Ocean Services; accessed at: http://oceanservice.noaa.gov/facts/seiche.html [Accessed 12/6/2019].

National Oceanic and Atmospheric Administration, Great Lakes Environmental Research Laboratory., 2019. Historical Ice Cover. accessed at: http://www.glerl.noaa.gov/data/ice/

National Oceanic and Atmospheric Administration, National Ocean Service., 2019. What is a seiche? accessed at: https://oceanservice.noaa.gov/facts/seiche.html

New York State Department of Environmental Conservation, "Great Lakes: Areas of Concern", accessed at: http://www.dec.ny.gov/lands/91213.html

New York State Division of Homeland Security., 2014. *NYS Standard Multi-Hazard Mitigation Plan (State Mitigation Plan).*

Palmer, M. D., and Izatt, J. B., 1972. Lake movements with partial ice cover. *Limnology and Oceanography*, Wiley Online Library, 17(3), 403–409.

Platzman, G. W., and Rao, D. B., 1964a. Spectra of Lake Erie water levels. *Journal of Geophysical Research*, Wiley Online Library, 69(12), 2525–2535.

Platzman, G. W., and Rao, D. B., 1964b. *The free oscillations of Lake Erie. Studies on Oceanography* (Hidalra volume) (I<. Yoshida, editor). University of Washington Press, 359-382.

Roelvink, D., Reniers, A., Van Dongeren, A. P., de Vries, J. van T., McCall, R., and Lescinski, J., 2009. Modelling storm impacts on beaches, dunes, and barrier islands. *Coastal engineering*, Elsevier, 56(11–12), 1133–1152.

Roelvink, D., Reniers, A., Van Dongeren, A., de Vries, J., Lescinski, J., and McCall, R., 2010. *XBeach model description and manual*. Unesco-IHE Institute for Water Education, Deltares and Delft University of Technology.

Russell, P. E., 1993. Mechanisms for beach erosion during storms. *Continental Shelf Research*, Elsevier, 13(11), 1243–1265.

Saha, S., Moorthi, S., Pan, H.-L., Wu, X., Wang, J., Nadiga, S., Tripp, P., Kistler, R., Woollen, J., Behringer, D., and others., 2010. The NCEP climate forecast system reanalysis. *Bulletin of the American Meteorological Society*, American Meteorological Society, 91(8), 1015–1058.

Saha, S., Moorthi, S., Wu, X., Wang, J., Nadiga, S., Tripp, P., Behringer, D., Hou, Y.-T., Chuang, H., Iredell, M., Ek, M., Meng, J., Yang, R., Mendez, M. P., van den Dool, H., Zhang, Q., Wang, W., Chen, M., and Becker, E., 2011. *NCEP Climate Forecast System Version 2 (CFSv2) 6-hourly Products*. Research Data Archive at the National Center for Atmospheric Research, Computational and Information Systems Laboratory, Boulder CO.

Saharis, Angshuman, Zhu, Zhenduo, and Atkinson, Joseph, 2021. Compound flooding from lake seiche and river flow in a freshwater coastal river. Accepted for publication, *Journal of Hydrology*.

Sallenger Jr, A. H., 2000. Storm impact scale for barrier islands. *Journal of Coastal Research*, 16(3).

Sklar, A., 1973. Random variables, joint distribution functions, and copulas. *Kybernetika*, 9(6): 449-460.

Sogut, E., and Farhadzadeh, A., 2018. Alongshore Variability of Coastal Morhodynamics in Eastern Lake Erie due to Low Frequency Oscillations of Lake Level. *Coastal Engineering Proceedings*, 1(36), 23.

Thomas, R. L., Jaquet, J.-M., Kemp, A. L. W., and Lewis, C. F. M., 1976. Surficial sediments of Lake Erie. *Journal of the Fisheries Board of Canada*, NRC Research Press, 33(3), 385–403.

Tomasicchio, G. R., D'Alessandro, F., and Barbaro, G., 2011. Composite modelling for large-scale experiments on wave--dune interaction. *Journal of Hydraulic Research*, Taylor & Francis, 49(sup1), 15–19.

Trebitz, A. S. 2006. Characterizing seiche and tide-driven daily water level fluctuations affecting coastal ecosystems of the Great Lakes. *Journal of Great Lakes Research*, BioOne, 32(1), 102–116.

US EPA., 2020. About the Great Lakes National Program Office (GLNPO) | US EPA. [online] Available at: https://www.epa.gov/aboutepa/about-great-lakes-national-program-office-glnpo [Accessed 23 Jan. 2020].

United States Environmental Protection Agency., 2019. Lake Erie. accessed at: https://www.epa.gov/greatlakes/lake-erie

US Environmental Protection Agency, Great Lakes Areas of Concern (AOCs); accessed at: http://www.epa.gov/greatlakes/aoc/index.html

Wang, J., Hu, H., Schwab, D., Leshkevich, G., Beletsky, D., Hawley, N., and Clites, A., 2010. Development of the Great Lakes ice-circulation model (GLIM): application to Lake Erie in 2003--2004. *Journal of Great Lakes Research*, Elsevier, 36(3), 425–436.

Wang, L. et al., 2018. Using Copulas to Evaluate Rationality of Rainfall Spatial Distribution in a Design Storm. *Water*, 10(6): 758.

Westerink, J. J., Luettich, R. A., Feyen, J. C., Atkinson, J. H., Dawson, C., Roberts, H. J., Powell, M. D., Dunion, J. P., Kubatko, E. J., and Pourtaheri, H., 2008. A basin-to channel-scale unstructured grid hurricane storm surge model applied to southern Louisiana. *Monthly weather review*, 136(3), 833–864.

Wickham, J., Homer, C., Vogelmann, J., McKerrow, A., Mueller, R., Herold, N., and Coulston, J., 2014. The multi-resolution land characteristics (MRLC) consortium - 20 years of development and integration of USA national land cover data. *Remote Sensing*, 6(8), 7424-7441.

Wright, L. D., and Short, A. D., 1984. Morphodynamic variability of surf zones and beaches: a synthesis. Marine geology, Elsevier, 56(1–4), 93–118.

Xu, H., Xu, K., Lian, J., Ma, C., 2019. Compound effects of rainfall and storm tides on coastal flooding risk. *Stochastic Environmental Research and Risk Assessment*, 33(7): 1249-1261.

Yen, B.C., González-Castro, J.A., 2000. Open-channel capacity determination using hydraulic performance graph. *Journal of Hydraulic Engineering*, 126(2): 112-122.

Zhang, Q., Xiao, M., Singh, V.P., Chen, X., 2013. Copula-based risk evaluation of hydrological droughts in the East River basin, China. *Stochastic Environmental Research and Risk Assessment*, 27(6): 1397-1406.

Zheng, F., Westra, S., Leonard, M., Sisson, S.A., 2014. Modeling dependence between extreme rainfall and storm surge to estimate coastal flooding risk. *Water Resources Research*, 50(3): 2050-2071.

Appendix A

The coastal structure survey of Eastern Lake Erie resulted in the following preliminary report where the specifications of various shore protection structures and their performance were analyzed and reported. The georeferenced data were stored on a dedicated webpage on Farhadzadeh's research laboratory website and can be accessed at https://you.stonybrook.edu/cherl/lake-erie/

Structure 1

Figure A-1. Left Panel: Location of STR1 in Lake Erie, Right Panel: A Closer Look at the Structure Location

STR1 is an approximately 245-meter-long breakwater constructed to protect Monroe Marina, Barcelona Harbor Pier, and Daniel Reed Memorial Pier.

Aerial images from 1994 to 2016 available on Google Earth show that the structure has not experienced any noticeable damage.

Structure 2

Figure A-2. Left Panel: Location of STR2 in Lake Erie, Right Panel: A Closer Look at the Structure Location

STR2 is an approximately 260-meter-long offshore breakwater constructed to protect Monroe Marina, Barcelona Harbor Pier, and Daniel Reed Memorial Pier.

Aerial images from 1994 to 2016 available on Google Earth show that the structure has not experienced any noticeable damage.

Structure 3

Figure A-3. Left Panel: Location of STR3 in Lake Erie, Right Panel: A Closer Look at the Structure Location

STR3 is an approximately 235-meter-long wharf belongs to Barcelona Harbor Pier and Daniel Reed Memorial Pier.

Aerial images from 1994 to 2016 available on Google Earth show that the structure has not experienced any noticeable damage.

Structure 4

Figure A-4. Left Panel: Location of STR4 in Lake Erie, Right Panel: A Closer Look at the Structure Location

STR4 is an approximately 35-meter-long revetment constructed to protect the eastern section of Barcelona Harbor Pier and Daniel Reed Memorial Pier from wave effect.

Aerial images from 1994 to 2016 available on Google Earth show that the structure has experienced noticeable damage. It is observed that due to the wave effect a considerable amount of armor layer protection is lost.

Structure 5

No data available.

Structure 6

No data available.

Structure 7

Figure A-5. Left Panel: Location of STR7 in Lake Erie, Right Panel: A Closer Look at the Structure Location

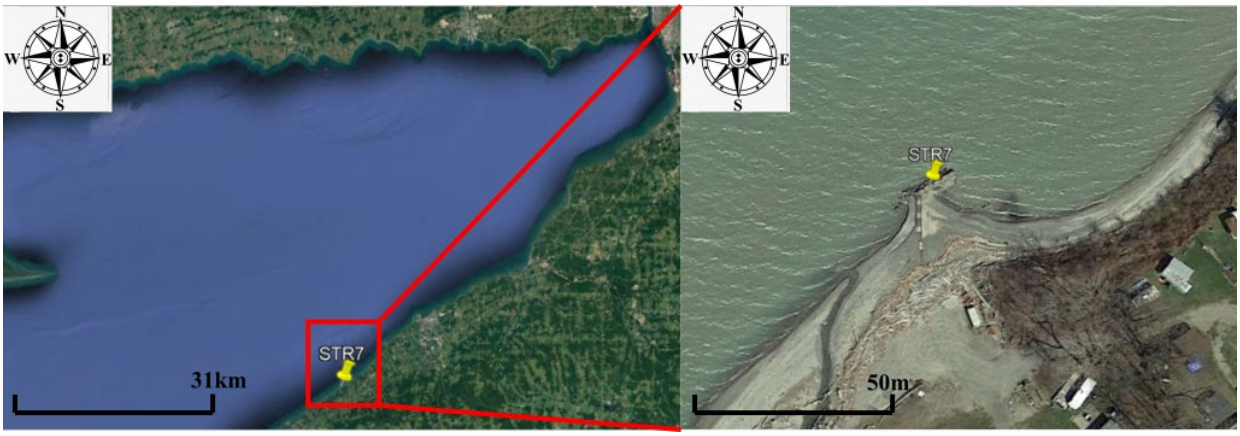

STR7 is an approximately 35-meter-long groin constructed to stabilize beach erosion near the DJ's campground.

Aerial images from 1994 to 2016 available on Google Earth show that the structure helped the shoreline stabilization for the area. Although there are yearly changes along the shoreline, in general, shoreline advanced seaward.

Structure 8

Figure A-6. Left Panel: Location of STR8 in Lake Erie, Right Panel: A Closer Look at the Structure Location

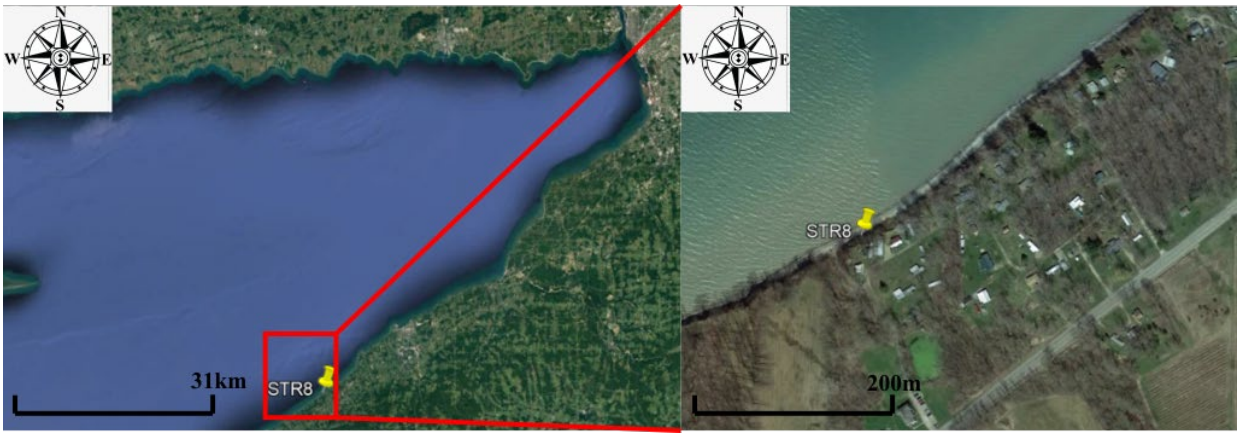

STR8 is an approximately 45-meter-long seawall constructed to protect the near-coast structure from flooding on Klinger Rd.

Aerial images from 1994 to 2016 available on Google Earth show the structure constructed after 2014, and it has not experienced any noticeable damage since then.

Structure 9

Figure A-7. Left Panel: Location of STR9 in Lake Erie, Right Panel: A Closer Look at the Structure Location

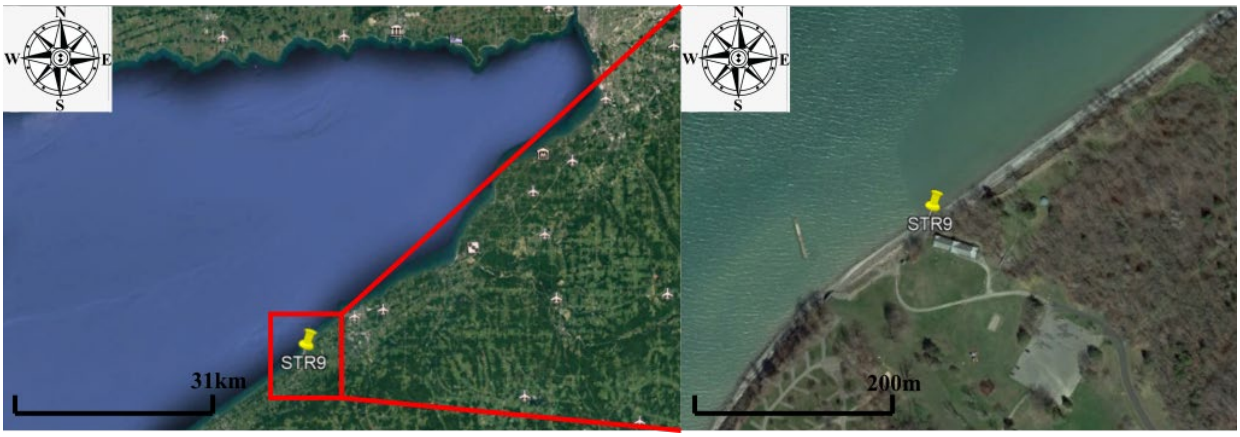

STR9 is an approximately 40-meter-long damped rock placed to prevent erosion both on the beach and on the bluff due to wave effect in Lake Erie State Park.

Aerial images from 1994 to 2016 available on Google Earth show that there is a significant shoreline recession on the beach. The rocks were damped in the area after 2004 to prevent erosion; however, it is observed that due to the wave effect a considerable amount of rock protection has been lost.

Structure 10

Figure A-8. Left Panel: Location of STR10 in Lake Erie, Right Panel: A Closer Look at the Structure Location

STR10 is an approximately 100-meter-long rock revetment constructed to prevent erosion on the bluff due to wave effect near Parkview Ln. Aerial images from 1994 to 2016 available on Google Earth show that there is a significant shoreline recession on the beach. The revetment was constructed after 2009 to prevent erosion, and it is observed that the structure has not experienced any noticeable damage since then.

Structure 11

Figure A-9. Left Panel: Location of STR11 in Lake Erie, Right Panel: A Closer Look at the Structure Location

STR11 is approximately 50-meter-long rock revetment constructed to prevent erosion on the bluff due to wave effect near Parkview Ln.

Aerial images from 1994 to 2016 available on Google Earth show that there is a significant shoreline recession on the beach. The revetment was constructed after 2016 to prevent erosion, and it is observed that the structure has not experienced any noticeable damage since then.

Structure 12

Figure A-10. Left Panel: Location of STR12 in Lake Erie, Right Panel: A Closer Look at the Structure Location

STR12 is an approximately 130-meter-long seawall constructed to prevent erosion due to wave effect near Swede Rd. Aerial images from 1994 to 2016 available on Google Earth show that there is a significant shoreline recession on the beach. The structure has not experienced any noticeable damage.

Structure 13

Figure A11: Left Panel: Location of STR13 in Lake Erie, Right Panel: A Closer Look at the Structure Location

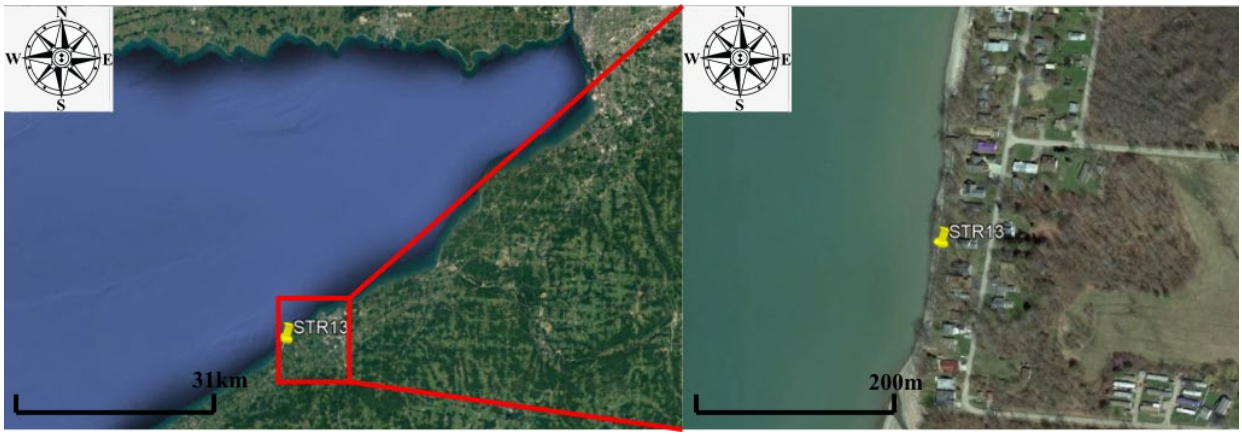

STR13 is an approximately 240-meter-long seawall constructed to prevent erosion due to wave effect near Patterson Ln.

Aerial images from 1994 to 2016 available on Google Earth show that there is a significant shoreline recession on the beach. The structure has not experienced any noticeable damage.

Structure 14

Figure A-12. Left Panel: Location of STR14 in Lake Erie, Right Panel: A Closer Look at the Structure Location

STR14 is an approximately 160-meter-long seawall constructed to prevent erosion due to wave effect near Patterson Ln.

Aerial images from 1994 to 2016 available on Google Earth show that there is a significant shoreline recession on the beach. The structure has not experienced any noticeable damage.

Structure 15

Figure A-13. Left Panel: Location of STR15 in Lake Erie, Right Panel: A Closer Look at the Structure Location

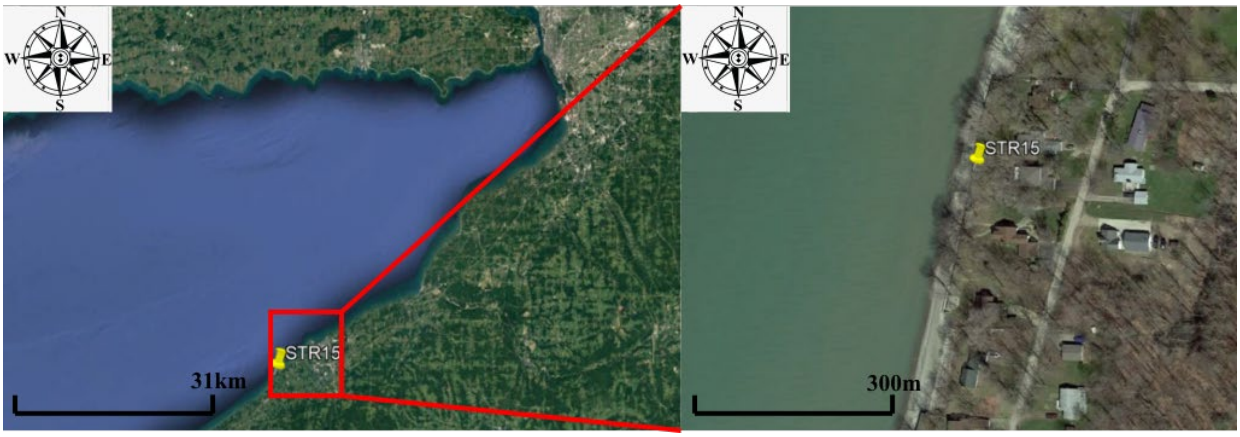

STR15 is an approximately 120-meter-long seawall constructed to prevent erosion due to wave effect near Patterson Ln.

Aerial images from 1994 to 2016 available on Google Earth show that there is a significant shoreline recession on the beach. The structure has not experienced any noticeable damage.

Structure 16

Figure A-14. Left Panel: Location of STR16 in Lake Erie, Right Panel: A Closer Look at the Structure Location

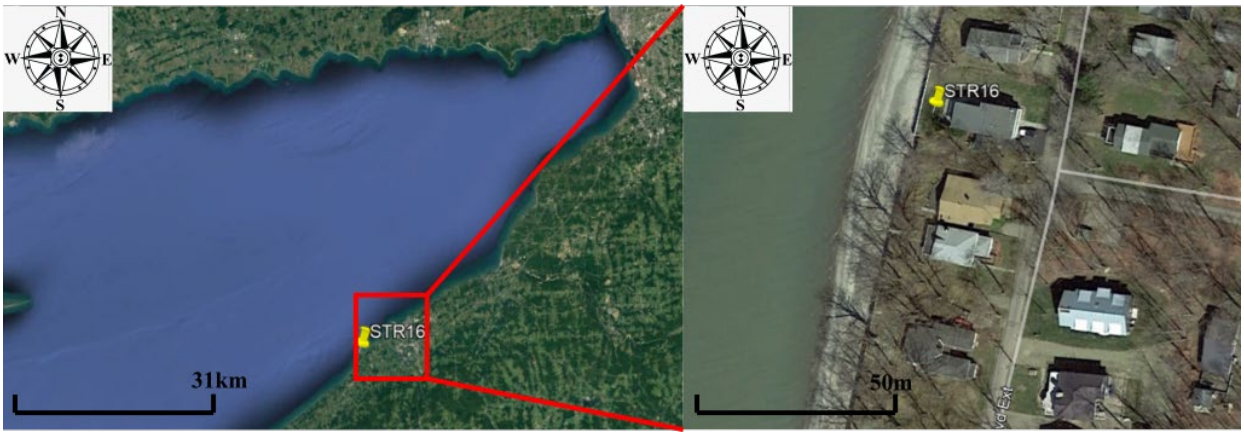

STR16 is an approximately 850-meter-long seawall constructed to prevent erosion due to wave effect near Lakeside Blvd Ext.

Aerial images from 1994 to 2016 available on Google Earth show that there is a significant shoreline recession on the beach. The structure has not experienced any noticeable damage.

Structure 17

Figure A-15. Left Panel: Location of STR17 in Lake Erie, Right Panel: A Closer Look at the Structure Location

STR17 is an approximately 400-meter-long revetment and seawall combination constructed to prevent erosion due to wave effect near Lakeside Blvd Ext. Aerial images from 1994 to 2016 available on Google Earth show that there is a significant shoreline recession on the beach. The structure has not experienced any noticeable damage.

Structure 18

Figure A-16. Left Panel: Location of STR18 in Lake Erie, Right Panel: A Closer Look at the Structure Location

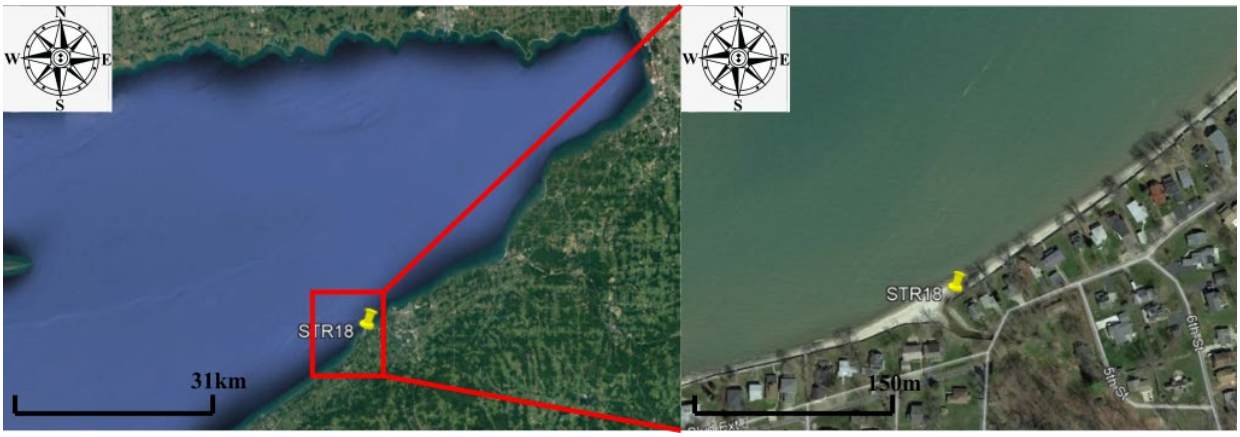

STR18 is an approximately 950-meter-long seawall constructed to prevent erosion due to wave effect near Lakeside Blvd Ext. Furthermore, the extension of the wall towards the upstream of the nearby river stabilized the river mouth. Aerial images from 1994 to 2016 available on Google Earth show that there is a significant shoreline recession on the beach. The structure has not experienced any noticeable damage.

Structure 19

Figure A-17. Left Panel: Location of STR19 in Lake Erie, Right Panel: A Closer Look at the Structure Location

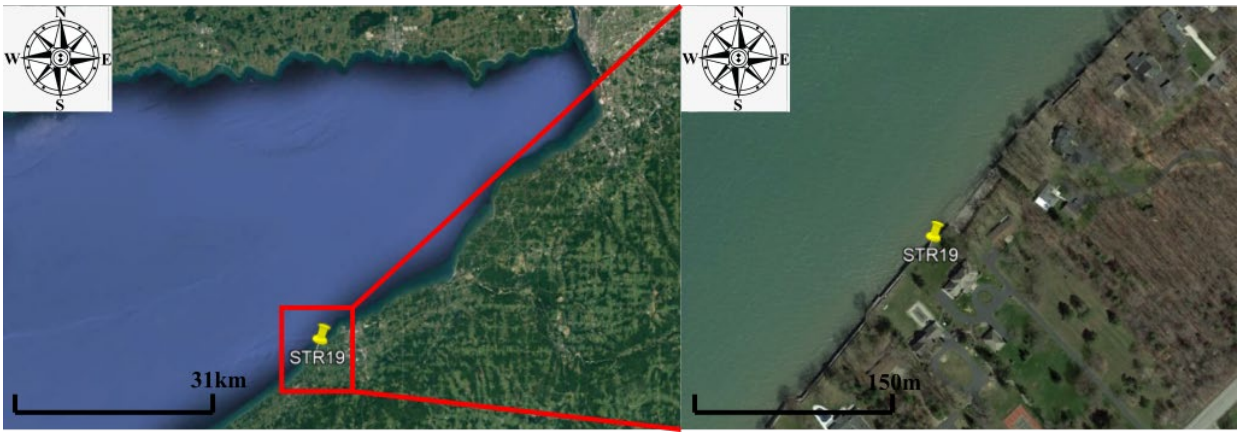

STR19 is an approximately 1000-meter-long seawall constructed to prevent erosion due to wave effect near Bayshore Dr. Aerial images from 1994 to 2016 available on Google Earth show that there is a significant shoreline recession on the beach. The structure has not experienced any noticeable damage.

Structure 20

Figure A-18. Left Panel: Location of STR20 in Lake Erie, Right Panel: A Closer Look at the Structure Location

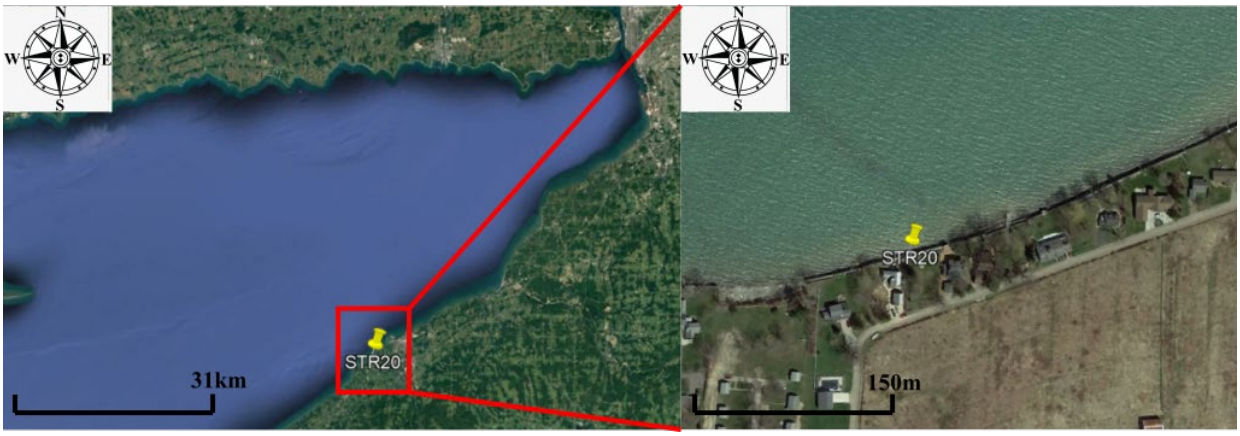

STR20 is an approximately 1700-meter-long seawall constructed to prevent erosion due to wave effect near Morewood Dr. Aerial images from 1994 to 2016 available on Google Earth show that there is a significant shoreline recession on the beach. The structure has not experienced any noticeable damage.

Structure 21

Figure A-19. Left Panel: Location of STR21 in Lake Erie, Right Panel: A Closer Look at the Structure Location

STR21 is an approximately 50-meter-rock revetment constructed to prevent bluff erosion due to wave effect near Shorewood Dr. E. Aerial images from 1994 to 2016 available on Google Earth show that there is a significant shoreline recession on the beach. The structure experienced a considerable amount of damage due to wave action, and while it was repaired, it seems that the structure will need additional repair work.

Structure 22

Figure A-20. Left Panel: Location of STR22 in Lake Erie, Right Panel: A Closer Look at the Structure Location

STR22 is an approximately 170-meter-long seawall constructed to prevent erosion due to wave effect near Lake Shore Dr. W. Aerial images from 1994 to 2016 available on Google Earth show that there is a significant shoreline recession on the beach. The structure has not experienced any noticeable damage.

Structure 23

Figure A-21. Left Panel: Location of STR23 in Lake Erie, Right Panel: A Closer Look at the Structure Location

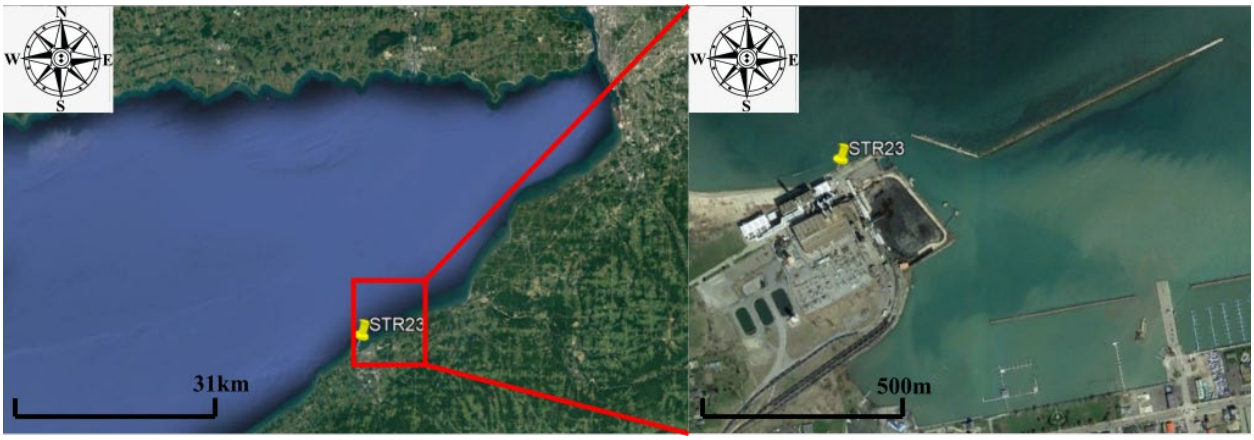

STR23 is an approximately 220-meter-long vertical wall belongs to NRG Dunkirk Operations Inc.

Aerial images from 1994 to 2016 available on Google Earth show that the structure has not experienced any noticeable damage.

Structure 24

Figure A-22. Left Panel: Location of STR24 in Lake Erie, Right Panel: A Closer Look at the Structure Location

STR24 is an approximately 850-meter-long offshore breakwater constructed to protect both wharf that belongs NRG Dunkirk Operations Inc and nearby marinas.

Aerial images from 1994 to 2016 available on Google Earth show that the trunk of the breakwater is damaged, and it has not been repaired.

Structure 25

Figure A-23. Left Panel: Location of STR25 in Lake Erie, Right Panel: A Closer Look at the Structure Location

STR25 is an approximately 250-meter-long quay wall that belongs to NRG Dunkirk Operations Inc.

Aerial images from 1994 to 2016 available on Google Earth show that the structure has not experienced any noticeable damage.

Structure 26

Figure A-24. Left Panel: Location of STR26 in Lake Erie, Right Panel: A Closer Look at the Structure Location

STR25 is an approximately 400-meter-long revetment constructed to protect the eastern section of the quay wall that belongs to NRG Dunkirk Operations Inc.

Aerial images from 1994 to 2016 available on Google Earth show that there are minor damages.

Structure 27

Figure A25: Left Panel: Location of STR27 in Lake Erie, Right Panel: A Closer Look at the Structure Location

STR27 is an approximately 200-meter-long revetment constructed to reduce wave reflection and overtopping, mainly due to ship waves, near Lake Shore Dr. W and N Woodrow Ave. Aerial images from 1994 to 2016 available on Google Earth show that the structure constructed on the seaside face of the wall has not experienced any noticeable damage.

Structure 28

Figure A-26. Left Panel: Location of STR28 in Lake Erie, Right Panel: A Closer Look at the Structure Location

STR28 is an approximately 370-meter-long offshore breakwater constructed to protect piers near Lake Shore Dr. W from direct wave impact. Aerial images from 1994 to 2016 available on Google Earth show that the structure has not experienced any noticeable damage.

Structure 29

Figure A-27. Left Panel: Location of STR29 in Lake Erie, Right Panel: A Closer Look at the Structure Location

STR29 is an approximately 450-meter-long vertical wall constructed to protect piers and the park near Lake Shore Dr. W from direct wave impact.

Aerial images from 1994 to 2016 available on Google Earth show that the structure has not experienced any noticeable damage.

Structure 30

Figure A-28. Left Panel: Location of STR30 in Lake Erie, Right Panel: A Closer Look at the Structure Location

STR30 is an approximately 350-meter-long pier near Lake Shore Dr. W from direct wave impact.

Aerial images from 1994 to 2016 available on Google Earth show that the structure has not experienced any noticeable damage.

Structure 31

Figure A-29. Left Panel: Location of STR31 in Lake Erie, Right Panel: A Closer Look at the Structure Location

STR31 is an approximately 370-meter-long breakwater constructed to protect the marina near Lake Shore Dr. W from direct wave impact. Aerial images from 1994 to 2016 available on Google Earth show that the structure has not experienced any noticeable damage. However, it seems that there is a sedimentation problem in the marina.

Structure 32

Figure A30: Left Panel: Location of STR32 in Lake Erie, Right Panel: A Closer Look at the Structure Location

STR32 is an approximately 400 meter-long quay wall that belongs to the marina near Lake Shore Dr. W.

Aerial images from 1994 to 2016 available on Google Earth show that the structure has not experienced any noticeable damage.

Structure 33

Figure A-31. Left Panel: Location of STR33 in Lake Erie, Right Panel: A Closer Look at the Structure Location

STR33 is an approximately 1150-meter-long wall constructed to protect residential buildings and Wright Parker Dr. from direct wave impact.

Aerial images from 1994 to 2016 available on Google Earth show that there is a significant shoreline recession on the beach. The structure has not experienced any noticeable damage.

Structure 34

Figure A-32. Left Panel: Location of STR34 in Lake Erie, Right Panel: A Closer Look at the Structure Location

STR34 is an approximately 90-meter-long revetment constructed to protect Laker Rd. from direct wave impact. Aerial images from 1994 to 2016 available on Google Earth show that the structure is significantly damaged, and it has not been repaired.

Structure 35

Figure A-33. Left Panel: Location of STR35 in Lake Erie, Right Panel: A Closer Look at the Structure Location

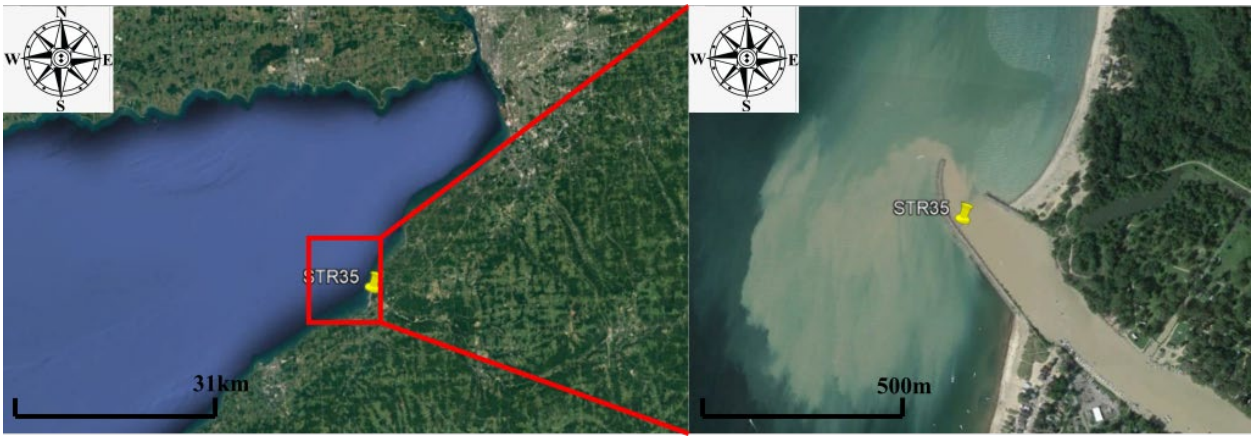

STR35 is an approximately 500-meter-long jetty constructed to both protect and stabilize the mouth of Cattaraugus Creek. Aerial images from 1994 to 2016 available on Google Earth show that jetty has stabilized the river mouth and it has not experienced any noticeable damage.

Structure 36

Figure A-34. Left Panel: Location of STR36 in Lake Erie, Right Panel: A Closer Look at the Structure Location

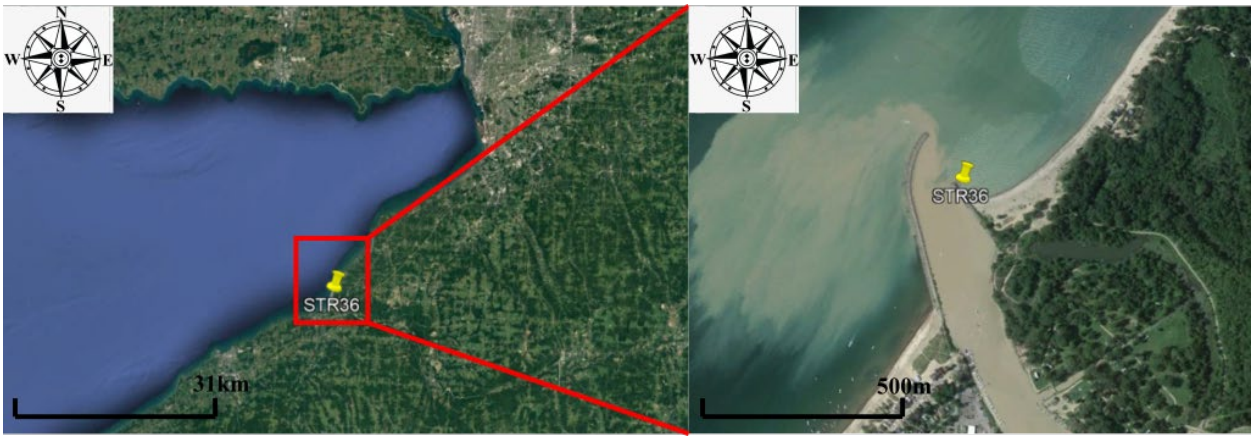

STR36 is an approximately 180-meter-long jetty constructed to both protect and stabilize the mouth of Cattaraugus Creek. Aerial images from 1994 to 2016 available on Google Earth show that jetty has stabilized the river mouth and it has not experienced any noticeable damage.

Structure 37

No data

Structure 38

Figure A-35. Left Panel: Location of STR38 in Lake Erie, Right Panel: A Closer Look at the Structure Location

STR38 is an approximately 50-meter-long wall constructed to protect residential buildings and Shorecliff road from direct wave impact. Aerial images from 1994 to 2016 available on Google Earth show that the structure has not experienced any noticeable damage.

Structure 39

Figure A-36. Left Panel: Location of STR39 in Lake Erie, Right Panel: A Closer Look at the Structure Location

STR39 is an approximately 100-meter-long wall constructed to protect residential buildings and Waterfront Rd from direct wave impact. Aerial images from 1994 to 2016 available on Google Earth show that there is a significant shoreline recession on the beach. The structure has not experienced any noticeable damage.

Structure 40

Figure A-37. Left Panel: Location of STR40 in Lake Erie, Right Panel: A Closer Look at the Structure Location

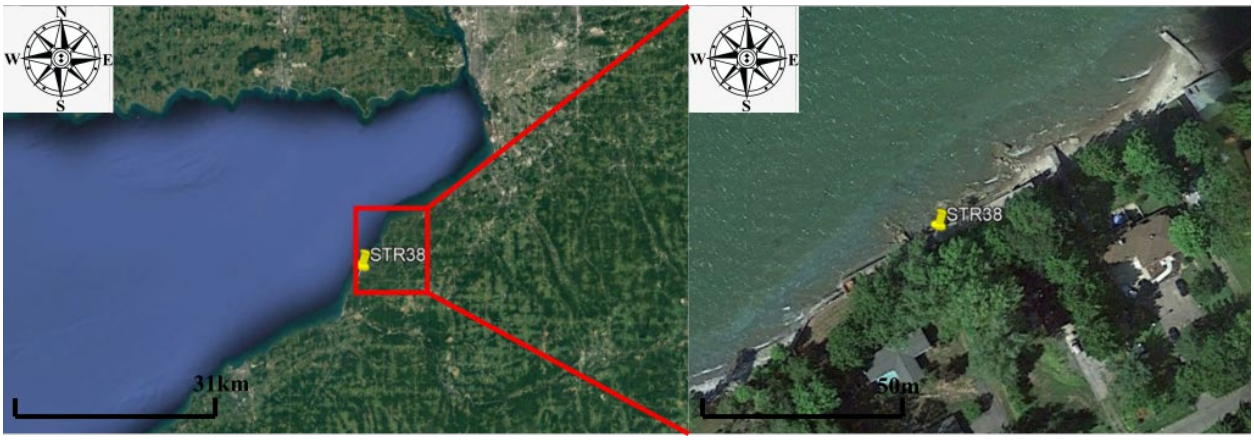

STR40 is an approximately 100-meter-long revetment constructed to protect residential buildings and Waterfront Rd. from direct wave impact. Aerial images from 1994 to 2016 available on Google Earth show the structure is damaged, and it has not been repaired.

Structure 41

Figure A-38. Left Panel: Location of STR41 in Lake Erie, Right Panel: A Closer Look at the Structure Location

STR41 is approximately 15-meter-long wall constructed to protect beach and boat yard near Waterfront Rd from direct wave impact. Aerial images from 1994 to 2016 available on Google Earth show that there is a significant shoreline recession on the beach. The structure has not experienced any noticeable damage.

Structure 42

Figure A-39. Left Panel: Location of STR42 in Lake Erie, Right Panel: A Closer Look at the Structure Location

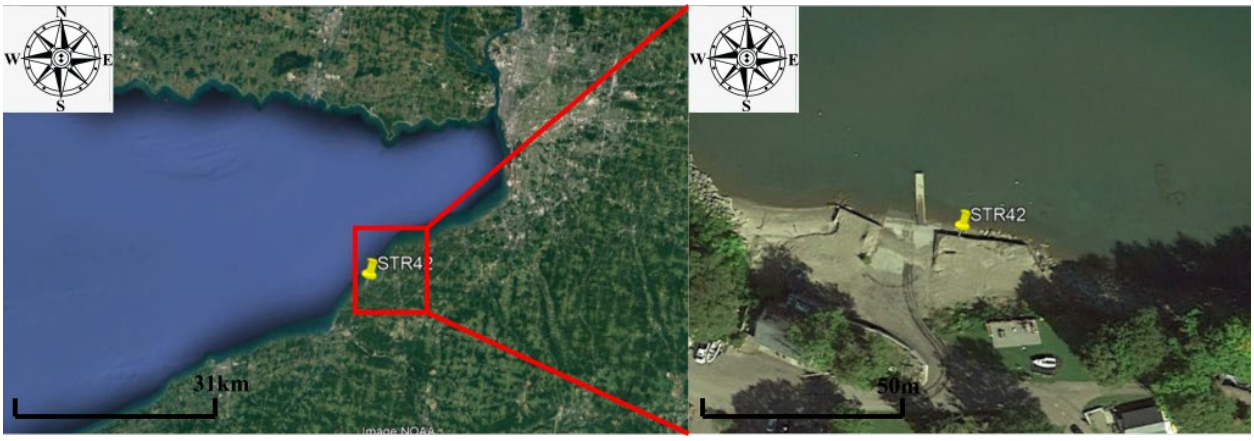

STR42 is an approximately 30-meter-long wall constructed to protect beach and boat yard near Waterfront Rd. from direct wave impact. Aerial images from 1994 to 2016 available on Google Earth show that there is a significant shoreline recession on the beach. The structure has not experienced any noticeable damage.

Structure 43

Figure A-40. Left Panel: Location of STR43 in Lake Erie, Right Panel: A Closer Look at the Structure Location

STR43 is an approximately 25-meter-long revetment constructed to prevent erosion due to wave effect near Waterfront Rd.

Aerial images from 1994 to 2016 available on Google Earth show that there is a significant shoreline recession on the beach. The structure is slightly damaged.

Structure 44

Figure A41: Left Panel: Location of STR44 in Lake Erie, Right Panel: A Closer Look at the Structure Location

STR44 is a wall constructed to prevent erosion due to wave effect near Lakeshore Rd. Aerial images from 1994 to 2016 available on Google Earth show that there is a significant shoreline recession on the beach. The structure has not experienced any noticeable damage.

Structure 45

Figure A-42. Left Panel: Location of STR45 in Lake Erie, Right Panel: A Closer Look at the Structure Location

STR45 is an approximately 10-meter-long groin constructed to prevent erosion due to wave effect near Lakeside Rd. Aerial images from 1994 to 2016 available on Google Earth show that there is a significant shoreline recession on the beach. It seems that the groin slowed down the beach recession.

Structure 46

Figure A-43. Left Panel: Location of STR46 in Lake Erie, Right Panel: A Closer Look at the Structure Location

STR46 is an approximately 10-meter-long groin constructed to prevent erosion due to wave effect near Lakeside Rd. Aerial images from 1994 to 2016 available on Google Earth show that there is a significant shoreline recession on the beach. It seems that the groin slowed down the beach recession.

Structure 47

Figure A-44: Left Panel: Location of STR47 in Lake Erie, Right Panel: A Closer Look at the Structure Location

STR47 is an approximately 550-meter-long wall constructed to protect residential buildings and Roat Dr. from direct wave impact. Aerial images from 1994 to 2016 available on Google Earth show that there is a significant shoreline recession on the beach. The structure has not experienced any noticeable damage.

Structure 48

Figure A-45. Left Panel: Location of STR48 in Lake Erie, Right Panel: A Closer Look at the Structure Location

STR48 is an approximately 300-meter-long breakwater constructed to protect Sturgeon Point marina from direct wave impact.

Aerial images from 1994 to 2016 available on Google Earth show that the structure has not experienced any noticeable damage.

Structure 49

Figure A-46. Left Panel: Location of STR49 in Lake Erie, Right Panel: A Closer Look at the Structure Location

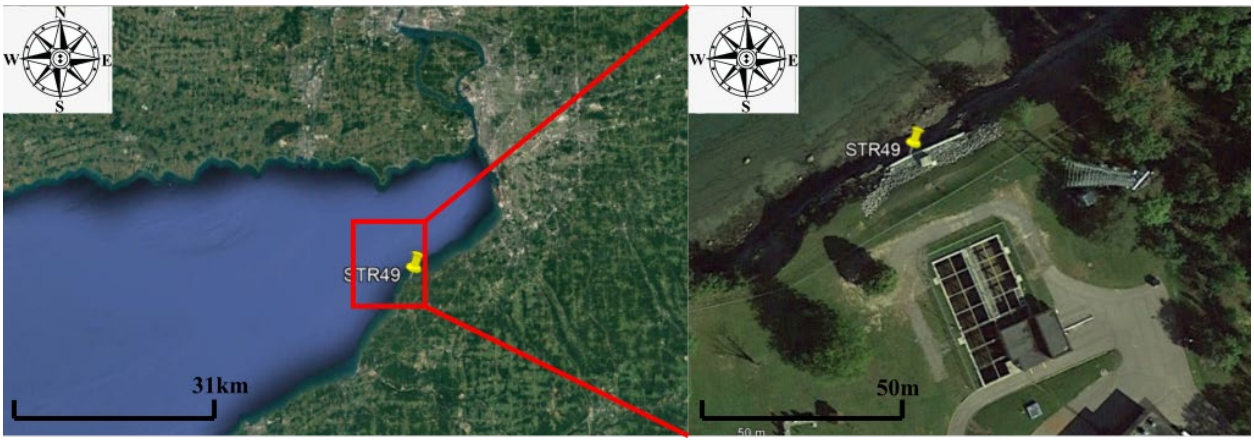

STR49 is an approximately 20-meter-long wall constructed to protect nearby structure from erosion.

Aerial images from 1994 to 2016 available on Google Earth show that there is a significant shoreline recession on the beach. The structure was constructed in 2016, and it has not experienced any noticeable damage since then.

Structure 50

Figure A-47. Left Panel: Location of STR50 in Lake Erie, Right Panel: A Closer Look at the Structure Location

STR50 is an approximately 65-meter-long wall constructed to protect nearby structures on Woodmere Rd. from erosion. Aerial images from 1994 to 2016 available on Google Earth show that there is a significant shoreline recession on the beach. The structure has not experienced any noticeable damage.

Structure 51

Figure A-48. Left Panel: Location of STR51 in Lake Erie, Right Panel: A Closer Look at the Structure Location

STR51 is an approximately 65-meter-long wall constructed to protect nearby structures on Woodmere Rd. from erosion.

Aerial images from 1994 to 2016 available on Google Earth show that there is a significant shoreline recession on the beach. The structure has not experienced any noticeable damage.

Structure 52

Figure A-49. Left Panel: Location of STR52 in Lake Erie, Right Panel: A Closer Look at the Structure Location

STR52 is an approximately 250-meter-long rock wall constructed to protect nearby structures from erosion.

Aerial images from 1994 to 2016 available on Google Earth show that there is a significant shoreline recession on the beach. The structure is damaged, and it has not been repaired.

Structure 53

Figure A-50. Left Panel: Location of STR53 in Lake Erie, Right Panel: A Closer Look at the Structure Location

STR53 is an approximately 1250-meter-long wall constructed to protect nearby structures on Lake Shore Rd. from erosion.

Aerial images from 1994 to 2016 available on Google Earth show that there is a significant shoreline recession on the beach. The structure has not experienced any noticeable damage.

Structure 54

Figure A-51. Left Panel: Location of STR54 in Lake Erie, Right Panel: A Closer Look at the Structure Location

STR54 is an approximately 700-meter-long wall constructed to protect nearby structures on Lake Shore Rd. from erosion.

Aerial images from 1994 to 2016 available on Google Earth show that there is a significant shoreline recession on the beach. The structure has not experienced any noticeable damage.

Structure 55

Figure A-52. Left Panel: Location of STR55 in Lake Erie, Right Panel: A Closer Look at the Structure Location

STR55 is an approximately 10-meter-long groin constructed near the structure on Lake Shore Rd. from erosion.

Aerial images from 1994 to 2016 available on Google Earth show that there is a significant shoreline recession on the beach. The groin was constructed around 2011. It is damaged and has not been repaired.

Structure 56

Figure A-53. Left Panel: Location of STR56 in Lake Erie, Right Panel: A Closer Look at the Structure Location

STR56 is an approximately 75-meter-long revetment constructed to protect Lake Shore Rd. from direct wave impact.

Aerial images from 1994 to 2016 available on Google Earth show that the structure was constructed around 2011. It is damaged and has not been repaired.

Structure 57

Figure A-54. Left Panel: Location of STR57 in Lake Erie, Right Panel: A Closer Look at the Structure Location

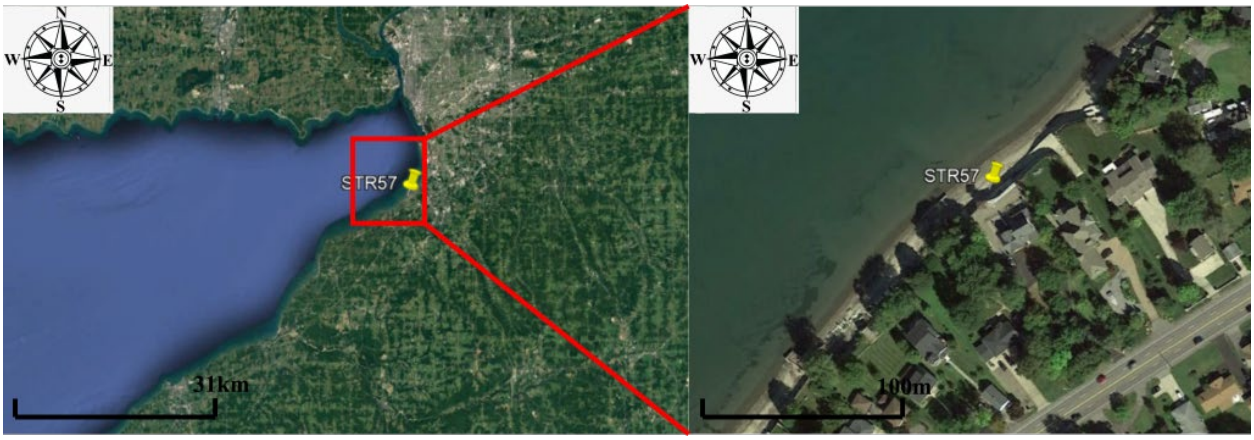

STR57 is an approximately 1000-meter-long wall and rock revetment constructed to protect residential buildings near Lake Shore Rd. from direct wave impact.

Aerial images from 1994 to 2016 available on Google Earth show that there is a significant shoreline recession on the beach. The structure has not experienced any noticeable damage.

Structure 58

Figure A-55. Left Panel: Location of STR58 in Lake Erie, Right Panel: A Closer Look at the Structure Location

STR58 is an approximately 200-meter-long rock revetment constructed to protect fill area from direct wave impact.

Aerial images from 1994 to 2016 available on Google Earth show that the structure has not experienced any noticeable damage.

Structure 59

Figure A-56. Left Panel: Location of STR59 in Lake Erie, Right Panel: A Closer Look at the Structure Location

STR59 is an approximately 70-meter-long rock revetment constructed to protect Lake Shore Rd. from direct wave impact.

Aerial images from 1994 to 2016 available on Google Earth show that the structure was constructed around 2009, and it has not experienced any noticeable damage since then.

Structure 60

Figure A57: Left Panel: Location of STR60 in Lake Erie, Right Panel: A Closer Look at the Structure Location

STR60 is an approximately 390-meter-long revetment constructed to protect Lake Shore Rd. from direct wave impact.

Aerial images from 1994 to 2016 available on Google Earth show that the structure was constructed in 2016, and it has not experienced any noticeable damage since then.

Structure 61

Figure A-58. Left Panel: Location of STR61 in Lake Erie, Right Panel: A Closer Look at the Structure Location

STR60 is an approximately 600-meter-long wall constructed to protect Lake Shore Rd. from direct wave impact.

Aerial images from 1994 to 2016 available on Google Earth show that the structure has not experienced any noticeable damage.

Structure 62

Figure A-59. Left Panel: Location of STR62 in Lake Erie, Right Panel: A Closer Look at the Structure Location

STR60 is an approximately 225-meter-long revetment constructed to protect nearby structure and Lake Shore Rd. from direct wave impact.

Aerial images from 1994 to 2016 available on Google Earth show that the structure was constructed around 2011 and it has not experienced any noticeable damage since then.

Structure 63

Couldn’t find (probably missed in numbering)

Structure 64

Figure A-60. Left Panel: Location of STR64 in Lake Erie, Right Panel: A Closer Look at the Structure Location

STR64 is an approximately 800-meter-long wall constructed to protect residential buildings near S. Shore Dr. from direct wave impact.

Aerial images from 1994 to 2016 available on Google Earth show that there is a significant shoreline recession on the beach. The structure has not experienced any noticeable damage.

Structure 65

Figure A-61. Left Panel: Location of STR65 in Lake Erie, Right Panel: A Closer Look at the Structure Location

STR65 is an approximately 30-meter-long groin constructed to protect beach from erosion.

Aerial images from 1994 to 2016 available on Google Earth show that the structure is damaged and has not been repaired. Since it is not repaired, the structure is not functioning properly; therefore, there is a significant shoreline recession on the beach.

Structure 66

Figure A-62. Left Panel: Location of STR66 in Lake Erie, Right Panel: A Closer Look at the Structure Location

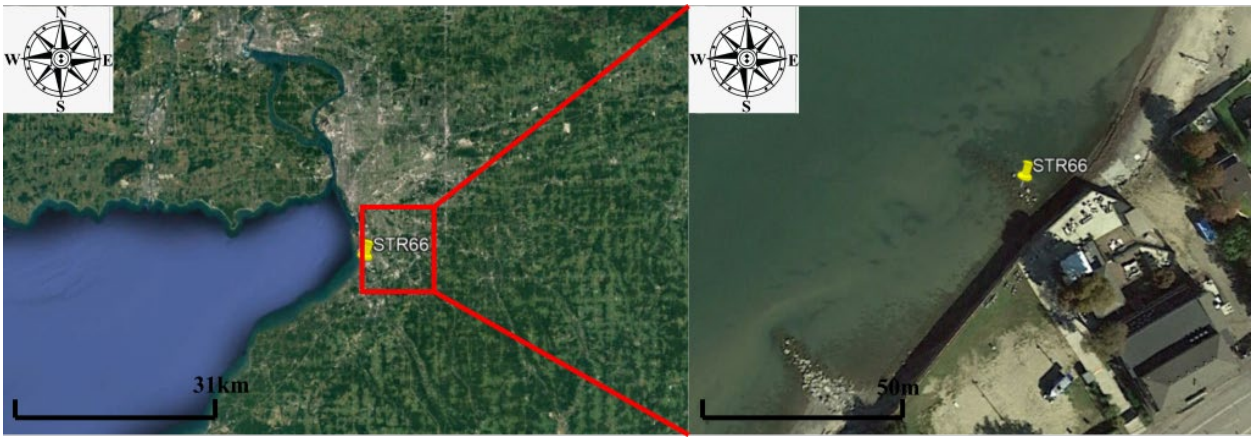

STR66 is an approximately 30-meter-long groin constructed to protect beach from erosion.

Aerial images from 1994 to 2016 available on Google Earth show that the structure is damaged and has not been repaired. Since it is not repaired, the structure is not functioning properly; therefore, there is a significant shoreline recession on the beach.

Structure 67

Figure A-63. Left Panel: Location of STR67 in Lake Erie, Right Panel: A Closer Look at the Structure Location

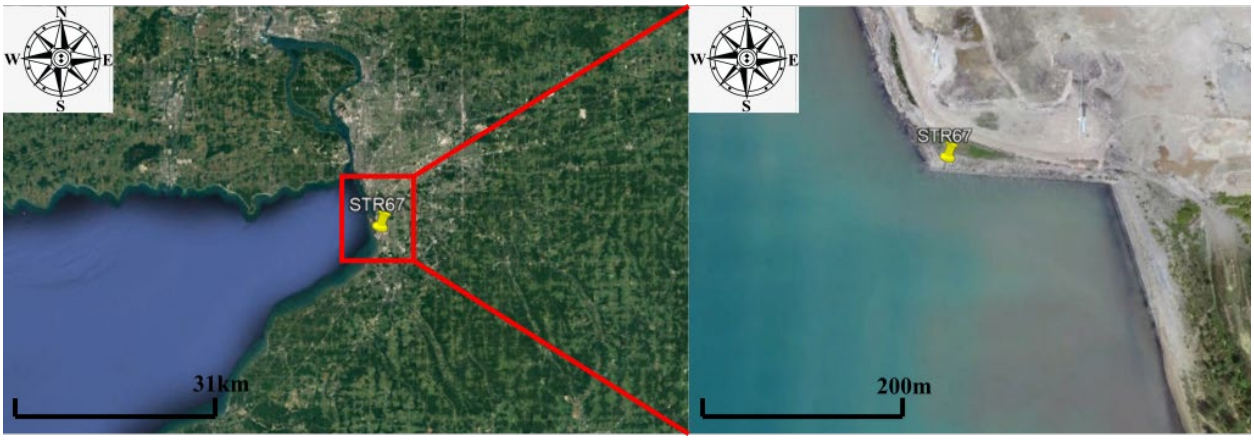

STR67 is an approximately 210-meter-long revetment constructed to protect fill area on which wind turbines are constructed from direct wave impact.

Aerial images from 1994 to 2016 available on Google Earth show that the structure has not experienced any noticeable damage.

Structure 68

Figure A-64. Left Panel: Location of STR68 in Lake Erie, Right Panel: A Closer Look at the Structure Location

STR68 is an approximately 65-meter-long jetty constructed to stabilize the river mouth.

Aerial images from 1994 to 2016 available on Google Earth show that the structure has not experienced any noticeable damage.

Structure 69

Figure A-65. Left Panel: Location of STR69 in Lake Erie, Right Panel: A Closer Look at the Structure Location

STR69 is an approximately 65-meter-long jetty constructed to stabilize the river mouth.

Aerial images from 1994 to 2016 available on Google Earth show that the structure has not experienced any noticeable damage.

Structure 70

Figure A-66. Left Panel: Location of STR70 in Lake Erie, Right Panel: A Closer Look at the Structure Location

STR70 is an approximately 1650-meter-long breakwater.

Aerial images from 1994 to 2016 available on Google Earth show that the structure has not experienced any noticeable damage.

Structure 71

Figure A-67. Left Panel: Location of STR71 in Lake Erie, Right Panel: A Closer Look at the Structure Location

STR71 is an approximately 3100 meter-long offshore breakwater constructed to protect coastal structures along the Buffalo coastline from direct wave impact.

Aerial images from 1994 to 2016 available on Google Earth show that the structure has not experienced any noticeable damage.

Structure 72

Figure A-68. Left Panel: Location of STR72 in Lake Erie, Right Panel: A Closer Look at the Structure Location

STR72 is an approximately 1200-meter-long breakwater constructed to protect NFTA marina from direct wave impact.

Aerial images from 1994 to 2016 available on Google Earth show that the structure has not experienced any noticeable damage.

Structure 73

Figure A-69. Left Panel: Location of STR73 in Lake Erie, Right Panel: A Closer Look at the Structure Location

STR73 is an approximately 400-meter-long revetment constructed to shoreline from direct wave impact and erosion.

Aerial images from 1994 to 2016 available on Google Earth show that the structure was constructed around 2011, and it has not experienced any noticeable damage since then.

Structure 74

Figure A-70. Left Panel: Location of STR74 in Lake Erie, Right Panel: A Closer Look at the Structure Location

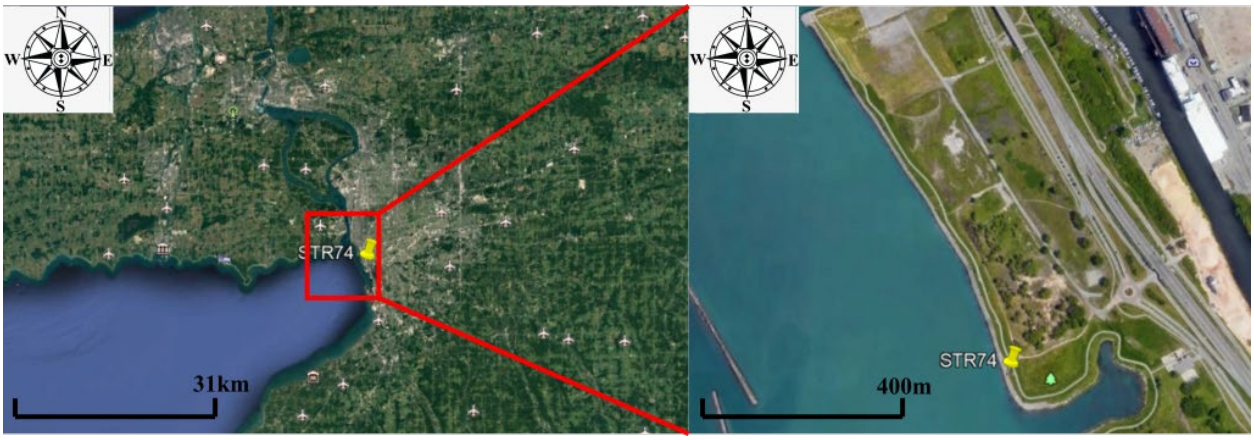

STR74 is an approximately 1100-meter-long revetment constructed to shoreline from direct wave impact and erosion.

Aerial images from 1994 to 2016 available on Google Earth show that the structure was constructed around 2011, and it has not experienced any noticeable damage since then.

Structure 75

Figure A-71. Left Panel: Location of STR75 in Lake Erie, Right Panel: A Closer Look at the Structure Location

STR75 is an approximately 1900-meter-long offshore breakwater constructed to protect coastal structures along the Buffalo coastline from direct wave impact.

Aerial images from 1994 to 2016 available on Google Earth show that the structure has not experienced any noticeable damage.

Structure 76

Figure A-72. Left Panel: Location of STR76 in Lake Erie, Right Panel: A Closer Look at the Structure Location

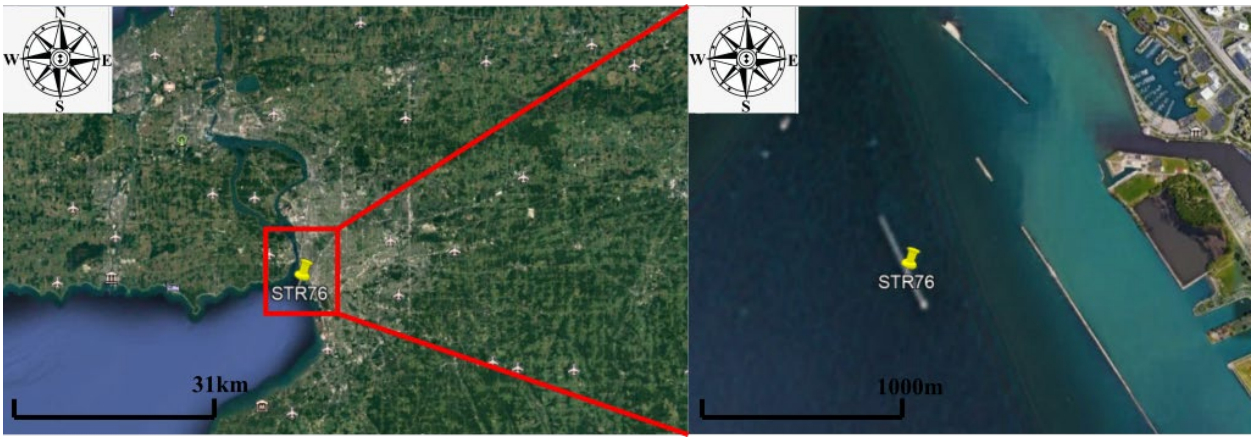

STR76 is an approximately 550-meter-long offshore breakwater constructed to protect coastal structures along the Buffalo coastline from direct wave impact.

Aerial images from 1994 to 2016 available on Google Earth show that the structure has not experienced any noticeable damage.

Structure 77

Figure A-73. Left Panel: Location of STR77 in Lake Erie, Right Panel: A Closer Look at the Structure Location

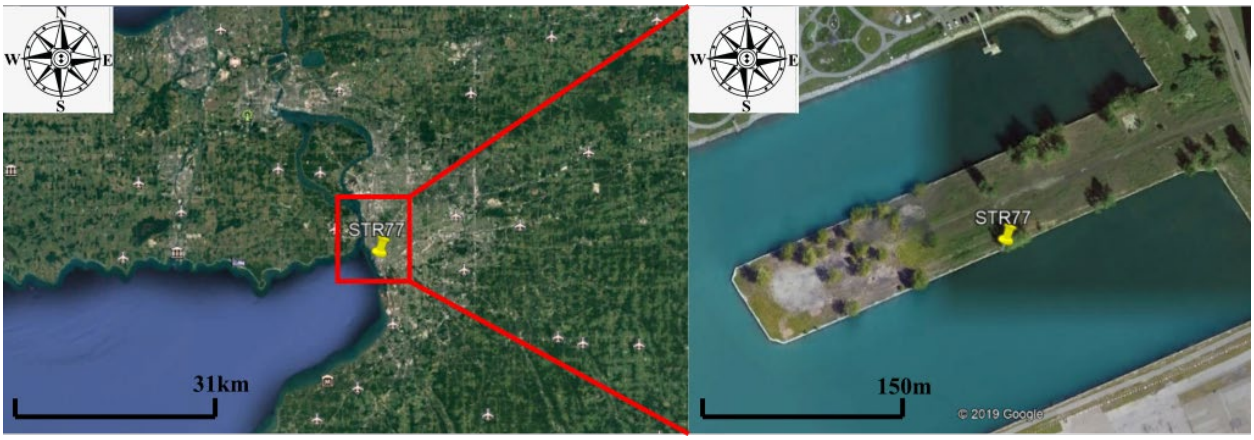

STR77 is an approximately 1300-meter-long wall constructed to protect shoreline from erosion.

Aerial images from 1994 to 2016 available on Google Earth show that the structure has not experienced any noticeable damage.

Structure 78

Figure A-74. Left Panel: Location of STR78 in Lake Erie, Right Panel: A Closer Look at the Structure Location

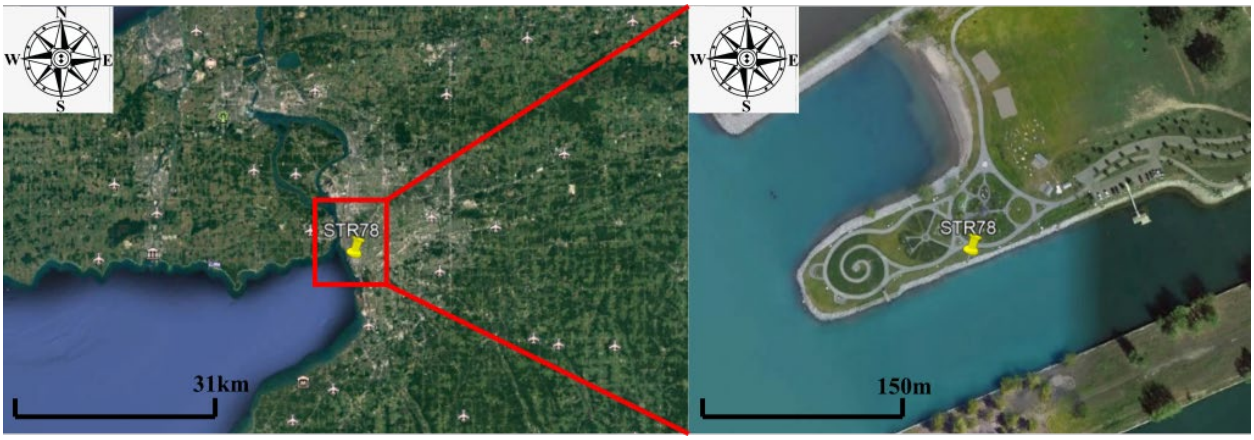

STR78 is an approximately 550-meter-long revetment constructed to protect shoreline from erosion.

Aerial images from 1994 to 2016 available on Google Earth show that the structure was constructed around 2011 and it has not experienced any noticeable damage since then.

Structure 79

Figure A-75. Left Panel: Location of STR79 in Lake Erie, Right Panel: A Closer Look at the Structure Location

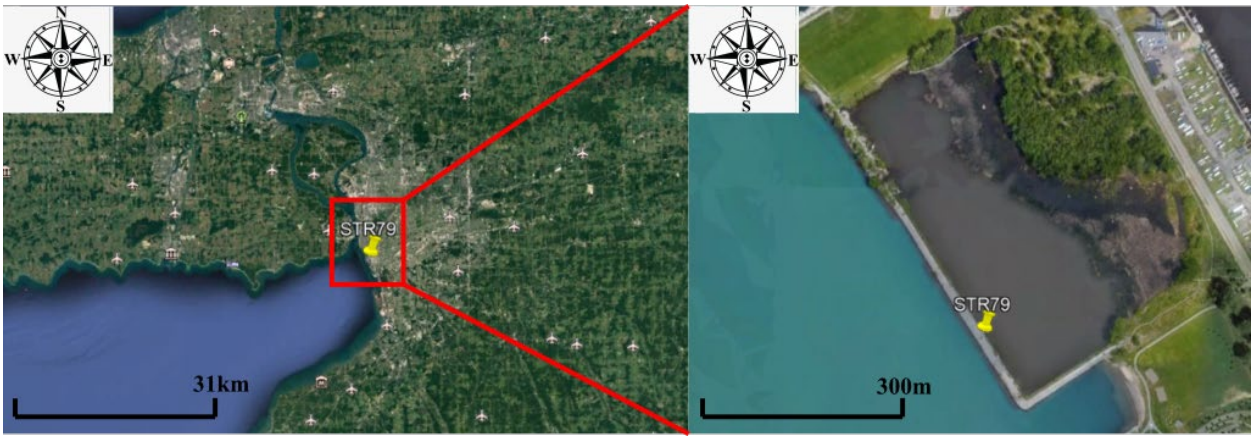

STR79 is an approximately 550-meter-long revetment constructed to protect the pond from the direct wave impact.

Aerial images from 1994 to 2016 available on Google Earth show that the has not experienced any noticeable damage.

Structure 80

Figure A76: Left Panel: Location of STR80 in Lake Erie, Right Panel: A Closer Look at the Structure Location

STR80 is an approximately 150-meter-long offshore breakwater.

Aerial images from 1994 to 2016 available on Google Earth show that the has not experienced any noticeable damage.

Structure 81

Figure A-77. Left Panel: Location of STR81 in Lake Erie, Right Panel: A Closer Look at the Structure Location

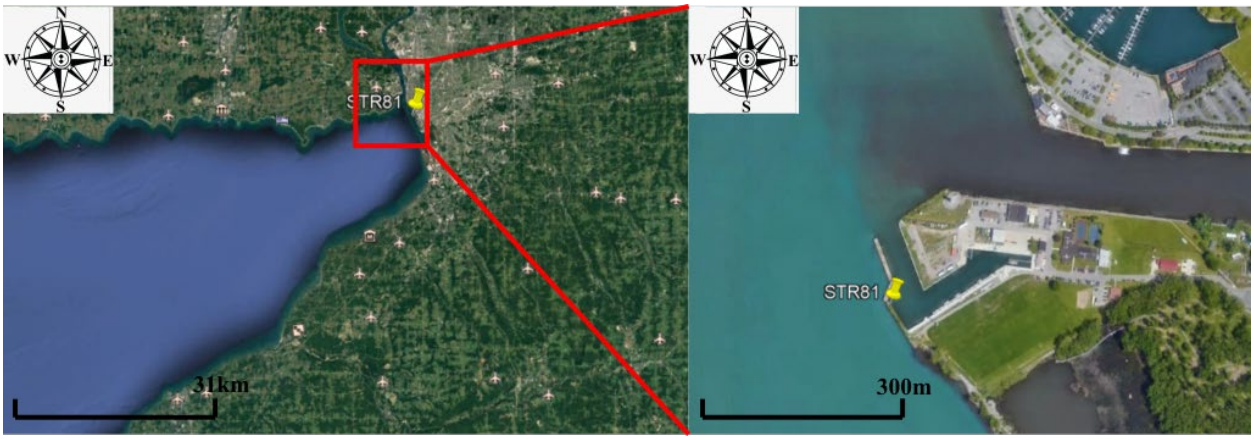

STR81 is an approximately 120-meter-long breakwater constructed to protect the port.

Aerial images from 1994 to 2016 available on Google Earth show that the has not experienced any noticeable damage.

Structure 82

Figure A-78. Left Panel: Location of STR82 in Lake Erie, Right Panel: A Closer Look at the Structure Location

STR82 is an approximately 85-meter-long wall constructed to protect shoreline from erosion.

Aerial images from 1994 to 2016 available on Google Earth show that the has not experienced any noticeable damage.

Structure 83

Figure A-79: Left Panel: Location of STR83 in Lake Erie, Right Panel: A Closer Look at the Structure Location

STR83 is an approximately 400-meter-long revetment constructed to protect shoreline from erosion.

Aerial images from 1994 to 2016 available on Google Earth show that the has not experienced any noticeable damage.

Structure 84

Figure A-80. Left Panel: Location of STR84 in Lake Erie, Right Panel: A Closer Look at the Structure Location

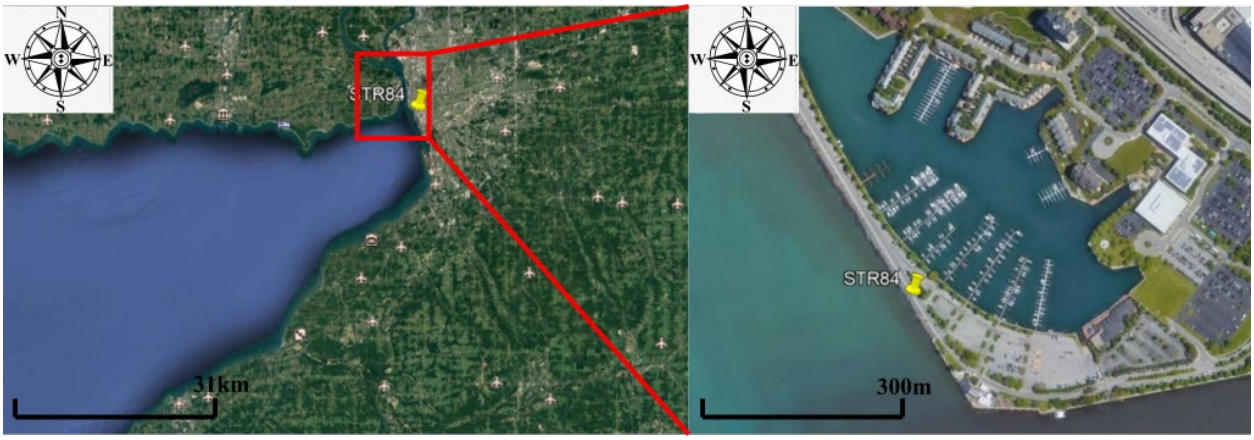

STR84 is an approximately 600-meter-long breakwater constructed to protect Buffalo Erie Basin marina from direct wave impact.

Aerial images from 1994 to 2016 available on Google Earth show that the has not experienced any noticeable damage.

Structure 85

Figure A-81. Left Panel: Location of STR85 in Lake Erie, Right Panel: A Closer Look at the Structure Location

STR85 is an approximately 650-meter-long offshore breakwater.

Aerial images from 1994 to 2016 available on Google Earth show that the has not experienced any noticeable damage.

Structure 86

Figure A-82. Left Panel: Location of STR86 in Lake Erie, Right Panel: A Closer Look at the Structure Location

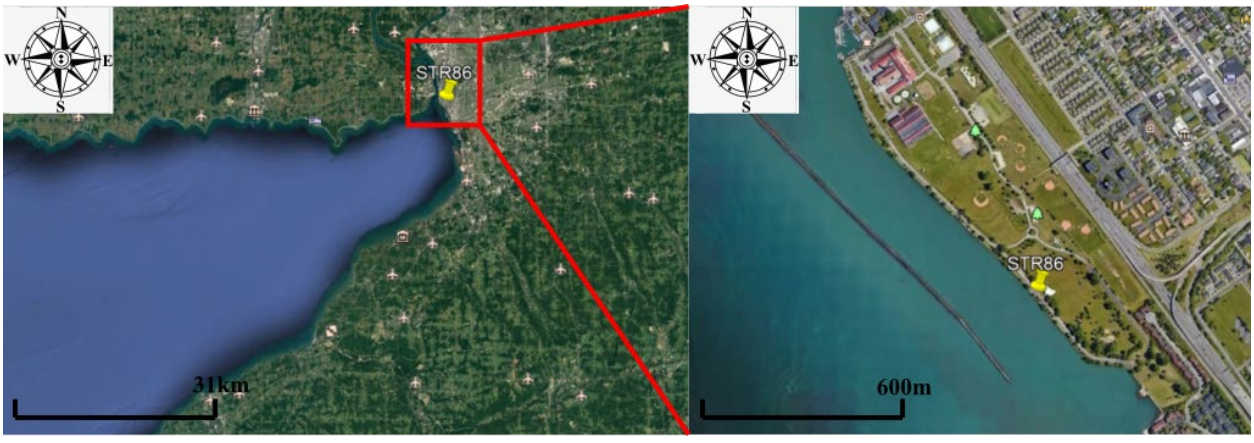

STR86 is an approximately 2000-meter-long revetment constructed to protect shoreline from erosion.

Aerial images from 1994 to 2016 available on Google Earth show that the has not experienced any noticeable damage.

Structure 87

Figure A-83. Left Panel: Location of STR87 in Lake Erie, Right Panel: A Closer Look at the Structure Location

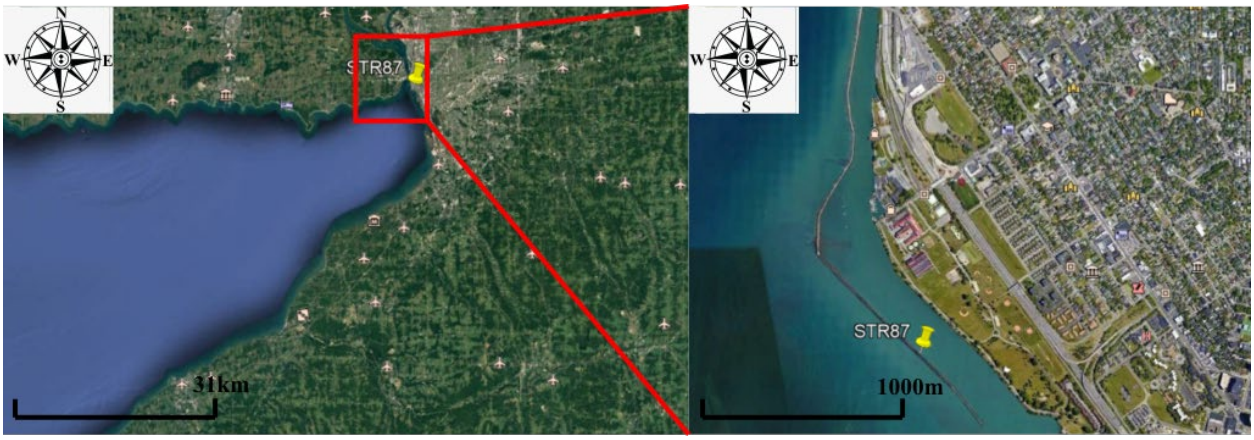

STR87 is an approximately 3200-meter-long offshore breakwater.

Aerial images from 1994 to 2016 available on Google Earth show that the has not experienced any noticeable damage.

Appendix B

Seiche and Storm Surge

What is a Seiche ("say-sh")

A seiche is a standing wave oscillating in a body of water. A seiche can occur in any semi- or fully-enclosed body of water. Seiches are typically caused when strong winds and rapid changes in atmospheric pressure push water from one end of a body of water to the other. When the wind stops, the water rebounds to the other side of the enclosed area. The water then continues to oscillate back and forth for hours or even days .

Image from a weather forecast on February 24, 2019 on WGRZ

Wind Set-up and Set-down

Ohio DNR

Lake Erie Seiches

Lake Erie is known for seiches, occurring when a strong wind blows along the lake's long axis, from Southwest (SW) to Northeast (NE), piling water up at Buffalo and causing a drawdown in Toledo.

Impacts of Seiches

When seiches occur, the affected area can be flooded. When there is ice, it can pile up and cause damage. The flooding from seiches can increase erosion and change the shape of the coastline. Over a 1-year period, seiches were observed to be the cause of 1.5% of coastline changes (erosion and accretion), in Buffalo, NY.

In 1844, a 22-foot seiche breached a 14-foot-high seawall, killing 78 people and damming the ice to the extent that Niagara Falls temporarily stopped flowing. As recently as November 2019, strong winds created waves in Lake Erie, leading to flooding near Buffalo, New York. More frequent wind storms from climate change may increase the occurrence of seiches. In winter, they can combine with other physical dynamics to toss walls of ice onshore.

Flooding from Seiches

The Federal Emergency Management Agency (FEMA) provides flood maps for 100 year discharge, but does not consider changes in downstream lake water level – combinations of seiche and high discharge can produce different results. The flood maps of the Buffalo River are not majorly impacted by seiches, but this may not be the case in other systems.

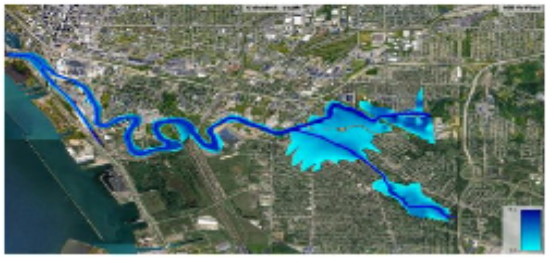

Flood map for 100-year flood and seiche combination.

Sea Grant New York

University at Buffalo
The State University of New York

NYSERDA, a public benefit corporation, offers objective information and analysis, innovative programs, technical expertise, and support to help New Yorkers increase energy efficiency, save money, use renewable energy, and reduce reliance on fossil fuels. NYSERDA professionals work to protect the environment and create clean-energy jobs. NYSERDA has been developing partnerships to advance innovative energy solutions in New York State since 1975.

To learn more about NYSERDA's programs and funding opportunities, visit nyserda.ny.gov or follow us on Twitter, Facebook, YouTube, or Instagram.

New York State Energy Research and Development Authority

17 Columbia Circle
Albany, NY 12203-6399

toll free: 866-NYSERDA
local: 518-862-1090
fax: 518-862-1091

info@nyserda.ny.gov
nyserda.ny.gov

State of New York
Kathy Hochul, Governor

New York State Energy Research and Development Authority
Richard L. Kauffman, Chair | Doreen M. Harris, President and CEO